Institute of condensed Matter and Nanosciences

Molecules, Solids and Reactivity

Bifunctional catalysts for the valorization of cellulose into sorbitol

by

Carlier Samuel

Supervisor:

Prof. Sophie Hermans

Examination board:

Prof. Eric Gaigneaux, Université catholique de Louvain, Belgium (president)

Prof. Sophie Hermans, Université catholique de Louvain, Belgium (supervisor)

Prof. Tom Leyssens, Université catholique de Louvain, Belgium

Prof. Patricia Luis Alconero, Université catholique de Louvain, Belgium

Dr. Vincent Dubois, LABIRIS, Belgium

Dr. Robert Wojcieszak, CNRS et Centrale Lille, France

Abstract

The aim of this PhD thesis was to elaborate a bifunctional catalyst that would allow biomass valorization, namely converting cellulose into sorbitol.

The first part of this work was devoted to the study of glucose hydrogenation into sorbitol. Catalysts composed of Ru nanoparticles deposited on carbon supports have been synthesized. Different sizes of Ru nanoparticles were prepared and the optimal size for this reaction has been established between 1 and 2 nm. Moreover, doping of carbon materials with nitrogen atoms has also been investigated. Efficient functionalization was confirmed by X-ray photoelectron spectroscopy and Boehm titration. Enhancement of the Ru activity by the presence of nitrogen in the support has been demonstrated for the direct transformation of cellobiose (two glucose units bound together) into sorbitol.

The second part of this thesis was dedicated to the study of cellobiose hydrolysis into glucose. Several carbon materials have been successfully covalently functionalized with sulfonic functions by a diazonium coupling method. Functionalized carbons displayed excellent acidity (confirmed by Boehm titration) and showed great selectivity in glucose as main hydrolysis product.

The last part of this manuscript dealt with the synthesis of bifunctional catalysts composed of Ru nanoparticles deposited on carbon supports functionalized by sulfonic functions. Despite cross-poisoning between the two active sites, optimization of the ratio between Ru and sulfur led to a bifunctional catalyst that outperformed non-acidic Ru/C catalysts. Sorbitol has been produced from cellobiose and more importantly from cellulose, in significant amounts compared to literature standards, with this bifunctional catalyst.

Acknowledgements

Tout d'abord, je voudrais remercier ma promotrice, le professeur Sophie Hermans pour m'avoir permis de faire ma thèse dans son laboratoire ainsi que pour avoir toujours cru en moi et pour m'avoir guidé tout au long de ces 7 années. Je n'aurais pas pu rêver d'une meilleure promotrice.

Je tiens à remercier le jury de thèse d'avoir pris le temps de lire ce manuscrit et d'aider à son amélioration lors de la défense privée.

J'aimerais également remercier les membres permanents des différents laboratoires qui sont là pour nous faciliter la vie : Jacqueline Boniver, Céline Brochier, Aurore Becquevort, Laurent Collard, Pierre Eloy, Gabriella Barozzino, François Devred et François Billard. Je tiens particulièrement à remercier Jean-François Statsijns pour son aide au quotidien et sa bonne humeur.

Je tiens maintenant à remercier les personnes avec qui j'ai passé la plus grande partie de mon temps durant cette thèse : Tommy pour toutes ces conversations One Piece, les concours de lancer de balle, les fous rires sur l'univers d'Harry Potter, Antonin avec qui j'ai eu la chance de voyager jusqu'au Japon et Nadia pour sa bonne humeur communicative. Grâce à vous j'ai passé de nombreux bons moments que je garderai en mémoire.

Un grand merci également à toutes les personnes avec qui j'ai pu collaborer durant cette thèse. Tout d'abord les trois étudiants que j'ai eu la chance d'encadrer : Jim, Martin et Julie. Viennent ensuite toutes les personnes du laboratoire B3 que j'ai côtoyées avec plaisir au fil des années : la petite Nath (la meilleure encadrante), la grande Nath, Nath B., Nathalie de la Torre, Seb D., Antoine, Dodji, Debobrata, Julien Mahy, Julien Mahin, Varun, Florence, Béatrice, Francisco, Arnaud, Jordan, Timothy, Sarah, Louise, Yang,

Jonathan, Maïté, Anne-Sophie, Rémi, Antonin E., Corentin, Fabien et Oriane. Merci à tous d'avoir rendu le travail au jour le jour si agréable.

Je souhaite aussi remercier toutes les personnes que j'ai rencontrées pendant l'assistanat que ce soit à Louvain-la-Neuve ou à Woluwé. Tout d'abord les personnes qui mettent tout en place pour qu'on travaille dans les meilleures conditions : Bernadette, Ramazan, Catherine, Nadine, Anne, Edouard, Pascale, Corentin et Agnès. Je tiens également à remercier les différents professeurs pour lesquels j'ai pu travailler comme assistant : Michel Devillers, Tom Leyssens, Geoffroy Hautier, Alexandru Vlad, Michael Singleton, Yann Garcia et Mark Rider. Viennent finalement les autres assistants avec qui j'ai eu le plaisir de donner des séances ou simplement de côtoyer au cours de ces années : Nadia, Tommy, Antoine R., Quentin, Cédric, Jérôme, Martin, Simon C., Simon DK, Ricky, Antoine D., Mika, Madeleine, Marine, Chloé, Louise, Véronique, Guillaume, Axel, Gabriel, Géraldine, Alixandre, Sophie et Yara.

Une petite pensée au groupe de foot L@B avec qui j'ai joué de très nombreux matchs entre amis avec Justin, Louis, Tommy, Antonin, Ricky, Robin, Martin, Timur, Nath B., Fred, Benoit, Boris, François K., François P., Gilles, Jason, Julien, Simon DK, Audric et Alex.

Un grand merci à Sharon pour son amour et son soutien. Merci d'être toujours là pour moi, de me donner confiance en moi et d'égayer chaque jour qui passe.

Finalement, je tiens à remercier ma famille : mes parents qui ont tout fait pour me donner la chance de faire les études dont je rêvais et qui ont toujours été fiers de ce que je faisais ainsi que mon frère qui m'a toujours soutenu et qui a toujours cru en moi.

Table of Content

Contents

Contents

List of abbreviations

AC	Activated coal or activated carbon
AFEX	Ammonia fiber explosion
BC	Bamboo carbonized
BET	Brunauer-Emmett-Teller
CB	Carbon black
CNF	Carbon nanofibers
CNT	Carbon nanotubes
CVD	Chemical vapor deposition
DNA	Deoxyribonucleic acid
DP	Degree of polymerization
EDA	Ethylenediamine
EDX	Energy dispersive X-ray
G	Graphene
GHG	Greenhouse gases
GNP	Graphene nanoplatelets
HMF	Hydroxymethylfurfural
HPA	Heteropolyacid
HR-TEM	High resolution Transmission electron microscopy
ICP	Inductively coupled plasma
IL	Ionic liquid
LCC	Lignin-carbohydrate complexes
LHT	Low heat treated
LHT-OX	Low heat treated oxidized
MWCNT	Multi walled carbon nanotube
RGO	Reduced graphene oxide

SBA	Santa Barbara Amorphous
SHF	Separate hydrolysis and fermentation
SSF	Simultaneous saccharification and fermentation
STEM	Scanning transmission electron microscopy
SWCNT	Single walled carbon nanotube
TEM	Transmission electron microscopy
TOC	Total organic content
TPD	Temperature programmed desorption
XPS	X-ray photoelectron spectroscopy
XRD	X-ray crystallography

Chapter I

Introduction

I.1 General context: Energy and chemicals sources

Since the industrial revolution, the energy demand has increased tremendously with the fast population growth. If we look at the last 25 years, growth in energy demand is still increasing[1]. Fossil resources such as coal, natural gas and oil have been mainly used to meet the increasing energy and chemicals demand. Nowadays these fossil resources still contribute for about 80 % of the global energy demand (Figure I-1). The use of green energy as hydroelectricity or renewables sources is increasing but still represents a small part of the global energy consumption. In the current context, the costs of fossil resources tend to rise while stocks shrink, which is expected to lead to a major crisis[2].

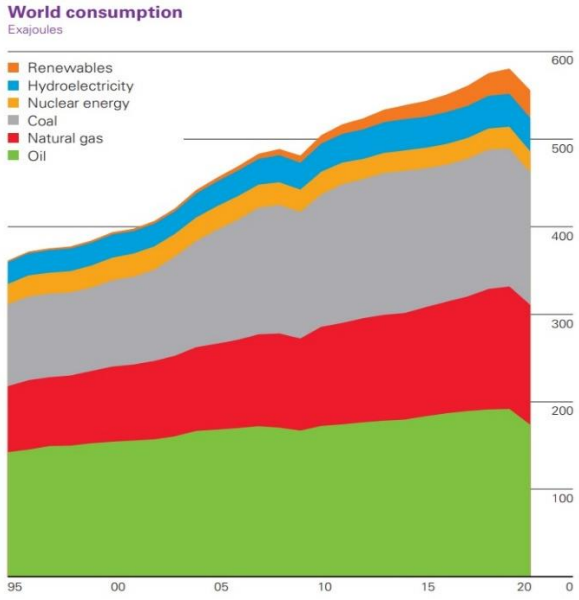

Figure I-1: World consumption of resources in exajoules since 1995 to 2020[3].

To avoid this scenario, alternatives resources have been studied. Biomass appears to be a promising solution to produce energy and chemicals as it is a renewable resource[4]. Moreover the utilization of biomass will limit the emission of greenhouse gases (GHG) such as CO_2. Biomass is using atmospheric CO_2 to grow and this CO_2 will be technically converted into fuels

and chemicals. This should lead to CO_2-neutral technologies[5]. However, separation and processing of the raw biomass to produce fuels and chemicals requires energy inputs and use of solvents or other reactants. Thus, CO_2 emissions must be taken into account for this energy and chemicals production. This is represented by the CO_2 emission that is not included in the loop (Figure I-2). Therefore CO_2 neutrality has not yet been reached and enhancing this type of process is one of the most important current challenge in order to replace fossil resources by biomass.

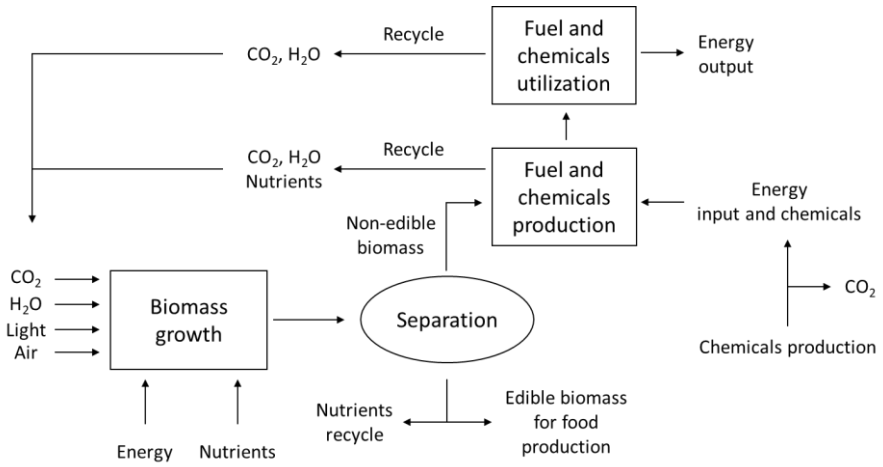

Figure I-2: Complete cycle from biomass growth to fuel production and utilization (adapted from[5])

I.2 Biomass classification

Biomass is classified in different generations depending on the origin of the feedstock used. The first generation is composed of food sources (corn, wheat, sugarcane, *etc*.). Ethical issues regarding their usage have been raised. Indeed, biofuels industries using first generation biomass will reduce the food availability and increase the price of these resources. It has been observed in the US, as the corn and wheat prices reached their highest point at the same time biofuels were produced[6]. Food security should not be threatened by the production of energies. This issue can be resolved by using

the second generation biomass, also known as lignocellulosic biomass which is non-edible. This biomass comes from by-products (sugarcane bagasse, wood residues, *etc*.), dedicated feedstocks (vegetative grasses grown on purpose, short rotation forests) and wastes (municipal cellulosic wastes)[7],[8]. Therefore this biomass will not compete with the food production and can be harvested without any ethical problem. It is composed mainly of cellulose (50-70 %), a polymer of glucose, hemi-cellulose (10-40 %), a polymer of pentoses and hexoses, and lignin (10-30 %), a polymer mainly composed of aromatics[4]. The exact proportion of each component depends on the type and origin of the feedstock[9]. Algae represents the third generation biomass. It is not in competition with food production or other crops and can be cultivated in shallow lagoons or closed ponds. Its production is easier and faster than conventional biomass and the oil yields obtained from it can exceed the ones from oilseed crops [10],[11],[12],[13]. The fourth generation biomass deviates from the others as it requires metabolic engineering of the algae. It is using DNA recombination and modifications of the algae properties in order to enhance biofuel production from it [14]. Table I-1 sums up the differences between each generation in terms of feedstock and processing technology to obtain biofuels or chemicals.

Table I-1: Biomass classification: feedstocks and process (adapted from [8])

Generation	Feedstocks	Processing technology
First	Edible sources: corn, wheat, sugarcane, animal fats	Esterification of oils; fermentation of sugars
Second	Lignocellulosic biomass: sugarcane bagasse, cereal straw, forest residues	Physico-chemical pretreatment and fermentation; catalytic and/or enzymatic transformation
Third	Algae	Algae harvesting and fermentation; oil extraction; thermochemical process
Fourth	Bio-engineered algae	Enhancement of algae properties by metabolic engineering; harvesting and fermentation; oil extraction; thermochemical process

I.3 Lignocellulosic biomass: Structure and pretreatments

As said above, lignocellulosic biomass is composed of cellulose, hemi-cellulose and lignin. Cellulose is a linear polysaccharide of glucose with a β-1,4 glycosidic bound between each unit and possesses high polymerization degree (over 10000)[15]. The structure of cellulose allows the formation of a lot of intra- and intermolecular hydrogen bonds that make it crystalline (Scheme I-1). Therefore cellulose polymers chains will stack on top of each other and form microfibrils. Several allomorphs of cellulose exist (cellulose type I, II, III and IV) depending on its crystallographic structure. Chemical and heat treatment can change the native cellulose (type I) into other types [16],[17].

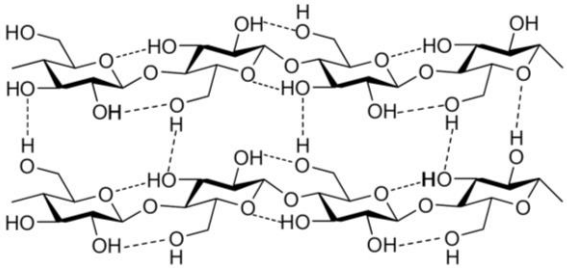

Scheme I-1: Representation of the cellulose structure (adapted from [18])

Hemi-cellulose is a heterogeneous branched polysaccharide composed of mainly pentoses (xylose and arabinose), hexoses (glucose, mannose, galactose) and sugar acids (glucuronic acid)[19]. Its composition varies depending on the type of biomass. Unlike cellulose, it is not crystalline and its polymerization degree is lower (around 200)[20]. Hemi-cellulose will form hydrogen bonds with cellulose and covalent bonds with lignin to create what is called lignin-carbohydrate complexes (LCC)[21].

Lignin is a polyphenolic polymer composed of three main units: *p*-coumaryl, coniferyl and sinapyl alcohols (Scheme I-2). The ratio between

these three units is varying depending on the type of biomass[22]. Lignin is hydrophobic and will give impermeability and protection to the plant.

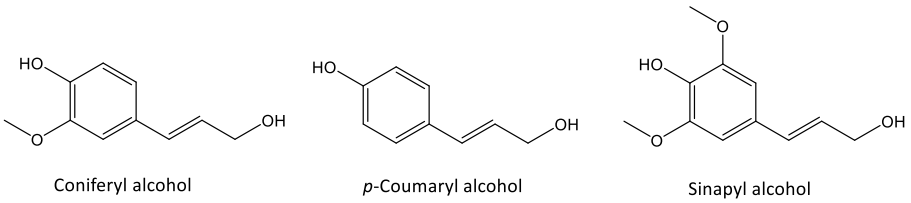

Scheme I-2: Representation of coniferyl alcohol, *p*-coumaryl alcohol and sinapyl alcohol

In most cases, microfibrils of cellulose are embedded in a matrix of hemi-cellulose and/or lignin. These microfibrils will arrange themselves into bundles or macrofibrils[23]. It is the combination of cellulose, hemi-cellulose and lignin that gives its high robustness to the plants (Figure I-3). Therefore the lignocellulosic biomass is very resistant to biological or chemical treatment. Lignocellulose is meant to give rigidity and strength to the plants, which means that its constituents are by essence resistant and cannot be easily transformed into other compounds. Therefore, producing biofuel and chemicals from it is highly challenging.

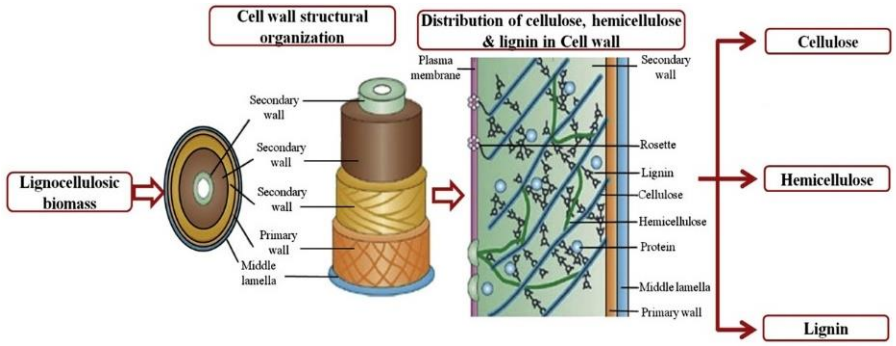

Figure I-3: Illustration of the lignocelullosic biomass framework (adapted from [23])

In order to valorize the lignocellulosic biomass, separation of the three components from each other is primordial to transform them individually into chemicals and fuels. Pretreatments of many types have been

imagined to break lignocellulosic biomass and making cellulose, hemi-cellulose and lignin more disposed to be transformed. As cellulose is the biomass part we are interested in in this work, we will focus on the impact of the pretreatments on the cellulose component.

Two main factors define the cellulose reactivity: its accessibility and its purity. Cellulose accessibility can be separated into micro-accessibility and macro-accessibility. Micro-accessibility refers to the accessibility of the inner structure of the cellulose like the β-1,4 glycosidic bonds. Macro-accessibility refers to the accessibility of the cellulose outer surface[24].

Micro-accessibility depends on two major factors: cellulose crystallinity and degree of polymerization. As said above, cellulose polymers are held together thanks to inter and intra-molecular hydrogen bonds, but also van der Waals forces or hydrophobic interactions. These arrangements will form crystals and reduce the accessibility and reactivity of the cellulose chains[25]. On the contrary, amorphous cellulose will be more easily transformed. It is important to mention that recrystallization of amorphous cellulose can occur in water due to high surface tension and the possibility of making hydrogen bonds[26]. Degree of polymerization (DP) is the average amount of β-1,4 linked anhydroglucose units. It is the key factor for the cellulose solubility. Indeed cellulose oligomers with DP of 2-6 are soluble in water while cellulose oligomers with DP of 7-13 are moderately soluble in hot water. When the DP is over 30, cellulose oligomers will have high similarity with 'bulk' cellulose and will be insoluble in water[27]. Obviously, solubility of the cellulose will enhance its reactivity. That is why pretreatments of cellulose that is decreasing both crystallinity and DP will help cellulose to be more reactive.

Macro-accessibility depends on external specific surface area which is determined by particle size, shape, and surface texture. In general, small

particles will display higher specific surface area which increases their reactivity[28]. Moreover the center of small particles will be more easily accessible to solvents and catalysts. Therefore reduction of the particle size by pretreatments will increase the cellulose reactivity[29]. Macro-accessibility of cellulose is dramatically decreased by the presence of a protective matrix composed of hemi-cellulose and lignin. These impurities will cause physical hindrance that will lower the cellulose reactivity. Moreover they can neutralize the catalysts. For example wood can neutralize mineral acid catalysts by ion-exchange between the inorganic cation in the wood and the protons in the reaction mixture[30]. This neutralization ability depends on the nature of the feedstock. Catalysts can also be inhibited by the impurities, as cellulases can be poisoned by lignin derivatives[31].

In summary, increasing the cellulose purity and the macro-accessibility while decreasing the degree of polymerization and the crystallinity of cellulose can boost the cellulose valorization in chemicals and fuels. Pretreatments will have a key role in the industrial processes of biomass valorization. Therefore it is a widely studied topic and several pretreatments processes will be developed in the following sections.

I.3.1 Physical milling

The main purpose of milling is to reduce the particle size, the degree of polymerization and the crystallinity of the lignocellulose in order to enhance its reactivity. There are several milling pretreatments possibilities: ball, two-roll, knife, hammer, vibro energy and freeze-milling[32]. Ball-milling is the most common pretreatment in research before carrying out catalytic or enzymatic reactions[33]. The improvement of cellulose reactivity with these types of pretreatments is considerable. However, the main drawback of milling is the huge energy consumption. Because of that its application to

industrial process is very limited. To overcome that problem, wet milling has been investigated as a less energy-consuming method. Unfortunately, the performances of wet milling have not yet reached the ones of dry milling[34].

Improvement of ball-milling with the addition of acids has been tried. Ball-milling of microcrystalline cellulose after impregnation with mineral acids decreases drastically its degree of polymerization. Cellulose powder obtained after that treatment is even soluble in water[35]. This pretreated cellulose can react more easily with catalysts to produce chemicals[36].

Reactions between solid cellulose and solid catalysts have been usually restricted by the weak interactions by collision between the two. Mix ball-milling of both cellulose and catalyst together has been studied to improve the interactions between both solids and increase their reactivity. Higher rate constant for cellulose conversion has been observed when implementing the mix ball-milling[37].

Physical milling and especially ball-milling is improving the reactivity of cellulose. The use of mineral acids or the mix ball-milling are interesting new concepts that can further enhance the cellulose reactivity. However this pretreatment technique remains costly. Moreover milling is limited to the activation of microcrystalline cellulose. Indeed milled lignocellulosic biomass can less easily be valorized because of the presence of the other components. Physical milling of lignocellulose must be combined with another method of pretreatment to purify cellulose.

I.3.2 Irradiation

There are several possible irradiation pretreatments that can be considered: microwave, ultrasound, electron beam and gamma ray. They can be applied either alone or combined with other pretreatment methods.

Microwaves are radio waves with frequencies between 300 MHz and 300 GHz. When these interact with organic matter, they are absorbed and their energy is transferred to organic molecules generating huge amounts of heat. Therefore this pretreatment method relies on the *in situ* generation of heat within the lignocellulosic substrate and reaction media. This method can generate higher reaction rates compared to common heating from external sources. It also leads to high lignin removal and increased sugar yields[38].

Although microwave irradiation has many advantages, the main drawbacks are the energy consumption and the cost of this method compared to conventional energy sources. Moreover for large-scale pretreatments of biomass, a large microwave irradiator is required, which is very costly and limits its use in large-scale operations[39]. Another disadvantage is the generation of high temperature and non-uniform heating of the biomass which leads to the formation of inhibitors that can lower yields[40].

Gamma rays and electron beams are ionizing radiations. It means that they will ionize atoms by removing electrons which will induce chemical changes. These two methods are reported to depolymerize and decompose lignocellulosic biomass[41]. Increase of the enzymatic digestibility of cellulose after irradiation with gamma rays has been shown[42].

Ultrasound irradiation is based on the creation of pressure differences within the reaction media (cavitation bubbles) and can cause erosion, cell wall collapse and enhancement of mass transfer which is improving the accessibility to lignocellulosic biomass[43]. It is also reported as a good method for delignification of the biomass[44].

I.3.3 Steam explosion

Steam explosion is a method where biomass is first treated with high pressure saturated steam. The pressure is then released quickly to atmospheric pressure which creates explosive decompression within the biomass structure. This method is usually initiated at a temperature between 160 °C and 260 °C and a corresponding pressure between 20 bar and 50 bar for several seconds to a few minutes[45]. During the process, hemi-cellulose is hydrolyzed by acetic acid coming from the hydrolysis of acetyl groups associated with it. Lignin is also decomposed due to the high temperature applied during the pretreatment. These two effects are making the cellulose more accessible and an increase of the catalytic/enzymatic activity has been shown after this type of process[46].

Addition of H_2SO_4 or CO_2 can improve the hydrolysis and remove completely the hemi-cellulose, using lower temperature and shorter process time. However, this can lead to the formation of degradation products that will inhibit enzymatic hydrolysis and fermentation. Therefore, the pretreated biomass needs to be washed with water to remove these side-products. This washing step will also decrease the global saccharification yield by removing all the soluble sugars produced during the process[47].

The main advantage of this pretreatment technique is the low energy requirement compared to other processes which implies lower cost. It is making this method one of the most adapted to industrial applications[25].

I.3.4 Ammonia fiber explosion (AFEX)

Ammonia fiber explosion (AFEX) is based on the same concept than steam explosion, except that liquid ammonia is used instead of steam. The process is using high pressure (15-20 bar) and moderate temperature (60-120 °C) for several minutes (under 30 minutes) and is followed by a

sudden pressure release[48]. Four parameters can be adjusted: ammonia loading, water loading, residence time and temperature. The optimization of these conditions can vary in function of the type of biomass that is pretreated. Ammonia gas quick expansion will cause huge physical disruption within the biomass structure and will lead to increased digestibility and accessibility[49].

The advantage of AFEX compared to steam explosion is that, because of the low boiling point of the ammonia, only solid materials are produced during the pretreatment. No mass loss is observed during the process. However, AFEX process is not altering the cellulose crystallinity because of the high concentration of water in the employed ammonia that will prevent the ammonia from entering within the cellulose structure[50].

AFEX is a promising method to activate biomass and especially cellulose for further chemical processing. The higher cost of ammonia and the environmental issues caused by its disposal are forcing the application of an efficient recovery and recycling of ammonia to be sustainable in an industrial application[51].

I.3.5 Acid pretreatment

Acid pretreatment is the most common method employed in the industry for transforming the lignocellulosic biomass. Sulfite pulping was already conducted in the 19th century to remove lignin by cleaving and sulfonating it to water-soluble products[52]. Nowadays acid pretreatment is using mainly HCl and H_2SO_4 but a lot a different acids have been tried out such as HF, HNO_3, H_3PO_4 and organic acids[53].

Depending on the severity of the pretreatment, we can have either the removal of hemi-cellulose or the hydrolysis of both cellulose and hemi-cellulose into monomers. Two main conditions are utilized: low acid

concentration with high temperature or high acid concentration with low temperature[54]. The use of concentrated acids with low temperature is more interesting because of the economic cost of high temperatures. However, concentrated acids will provoke degradation of the installation because of their corrosiveness. Recovery and disposal of the acids is also a major problem. Concentrated acids are giving a lot of lignocellulosic degradation products such as furfural and HMF that are well known inhibitors for microorganisms. Diluted acids are giving less degradation products but are less effective for hemi-cellulose solubilization. However higher temperatures and longer retention time can be applied to increase their activity[55].

Acid pretreatment of biomass can also be performed in alcohol media instead of water. The alcohol media will lead to alkylglucosides, xylosides and alkyl levulinate as products. Increase of reaction rate and yields have been observed as well as less production of inhibitors. For example, production of alkyl levulinates in alcohol from the cellulose has given higher yields than the production of levulinic acid in water. Brønsted acid sites are promoting the formation of alkyl levulinates, while Lewis acid sites are leading to levulinic acids in water[56].

Utilization of bifunctional catalysts is another approach to avoid unwanted products during the treatment. Hydrolytic hydrogenation will immediately hydrogenate the produced monomeric sugars to more stable sugar alcohols (especially sorbitol)[57]. Further acid-catalyzed dehydration of sugar alcohols can produce polyols such as sorbitan and isosorbide[58]. Sugar alcohols and their dehydration products are useful to produce fuels, chemicals and polymers[59].

I.3.6 Alkaline pretreatment

Alkaline pretreatment is employed since the 1940s, especially the Kraft pulping process that is providing high-quality cellulose fibers from wood by using NaOH and Na_2S for delignification[52]. This process is mainly used in the paper industry to produce wood pulp, which is the main component of paper, from sawdust and wood chips. Alkaline processes are efficient to remove lignin through the cleavage of lignin ether bonds and can solubilize hemi-cellulose by the saponification of intermolecular ester bonds between hemi-cellulose and lignin. Cellulose is more resistant to alkaline pretreatment than hemi-cellulose. However, depolymerization of cellulose can occur. Therefore, alkaline pretreatment is very useful to increase the cellulose accessibility and reactivity[45],[60].

NaOH, KOH, $Ca(OH)_2$ and ammonia are the most common bases used for alkaline pretreatment. Compared to the acid pretreatment, alkaline process is working at lower temperature but with higher residence time[61]. The major drawback is the need for neutralization of the slurry that has been formed[62].

Combination of two bases together has been studied to increase process performance. For example, NaOH and $Ca(OH)_2$ have been used for pretreatment of switchgrass at ambient condition[63]. Addition of an oxidant agent such as O_2 or H_2O_2 can improve the performances of the pretreatment by enhancing the lignin removal[64].

I.3.7 Oxidative pretreatment

Oxidizing agents such as H_2O_2, O_2, air, peracids and hypochlorite can be used for enhancing the cellulose accessibility by removing lignin from the biomass[65],[66]. H_2O_2 and O_2 are reacting as free radicals in alkaline solutions and are improving this type of treatment[67].

Ozone is also utilized as oxidative agent in what is called ozonolysis pretreatment. This method is degrading lignin and a part of hemi-cellulose. It is usually conducted at room temperature and avoids the formation of inhibitory compounds that would impede downstream processes like enzymatic hydrolysis or fermentation[68]. Huge quantities of ozone are required for this process and that makes it an expensive method[45].

Wet oxidation is a pretreatment that is using oxygen or air in aqueous media. The biomass is treated at temperatures between 150 °C and 200 °C and 10 to 20 bar of O_2 or air for short periods of time (below 30 minutes). At these temperatures, the process is exothermic and becomes self-supporting in term of energy as the reaction is proceeding[69]. Therefore, a careful control of the temperature during the pretreatment is needed to avoid too high temperatures. Hydrolytic processes and oxidative reactions are happening during the wet oxidation and are leading to the formation of acids. These acids are participating in the biomass treatment. All three parts of lignocellulosic biomass are affected. Lignin is cleaved and oxidated, while hemi-cellulose is depolymerized into monomers. Cellulose is partially degraded and becomes more accessible with an enhanced reactivity[70].

I.3.8 Organosolv fractionation

Organosolv pretreatment is based on the degradation and solubilization of hemi-cellulose and lignin in aqueous or non-aqueous solvents. This process is improving the cellulose purity as well as its accessibility and reactivity[71]. Several organic solvents have been investigated: alcohols, esters, glycols, ketones, organic acids, esters and phenols[72]. The process can be carried out auto-catalytically at high temperature (between 185-210 °C) or with the addition of a catalyst, usually acids catalysts such as HCl, H_2SO_4 or oxalic acid[73].

Organosolv process has been studied for paper manufacturing where high cellulose purity, high fiber strength and high crystallinity are required. It also has been investigated as a pretreatment prior to enzymatic hydrolysis for which a high cellulose reactivity is needed[74]. Organosolv process is interesting for its fractionation ability. Indeed, at the end of the process, three separate, high quality streams can be obtained: a solid pulp enriched in cellulose, a high purity lignin precipitate and an aqueous mixture of hemi-cellulose products and extractive products (minerals and proteins)[71]. This process is very useful to further valorize lignin for a wide variety of applications[75]. The precipitated lignin can be redissolved in an adequate solvent and valorized.

The main drawbacks of this method are the low boiling point of organic solvents as well as their flammability and volatility. Moreover, the use of such organic solvents can be costly and it has been established that organic solvents can have inhibitory effects on enzymatic hydrolysis and microorganisms. That is why the removal of organic solvents is important and the recyclability of these solvents is even better to decrease the operation cost[76],[45].

I.3.9 Cellulose solvents

Cellulose low solubility in water is caused by both hydrogen bonding and hydrophobic interactions within cellulose structure. Other solvents that could overcome these interactions and solubilize cellulose have been investigated. These solvents can be divided in two categories: non-derivatizing and derivatizing solvents[77]. Non-derivatizing solvents will apply a physical dissolution of the cellulose by intermolecular interactions. These solvents include inorganic complexes (copper (II) ethylenediamine), molten salt hydrates ($ZnCl_2.4H_2O$), DMSO-based solvents, tertiary amine

oxide and ionic liquids[78],[79]. On the other hand, derivatizing solvents will alter cellulose by the formation of unstable ether, ester or acetal derivatives. They include trifluoroacetic acid, formic acid and DMF/N_2O_4[78].

Ionic liquids in particular are very interesting as solvents to dissolve cellulose. Ionic liquids are organic salts composed generally of large organic cations and small inorganic anions. Hydrogen bonds can be formed between the ions of the ionic liquids and the protons of hydroxyl groups in the cellulose. These interactions lead to the disruption of the internal network in the lignocellulose[55]. During the process with ionic liquids, cellulose is usually recovered, after its dissolution, through precipitation by the addition of solvent such as water or alcohol[80]. Cellulose obtained by this way displays a decreased or modified crystallinity (sometimes cellulose of type II is formed), which is making it more accessible and more reactive to further treatments[81]

The main drawbacks of the ionic liquids pretreatment is the very high cost of ionic liquids and their ability of deactivate catalysts and enzymes in downstream processes[82]. Their recovery and recyclability are therefore needed to be applicable at industrial level. Studies are very intensive in this subject and a concept where ionic liquids are synthesized from lignin and hemi-cellulose has been imagined. This could lead to a closed loop biorefinery process[83].

I.3.10 Biological pretreatment

Biological pretreatment is using microorganisms, mainly white, brown and soft-rot fungi, to convert lignocellulosic biomass into more accessible compounds for hydrolysis and subsequent transformation[84]. These microorganisms produce a battery of enzymes with different specificities (cellulolytic enzymes or cellulases) that act together with

synergy[85]. White-rot fungi appears to be the most effective to remove lignin from the biomass. Parameters such as particle size, moisture content, pretreatment time and temperature can affect the efficiency of the biomass degradation and hydrolysis yield[86].

This type of process is not costly in comparison with other pretreatments. It takes advantage of the enzymes of the fungi to delignify and enhance lignocellulosic biomass reactivity[87]. Moreover this pretreatment does not require chemicals and high amount of energy. However main drawbacks of this method are long process time, large space requirement and the need to monitor microorganisms growth during the process. These disadvantages are limiting the use of biological pretreatment as a commercial method[88].

Another way to perform biological conversion of cellulose is to use isolated cellulosic enzymes such as cellulases[89]. However, microcrystalline cellulose is resistant to enzymatic hydrolysis. Therefore, increasing efficiency, stability and recovery of these enzymes is crucial, as well as eliminating inhibitors such as cellobiose (simplest glucose oligomer, composed of two glucose units). However, the production and purifications of such enzymes are very costly[85].

Finally, fermentation of the products coming from cellulose hydrolysis is an interesting possibility to produce fuels, especially ethanol. Microorganisms such as *S. cerevisiae*, *Zymomonas mobilis*, and *Kluyveromyces marxianus* can be used for the fermentation. In most processes, cellulose hydrolysis is performed prior to the fermentation step. It is called the SHF (separate hydrolysis and fermentation) process[90]. It allows to perform both steps in optimal conditions. Once the hydrolysis has been performed, the medium is centrifugated (non-hydrolyzed solid is discarded) and the fermentative microorganism is inoculated to the liquid

medium. The main drawback of this method is the partial inhibition of enzymes during the hydrolysis because of the accumulation of glucose and cellobiose. To overcome this problem, SSF (simultaneous saccharification and fermentation) process has been imagined. Cellulases and microorganisms are inoculated in the medium at the same time. The glucose produced by the cellulose hydrolysis will be directly used by the yeast, preventing the inhibition of the enzymes[91]. Several studies have shown better results with the SSF process compared with the SHF process[92].

I.3.11 Lignin first biorefinery

Several pretreatments have shown excellent abilities to remove lignin from the lignocellulosic biomass, which can then be valorized separately into chemicals and fuels. Since a few years, a new method to achieve both delignification and valorization of the lignin has been developed and is called lignin first biorefinery. In this method, the lignin from the lignocellulosic biomass is depolymerized to high yield of monomers and oligomers by chemocatalytic processes while the cellulose and hemi-cellulose are left as a solid. Hemi-cellulose can be solubilized more easily than cellulose and its presence in the solid pulp is depending on the conditions of the treatment. This pretreatment can overcome the usual problems encountered with the isolated lignin valorization which are lignin recondensation and degradation during the pretreatment[93]. Therefore the cellulose obtained after this pretreatment will display higher purity than with other methods and would be valorized more easily.

Reductive catalytic fractionation, which is the most promising method, is using hydrogenation and hydrogenolysis with catalysts to depolymerize lignin and stabilize reactive intermediates to prevent degradation[94]. Removal of the lignin with good yield in monomers by this

method has been demonstrated[95]. The remaining cellulose and hemi-cellulose can be further valorized. Indeed by removing the lignin, the cellulose reactivity and accessibility are increased.

Other processes have been investigated to valorize the lignin. One of them is the oxidative catalytic fractionation which is carried out under milder conditions than the reductive fractionation and is based on lignin oxidation in aldehydes[96]. Photocatalysis has also been considered to remove lignin and transform it into ketones[97].

I.3.12 Summary of pretreatment methods

A wide variety of pretreatment methods have been described in the previous sections. A table that sums up all the techniques with their advantages/drawbacks is displayed below (Table I-2). All these techniques will impact differently the lignocellulosic biomass, with consequences for further uses. Moreover, the effect of each pretreatment can vary depending on the biomass source. The choice of the pretreatment will depend on the intended downstream valorization. If cellulose is the main target, pretreatments that remove hemi-cellulose and lignin will be preferred, such as AFEX or oxidative treatment. However, if lignin valorization is the main purpose, lignin first biorefinery or organosolv fractionation will be chosen.

Lignocellulosic biomass pretreatments are still widely studied and no perfect industrial process exists for now. Almost all pretreatment methods are costly and difficult to apply at industrial level. However, methods such as physical milling or irradiation can be used in research labs for more fundamental studies.

Table I-2: Comparison between several pretreatment methods for lignocellulosic biomass

Pretreatment	Sugar yield	Equipment cost	Advantages	Drawbacks	Ref.
Physical milling	Low	High	Decreases cellulose crystallinity and DP	High energy consumption; no hemi-cellulose or lignin removal	[32]
Irradiation	High	High	High lignin removal; increase of enzymatic digestibility	Batch process; enzyme's inhibitors production	[39]
Steam explosion	High	Moderate	Hemi-cellulose hydrolysis; alteration in lignin structure	Incomplete destruction of LCC	[45]
AFEX	High	High	Hemi-cellulose and lignin removal; no mass loss	Low efficiency for high lignin content biomass	[50]
Acid treatment	High	Moderate	Hydrolysis of cellulose and hemi-cellulose; alteration in lignin structure	Installation corrosion; waste disposal; enzyme's inhibitors formation	[54]
Alkaline treatment	High	Low	Hemi-cellulose and lignin removal	Long residence time; slurry neutralization	[63]
Oxidative treatment	Moderate	High	Lignin removal; hemi-cellulose dissolution; decrease of cellulose crystallinity	Utilization of large amount of ozone or oxidants	[70]
Organosolv fractionation	High	High	Hydrolysis of hemi-cellulose and lignin	Recovery and recycling of solvents	[76]
Cellulose solvents	Moderate	High	Cellulose dissolution; increase of cellulose accessibility	Recovery of solvents or ionic liquids; alteration of cellulose	[83]
Biological treatment	High	High	Lignin removal; decrease of cellulose crystallinity	Large space requirement; low hydrolysis rate; need to be monitored	[90]
Lignin first biorefinery	Low	High	Lignin removal and valorization	Catalyst recovery; down-stream product purification	[93]

[1] DP = Degree of polymerization; LCC = lignin-carbohydrate complexes; AFEX = ammonia fiber explosion

I.4 Cellulose valorization into high-value products by heterogeneous catalysts

Once it has been isolated from the lignocellulosic biomass, cellulose can be valorized into interesting chemicals. The most important molecule that can be obtained from cellulose is glucose, the monomer. Glucose is a chemical platform that can lead to the formation of 5-hydroxymethylfurfural, gluconic acid, sorbitol, adipic acid (monomer for nylon production)[98] and many other interesting chemicals[99] (Scheme I-3).

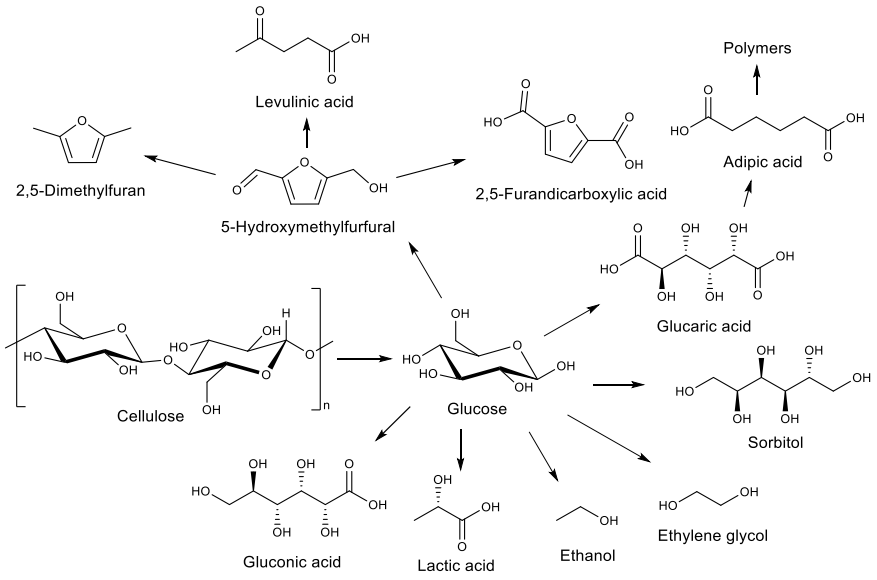

Scheme I-3: Glucose as a chemical platform

Therefore cellulose hydrolysis is an intensively investigated topic since many years. Hydrolysis processes to produce biofuel from cellulose were already studied since the 1920s. These were using dilute H_2SO_4, concentrated HCl or HF solutions to perform the hydrolysis. These processes have not been enough cost-effective to be applied in industries and have been eclipsed by the emergence of the cracking method in petroleum refining to produce fuels. Drawbacks such as the acid recovery, corrosion of the reactors, neutralization of the acid and chemical waste disposal are

making these technologies not very suitable for industrial applications[100]. That is why new methods for hydrolyzing the cellulose into glucose have been studied in recent years.

The pretreatment methods explained in the previous section that are hydrolyzing or solubilizing the cellulose can be applied as well on cellulose alone. For example, ionic liquids are thoroughly studied as solvents and catalysts for the hydrolysis reaction[101].

Enzymatic catalysis is one of the most promising alternative as explained in the previous section. However, even if it is performed on cellulose alone, the main drawback of this method is that glucose and cellobiose are inhibitors for cellulases[102].

Since homogeneous catalysis is accompanied by the drawbacks of reactor corrosion and waste disposal, heterogeneous catalysis has become a huge field of interest to overcome these problems. Numerous heterogenous catalysts for cellulose depolymerization have been developed such as metallic oxides, zeolites, acidic resins, functionalized silica and functionalized carbon materials. These will be detailed in the next sections.

I.4.1 Metal oxides

Metal oxides are composed of cations displaying Lewis acid sites and anions with Brønsted base sites. Two classes are existing: single metal oxides and mixed metal oxides. Metal oxides have activity in the hydrolysis of cellulose and can be used as solid acid catalysts. These solids contain mesopores which allow the reactants to access the active acid sites within the pores. Metal oxides such as Nb_2O_5, WO_3, TiO_2 and Ta_2O_5-WO_3 have been studied as heterogeneous acid catalysts[103–105]. However the catalytic activity reached by these metal oxides is not striking, therefore mixed metal oxides such as $HNbMoO_6$ have been studied[106]. This is a layered transition-metal

oxide, composed of several layers which allow a higher acidity, water-tolerance and an easy intercalation of saccharides in the strongly acidic interlayer galleries of the catalyst. Catalytic activity for cellobiose and starch hydrolysis by $HNbMoO_6$ has outperformed well-known acidic solids such as Amberlyst-15 and Nafion NR50. However, cellulose hydrolysis has only given low amount of glucose. Cellobiose has been preferentially produced probably because of the difference of intercalation behavior between glucose and cellobiose. This lack of performance can be attributed to the fact that protons of the solid acid sites are not easily accessible to the glycosidic linkage of the substrate.

Mixed metal oxides such as nanostructured Zn-Ca-Fe oxides have displayed good activity for hydrolyzing crystalline cellulose. Nanoscale diameter of the Zn-Ca-Fe oxide particles suspension can provide high amount of active sites per gram and has some characteristics similar to fluid solutions[107]. Moreover the presence of Fe is making the catalyst separable by magnetic filtration methods.

Mesoporous metal oxides with their high specific area, adjustable pore sizes and their enhanced thermal stability are also very interesting as catalysts for cellulose hydrolysis and will become an important research field in the future[108].

I.4.2 Ion-exchange resins

Ion-exchange resins are reticulated polymeric structure displaying high acidity. They have been used since many years as solid acid catalysts in organic reactions such as esterification, alkylation or condensation reactions[109,110]. In the 1960s they have been studied for cellulose hydrolysis but have displayed poor activity and degradation during the reaction[111]. More recently, acidic resins have been enhanced and the NKC-9 resin has

produced a yield of 26.9 % of glucose from cellulose hydrolysis (heated under microwave irradiation at 240 W during 3 minutes)[112].

One of the most well-known acidic resins is the Amberlyst-15. It is a macroreticulated styrene-divinylbenzene resin which is functionalized with sulfonic groups. Alone, Amberlyst-15 resin has difficulties to depolymerize cellulose but when it is combined with ionic liquids, the depolymerization is very effective. Ionic liquids solubilize cellulose and make it more accessible for the resin to perform its hydrolysis activity[113].

However, resins in general have poor hydrothermal stability and begin to degrade at around 120 °C. In order to overcome this issue, Nafion NR50 resin has been synthesized with higher hydrothermal stability. Nafion NR50 resin displays acidity similar to Amberlyst-15 but can be utilized at higher temperature. In combination with ionic liquids, a glucose yield of 35 % has been obtained from cellulose (at 160 °C during 4 h)[114].

I.4.3 Zeolites

Zeolites are microporous aluminosilicate minerals widely used as catalysts. In the zeolite structure, silicon is tetracoordinated while aluminum is tricoordinated. Therefore a cation is needed to maintain the electroneutrality. When this cation is a proton, the zeolite is called H-form zeolite and it displays Brønsted acidity. The number of Brønsted acid sites depends on the Al/Si atomic ratio; high ratios are giving high acidity[115]. Zeolites have shape-selective properties due to their micropores and can be extensively tunable to adjust acidic and textural properties. All these characteristics combined with their hydrothermal stability make them good candidates as catalysts for biomass valorization.

The main drawback of the zeolites for cellulose hydrolysis are their micropores. Indeed cellulose has large particle sizes and difficulties to

disperse into the inner core of the zeolites. For example no depolymerization of cellulose has been noticed using H-ZSM-5 or zeolite Y as catalysts[113]. Therefore combination of zeolites catalysts with pretreatment of cellulose is required to increase the activity. Ionic liquids or microwave assistance can depolymerize the cellulose and allow it to access the active sites of the zeolites[116,117].

Another way to improve the zeolites activity is to modify their properties. Increasing the pore size of the zeolites would enhance their activity. Mesoporous zeolites have been studied for hemi-cellulose hydrolysis and have shown promising results[118].

Loading of superacids on the zeolites would overcome the poor activity of the zeolites alone for cellulose hydrolysis. Heteropoly acids (HPA) for example can be incorporated into the zeolites by direct impregnation of the zeolite with an HPA solution as it has been done for SBA-15[119]. However the HPA will mostly go inside the zeolite and will not be accessible for the catalysis. Mixing HPA during zeolites synthesis can give a strong acid catalyst. HPA intrinsic acidity is maintained and HPA are also stabilized, reducing their leaching during the catalytic tests. With this preparation method, HPA will be localized both at the surface and inside the zeolite support as it has been shown for SBA-15[119]. Such bifunctional catalysts, prepared on SBA-15, have been tested on the hydroisomerization of *n*-decane into smaller alkanes but could be applied for the cellulose hydrolysis. Similar catalyst with zeolite can be imagined, where surface HPA catalysts could hydrolyze the cellulose into oligosaccharides and these oligomers could go inside the zeolites porosity and be further hydrolyzed into glucose[120].

I.4.4 Functionalized carbons

Carbon materials are usually synthesized by calcination of natural organic matter such as raw vegetable waste mainly (coconut shells, rise husks or fruit cores)[121] but also carbohydrates, starch, cellulose, glucose, *etc*.[122]. Sulfonic functions can be added onto the carbon materials to increase their acidity. Sulfonation of the carbon materials is usually achieved by using concentrated sulfuric acid[123], fuming sulfuric acid[124] or chlorosulfonic acid[125].

Acidic carbon materials have a tremendous potential for conversion of cellulose into glucose. Carbon materials usually possess phenolic functions (-OH) and carboxylic functions (-COOH) at their surface. These functions will manage to adsorb cellulose at the carbon surface and will increase the proximity between cellulose and the sulfonic functions. The activation energy of the reaction will therefore decrease and the global activity will be boosted[124]. Higher production of glucose and glucose oligomers from microcrystalline cellulose have been reported with sulfonated carbon materials in comparison with homogeneous sulfuric acid (at 100 °C during 3 h)[126]. These results bring out the outperformance of the acidic carbon materials in comparison with homogeneous acidic catalysts like H_2SO_4 concentrated solutions.

One of the main drawbacks of heterogenous catalysts in the conversion of cellulose is their recyclability. At the end of the reaction, separating the catalysts from the unreacted cellulose is tough. Introducing paramagnetic nanoparticles, such as Fe_3O_4, in the carbon materials seems to be an option. The catalyst would be separable by using a magnetic field. Such studies have already been carried out on functionalized silica (SBA)[127] and could be tried out on carbon materials.

Preparation of acidic carbon materials generates huge amount of waste and uses dangerous chemicals that are corrosive for the installations. Other methods of synthesis must be investigated to be more respectful of the environment and safer. For example, sucralose and *p*-toluenesulfonic acid have been used to directly synthesize an acidic carbon material, avoiding functionalization with sulfuric acid[128]. Moreover this synthesis is bringing chloride functions (-Cl) to the carbon surface that are helping to adsorb cellulose. A method developed by Bitter *et al.* is using an *in situ* diazonium coupling procedure to functionalize carbon materials with aryl sulfonic acid functions (Scheme I-4)[129]. The reaction is made by mixing sulfanilic acid and isoamyl nitrite at 30 °C. This catalyst synthesis is carried out under mild conditions and is avoiding potential hazards (sulfuric acids or unstable pre-formed diazonium salts).

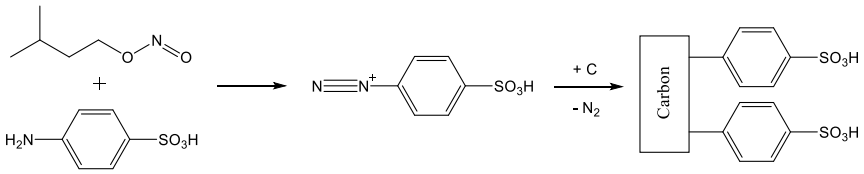

Scheme I-4: Functionalization of carbon materials with sulfonic functions (adapted from[129])

I.4.5 Summary

In the previous sections, many heterogenous catalysts have been presented for cellulose valorization. A summary of each catalyst with their composition and their activity can be found in Table I-3.

Table I-3: Comparison between several heterogeneous catalysts used for the hydrolysis of cellulose/cellobiose/starch

Catalyst	Hydrolysis conditions	Substrate	Yields	Ref.
$HNbMoO_6$ (mixed metal oxides)	100 °C, 200 mg of catalyst, 15 h	Starch (0.1 g)	Glucose = 21 %	[106]
Zn-Ca-Fe oxides	160 °C, 900 mg of catalyst, 20 h	Microcrystalline cellulose (2 g)	Glucose = 29 %	[107]
NKC-9 (sulfonated resin)	Microwave (240 W), 10 mg of catalyst, 3 min	Cellulose (0.1 g)	Glucose = 27 %	[112]
Amberlyst-15	150 °C, 25 mg of catalyst, 2 h	Cellobiose (0.3 g)	Glucose = 60 %	[130]
Nafion NR50 (sulfonated resin)	160 °C, 100 mg of catalyst, 4 h, ionic liquid	Microcrystalline cellulose (0.2 g)	Glucose = 35 %	[114]
H-ZSM-5 zeolite	150 °C, 50 mg of catalyst, 24 h	Milled cellulose (0.045 g)	Glucose = 12 %	[131]
AC-SO_3H (activated carbon sulfonated by H_2SO_4)	150 °C, 50 mg of catalyst, 24 h	Milled cellulose (0.045 g)	Glucose = 40 %	[131]
Sulfonated carbon-based solid	100 °C, 300 mg of catalyst, 3 h	Microcrystalline cellulose (0.025 g)	Glucose = 2 % Cellobiose = 15 %	[126]

Production of glucose from cellulose or simpler substrate such as starch or cellobiose require heterogenous catalysts that combine both high acidity and optimal solid properties. Indeed, microporous solid such as zeolite or resins are not adequate for large substrate like cellulose. That is why sulfonated carbon-based solids seem to be one of the most promising materials for cellulose valorization.

Glucose itself is not the main target of cellulose valorization. As it has been shown in Scheme I-3, many high value products can be obtained from glucose. In particular, sorbitol is a highly demanded molecule that can be produced by hydrogenating glucose and it will be the main target of this project. The next section will give some background information about this platform molecule.

I.5 Sorbitol

From all the molecules that can be produced from glucose, sorbitol is one of the most interesting. Sorbitol is a white crystalline powder that possesses around 60% relative sweetness compared with sucrose. Therefore it can be used as moisturizer, sweetener or softener in food industries, especially in diabetic food. Sorbitol has also applications in pharmaceutical field and is a chemical platform that can give biofuels. It is one of the top 12 important target molecules coming from biomass[132]. According to the IMARC group report, global sorbitol market reached a volume of 2.62 Million Tons in 2020 and the forecast predicts that it will still grow[133].

I.5.1 Sorbitol as a chemical platform

As said above, sorbitol is a chemical platform that can lead to many interesting chemicals. Isosorbide can be obtained by double dehydration of sorbitol over strong acid catalysts. First the cyclodehydration of sorbitol is giving two intermediates: 3,6-sorbitan and 1,4-sorbitan. These two intermediates are further dehydrated into isosorbide (Scheme I-5). Initially, isosorbide was produced by using homogeneous acidic catalysts such as H_2SO_4, HF or HCl at 20-140 °C. However a lot of heterogenous acidic catalysts have been studied to improve the process: zeolites, functionalized silica, zirconium phosphate catalysts are some of the promising alternatives[134,135]. Isosorbide can be used in pharmaceutical field[59] or as plastic monomer to produce poly-(ethylene-co-isosorbide), a bio-based alternative to polyethylene terephthalate[136]. It can also replace bisphenol A in the fabrication of polycarbonate and epoxy resins[137].

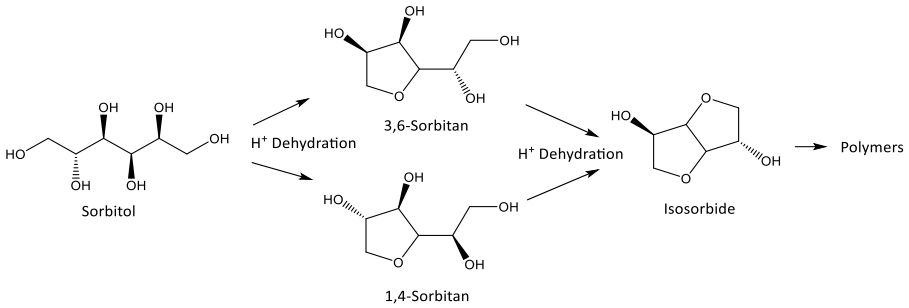

Scheme I-5: Double dehydration of sorbitol into isosorbide (adapted from [135])

Sorbitol can be transformed into glycols, such as ethylene glycol or 1,2-propylene glycol. Glycols are very important chemicals as they are extensively used to produce polymers such as polyethers, polyurethanes or polyester resins[138]. The conversion of sorbitol into glycols is carried out by a metal catalyzed dehydrogenation of sorbitol at more than 200 °C. This reaction can be accelerated by the addition of a basic promoter such as NaOH or $Ca(OH)_2$[139]. Most common catalysts for this transformation are Ru and Ni based catalysts with alkaline medium[140]. Ni is obviously less active than Ru but its use for the cleavage of C-C bonds can be interesting[141]. Several supports have been tested to support Ru and Ni active sites, such as metal oxides (SiO_2, Al_2O_3, ZrO_2 and TiO_2)[142] and carbon materials (carbon nanotubes and activated coal). Carbon nanotubes functionalization has shown an improvement of the catalytic activity of Ru nanoparticles for this reaction. Best results have been obtained with Ru supported on carbon nanotubes functionalized with $-NH_2$ moieties[143].

I.5.2 Food and pharmaceutical applications of sorbitol

Sorbitol has a low calorific value and is widely used as substitute of sugars in food applications. It is replacing sugars in diabetic foods, in sugar-free items like chocolate or chewing gum. Sorbitol liquid and syrup can

be used as softener and moisture stabilizers for all kinds of food such as cakes, dressings or ice cream[144].

Sorbitol is an excellent medicinal excipient. It will help to protect drug from degradation or inactivation and will prevent undesirable pharmacological or immunological effects. Sorbitol can also be introduced in the drug formulation as it can absorbs humidity, by changing its crystalline phase, to protect the active ingredients and keep the hardness of the medicine tablet[145]. Because of its poor absorption in small intestine and its water absorption properties, sorbitol can be used as laxative[146]. Sorbitol is also used as a key intermediate for the production of ascorbic acid (vitamin C) (Scheme I-7)[147],[148].

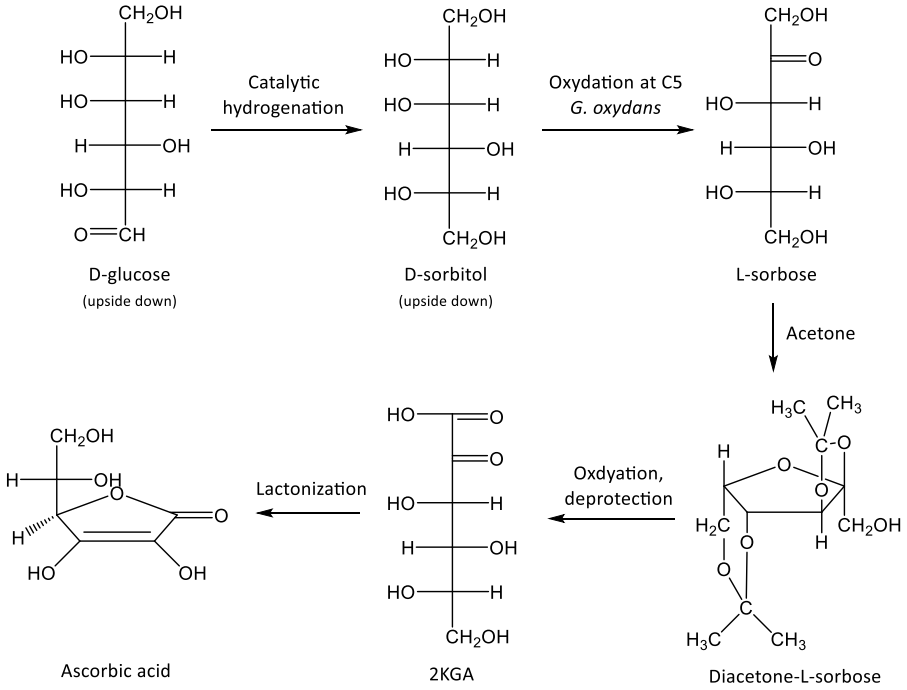

Scheme I-6: Ascorbic acid synthesis from D-glucose/D-sorbitol (G. oxydans stands for *Gluconobacter oxydans* and 2KGA stands for 2-keto-L-gulonic acid) (adapted from [148])

I.5.3 Sorbitol production

- **Production from glucose**

Sorbitol is produced industrially by catalytic hydrogenation of glucose. The most common industrial process is using batch-wise hydrogenation on Raney nickel catalysts promoted by electropositive metal atoms[149]. The utilization of supports in the catalysts preparation has been highly studied in order to increase the metal dispersion. Ni nanoparticles supported on supports such as SiO_2, TiO_2, Al_2O_3 or carbon have shown good results despite all catalysts were leaching[150]. The type of nickel precursors can have an impact on the catalyst activity. For example, Ni ethylenediamine complexes has led to small nanoparticles (between 2 and 3 nm) and a decrease of the Ni leaching has been demonstrated in comparison with bigger nanoparticles[151]. Modified Raney Ni has also been investigated. A skeletal Ni-P amorphous alloy has been synthesized by alkali Al leaching of amorphous Ni-Al-P precursor. This new catalyst has shown better activity than the simple Raney-Ni, apparently because of the promotion of Ni active sites by the P. The hypothesis given by the authors was that the disorder degree of the catalyst has been increased by adding P, resulting in a facilitated hydrogen flowing during the reaction[152].

To overcome the problem of Ni or metal promoter leaching and to further increase sorbitol selectivity, more stable and active catalysts have been investigated. Ruthenium catalysts have been widely studied for sorbitol production in recent years because of high stability and higher activity[153]. Selectivity in sorbitol of nearly 100 % can be obtained by using Ru/C catalyst under 40 bar of H_2. Moreover the Ru activity is proportional to its dispersion on the support[154].

Kinetic studies on the glucose transformation into sorbitol have been conducted. A first-order dependency with respect to hydrogen has been

observed for low concentrations of glucose, while at higher concentrations the reaction rate changed to zero-order behavior[155].

Ru is obviously more active than Ni for the transformation of glucose into sorbitol. However, studies to find the optimal carrier for Ru active sites as well as improving the recyclability of these catalysts are primordial given the high price of Ru.

- **Production from cellulose**

Production of sorbitol directly from cellulose is a very wide field of search in recent years. This transformation is requiring two steps: a hydrolysis and a hydrogenation. Therefore, combination of several catalysts or fabrication of bifunctional catalysts have been studied in order to conduct one-pot conversion of cellulose into sorbitol.

Transformation of cellulose into sorbitol is more challenging because of the cellulose insolubility in water media. As Ru is known to be very effective for the hydrogenation step, the main problem is to manage to hydrolyze cellulose into water-soluble oligomers. Ru/C catalysts have been used with the addition of small quantities of inorganic acid to enhance the hydrolysis step. Hexitols (mainly sorbitol and mannitol) yield of 66 % has been obtained at 463 K after 24h of reaction with 106 ppm of HCl[156].

As explained in the section I.4.4, functionalization of carbon materials with acidic functions such as -COOH or -SO_3H can increase the hydrolysis activity of the carbon catalyst. Sulfonic function is the most interesting one because it is a very strong acidic function. The most common method to functionalize carbon materials is the sulfonation-impregnation process, which consists in treating the carbon material in concentrated sulfonic acid under reflux (200 °C) during several hours[157]. Bifunctional catalyst using this type of functionalized support with Ru nanoparticles on it

has been investigated but only 8.6 % of sorbitol selectivity has been obtained with 19.6 % of cellulose conversion[157]. In order to improve the yields of this transformation, pretreatment of the cellulose, like the ones described in the section I.3, can be applied before the reaction. For example, when ball-milling is applied on microcrystalline cellulose before the reaction, the cellulose conversion is reaching 81 % with a selectivity into sorbitol of 58.7 %[157]. Wei *et al.* have developed catalysts using sulfonated cassava dregs (which is a side-product from the cassava starch extraction) as support with Ru nanoparticles on it and have obtained 85 % of sorbitol yield with 100 % of conversion on ball-milled microcrystalline cellulose. As they have reached 100 % of conversion, they managed to reuse their catalysts 5 times with a slight decrease of the activity[158].

As presented in the section I.3.9, ionic liquids are very interesting as solvents because of their ability to dissolve cellulose which can increase the hydrolytic depolymerization. A lot of studies about their use in combination with Ru catalysts have been done[159]. For example, combination between heterogeneous Ru catalyst with a homogenous Ru complex in 1-butyl-3-methylimidazolium under H_2 has given cellulose conversion of 50 % with a sorbitol selectivity of 74 %. It has been shown that the Ru complex is acting as a H_2 carrier by creating hydride compounds that are increasing H_2 solubility[159]. It has also been demonstrated that when metal nanoparticles are used with ionic liquids as solvents, these ILs have a positive impact on the stabilization of nanoparticles to avoid aggregation and maintain high surface area[160]. However separation of the targeted products from ionic liquids can be very difficult to perform. Biphasic systems have been studied in order to extract the products from the ionic liquids but extraction solvents usually display low separation coefficients regarding ionic liquids. There are also concerns about the corrosion of commonly used stainless steel equipment

by the ionic liquids. All these drawbacks need to be tackled to be able to use combination of ionic liquids with catalysts at an industrial level[161].

In order to simplify the study of cellulose transformation into sorbitol, cellobiose conversion has been investigated. Indeed cellobiose is the simplest model for cellulose as it contains only two glucose units bond together. The most important advantage of cellobiose is that it is soluble in water. Deng *et al.* have shown that Ru over carbon nanotubes (CNT) can achieve 87 % of sorbitol yield for the transformation of cellobiose[162]. In this work, the production of 3-β-D-glucopyranosyl-D-glucitol (cellobitol) from cellobiose has been highlighted when small Ru nanoparticles were used. This has been confirmed by the study of Palkovits *et al.* where it has been shown that two possible pathways can occur for the transformation of cellobiose into sorbitol (Scheme I-8)[163]. Cellobiose can be either hydrolyzed in glucose and then hydrogenated in sorbitol or hydrogenated in cellobitol before being hydrolyzed into glucose and sorbitol.

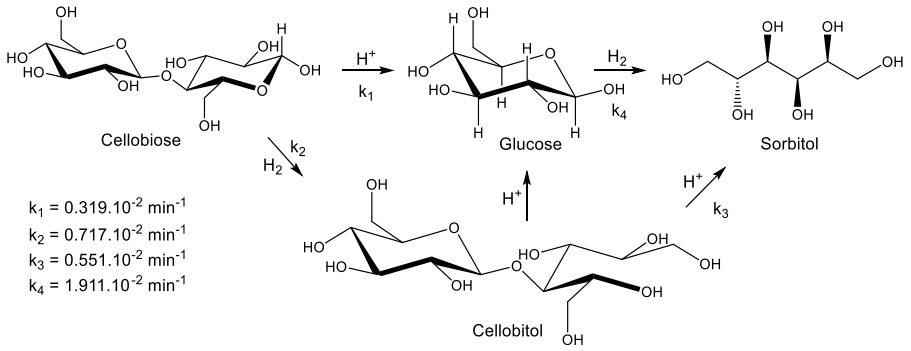

Scheme I-7: Two pathways for the transformation of cellobiose into sorbitol (adapted from [163])

The rate constants of each step have been estimated with a commercial Ru (5 wt. %)/C catalyst from Sigma. Hydrogenation rate constants (k_2 and k_4) are higher than hydrolysis rate constants (k_1 and k_3), meaning that hydrolysis is the rate-determining step. The pathway passing by the cellobitol intermediate is more favorable because the hydrolysis of

cellobitol (k_3) is higher than the hydrolysis of cellobiose (k_1). This explains why very low amount of glucose is detected at the end of the reaction[163].

Other noble metals such as platinum have been investigated to produce sorbitol from cellobiose. Excellent results with 91.5 % of sorbitol yield have been obtained with Pt/RGO (Reduced Graphene Oxide support). Other supports have been tested in the same work and their activities have been listed in the following order: Pt/RGO > Pt/CNT > Pt/AC > Pt/SiO_2 > Pt/G[164] where AC stands for Activated Carbon and G for Single layer Graphene.

As the transformation of cellobiose into sorbitol requires two different steps, bifunctional catalysts to improve both reactions at the same time have been studied. Polyoxometalates have been used as acidic supports for Ru active sites: Keggin-type Ru/$Cs_2PW_{12}O_{40}$ catalyst has shown excellent stability and activity[165]. Bifunctional catalysts using acidic supports such as Amberlyst-15 or functionalized silica (SBA-15) have shown good results with 81 % of sorbitol yield after 5h of reaction at 150 °C. Comparison with mechanical mixture of acidic support and standard Ru/C catalyst has given only 53 % of sorbitol yield, highlighting the benefits of having both active sites on the same catalyst[130].

As it has been demonstrated in sections I.4 and I.5, carbon materials are adequate for bearing acidic functions and for supporting metallic nanoparticles. Therefore they are the perfect materials to design bifunctional catalysts that can transform cellobiose or cellulose into sorbitol. The next section will review and describe all types of carbon materials that will be envisaged in this work.

I.6 Carbon materials

As said above, many types of catalysts are used for the transformation of cellulose into sorbitol. Heterogeneous catalysts are the most studied ones and especially supported on carbon materials which will be the supports of choice that will be used in the present work. Therefore, this last section of the Introduction will give the background knowledge about this particular class of solids.

Pure carbon structure can occur in a wide variety of configurations ranging from the ideal single-crystal hexagonal structure to the most disordered material, amorphous carbon. Natural carbon structures already display this variety, ranging from crystalline diamond to amorphous coal. Since many years, studies have unveiled many different carbon nanoscopic morphologies such as fullerenes, nanotubes (CNT), nanofibers (CNF), carbon black and finally graphene (Figure I-4) [166]. Graphene is a single sheet of fused aromatic rings forming a honeycomb lattice that is one atom thick.

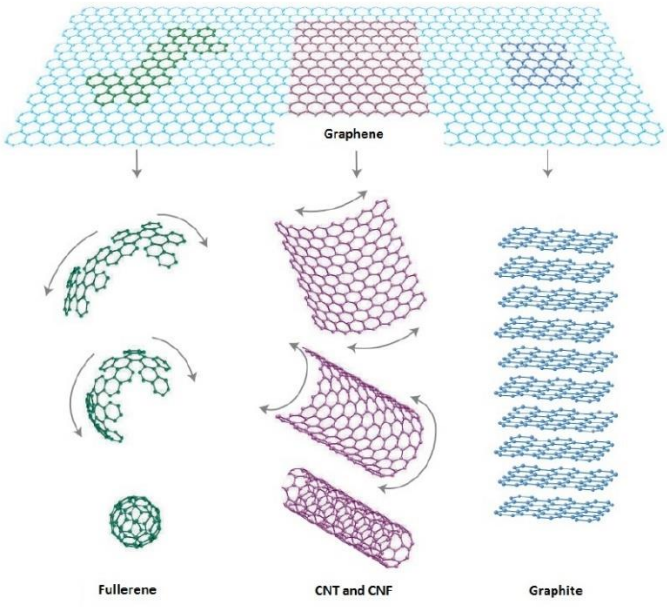

Figure I-4 : Carbon allotropes built from a single graphene sheet (adapted from [167])

I.6.1 Activated coal

Activated carbons or activated coals (AC) are an assembly of defective graphene layers linked together by weak attraction forces such as Van der Waals interactions (Figure I-5). Activated carbons are mainly amorphous with some crystalline zones and possess high specific surface area which make them very interesting for applications such as water or air filters or catalyst supports[168].

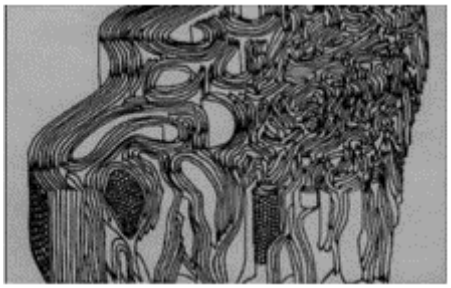

Figure I-5: Activated coal representation (adapted from [168])

Activated coal production is divided in two steps: carbonization and activation. Carbonization consists in pyrolysis under inert atmosphere at high temperature to remove the heteroatoms from the starting materials (organic compounds, biomass, …) and increase the carbon content. Carbon atoms rearrange to have a greater stability within the material structure and form an aromatic network. The removal of heteroatoms, the migration of carbon atoms and their rearrangement are creating spaces within the structure that constitute the carbon material porosity[168].

Activation can be carried out either physically or chemically. Physical activation is applied after the carbonization. Carbon material is submitted to a heat treatment with an activating compound such as CO_2 or water vapor. This treatment generates further porosity in the structure by removing

blocking residues and carbon atoms rearrangement. Chemical activation is performed at the same time as the carbonization step. In this process, carbonization is done with an activating agent such as phosphoric acid, zinc chloride or potassium hydroxide. These molecules dehydrate the structure and lead to an increased texture of the final material[169].

I.6.2 Carbon black

Carbon black is a particular carbon structure where graphene layers are overlapped and wrapped around an amorphous carbon core to lead to a spherical structure. These graphene domains are concentrically oriented around the core and are forming onion-like nanostructures which are called primary particles. These primary particles are assembling to constitute aggregates. Aggregates are very solid structures and only harsh conditions can separate primary particles from each other. These aggregates can bond together by weak Van der Waals forces to form agglomerates (Figure I-6). Unlike aggregates, agglomerates can be easily destroyed by mechanical constraints[170,171].

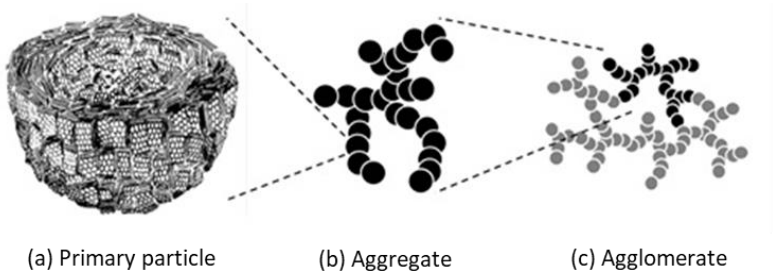

Figure I-6: Carbon black structure (adapted from[172])

Carbon black synthesis methods are numerous. The main processes are carbonization[173], pyrolysis[174], hydrolysis[175] or thermal plasma decomposition[176]. Yields of production are depending on the method, the

temperature and the carbon sources. Fossil resources such as fuel or acetylene have been widely used for carbon black production but new syntheses based on biomass waste or lignin have been developed in recent years[173]. Carbon black can be used as a reinforcing agent in rubber-based objects like tires, as a pigment in printing inks or in coatings and paints. It can also be used as a support for metallic nanoparticles to produce catalysts.

I.6.3 Carbon nanofibers and carbon nanotubes

Carbon nanofibers (CNF) and carbon nanotubes (CNT) are commonly made from the decomposition of carbonaceous gases (acetylene, ethylene, natural gas, *etc*.) by a process called chemical vapor deposition (CVD)[177]. If this reaction is non-catalyzed, it occurs at high temperature (>1300 °C for methane). Otherwise, a transition metal such as iron, nickel or cobalt, can catalyze the reaction and lower this temperature to a more energetically favorable one[178].

The mechanism of CNF or CNT synthesis is the following: hydrocarbon molecules adsorb on the surface of the metal catalyst and decompose to carbon species that can dissolve in the bulk of the metal. This decomposition is exothermic, leading to a hot metal surface. Then, those species diffuse to the other side of the nanoparticles and precipitate (endothermic), leading to a cooler nanoparticle face. In what is called the tip-growth model, the metal nanoparticle is lifted and remains at the tip of the CNF or CNT, leaving behind a hollow cylinder, which inner diameter is approximately the size of the nanoparticle. Excess carbon accumulates at the surface of the catalyst which migrates around the outer surface of the NP to form the graphitic layer of the nanofiber. This growth stops when the warm surface is encapsulated in this excess of carbon which subsequently prevents further carbonaceous gases decomposition. Then, it is possible to increase

the diameter of the formed CNF without elongating it by allowing pyrolysis[177]. Another growth mechanism exists: the base growth model. This mechanism occurs when particle adherence to the surface is strong. In this case, the carbon precipitates from the top surface of the particle and the CNT or CNF continues to grow upwards with the particle anchored on the substrate[179]. The final step consists in a mild acid treatment to remove the metal catalyst from the tip of the CNF or CNT[180]. Tarry residues can also be washed off by using a solvent to cleanse the carbon surface[181].

The difference between CNF and CNT is the angle (α) between the graphene sheets and the axis of the fiber[182]. If this angle equals to zero then it is called a nanotube. However, as soon as there is angle it is called a nanofiber (Figure I-7). Nanotubes diameter is generally narrower than the nanofibers diameter.

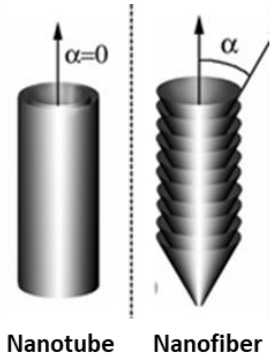

Figure I-7: Difference between a nanotube and a nanofiber (adapted from [182])

Depending on the value of the α angle, several nanofiber structures can be obtained (Figure I-8). When α = 0°, the nanofiber is called ribbon type, between 0° and 90°, it is the fishbone type and when α = 90°, it is the platelet type[183]. Moreover, these morphologies can exist in various shapes: coiled, helical, flat, braided, *etc*.

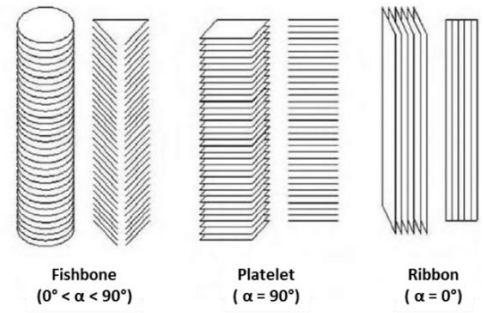

Figure I-8: Different nanofiber structures depending on the α angle (adapted from [183])

Two types of CNT exist: single walled carbon nanotubes (SWCNT) or multi walled carbon nanotubes (MWCNT) (Figure I-9). The SWCNT consists in a single graphene layer that is rolled up into a cylinder. The MWCNT is defined by two or more concentric shells of graphene layers[184]. In both cases, the diameter is a few nanometers while the length can be µm or even centimeters.

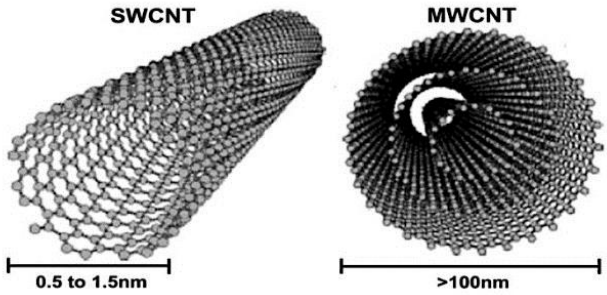

Figure I-9: Representation of a single walled carbon nanotube (on the left) and a multi-walled carbon nanotube (on the right) (adapted from [184])

I.6.4 Graphene nanoplatelets

Synthesis of single layer graphene has been widely studied in recent years[185]. After the first experimental isolation using scotch tape graphite exfoliation, the two main processes that have stood out are CVD 2D growth (usually on copper surfaces) and liquid phase exfoliation of graphite. However, the large scale manufacturing of pure graphene is still difficult

because of the low fabrication rate and high selling price. However, graphene nanoplatelets (GNP), which are carbon structures composed of few graphene layers stacked upon one another, with small lateral dimensions in the nano range, are combining large-scale production possibilities and low costs with outstanding physical properties[186].

GNPs are generally synthesized by liquid phase exfoliation procedure of graphite without further centrifugations steps that allow the separation of graphene single layers. The exfoliation procedure consists in sonication of graphite immersed into solvents with low surface tension or water with surfactants. Other fabrication processes are ball-milling[187], exposure of acid-intercalated graphite to microwave radiation[187] and wet-jet milling[188]. Depending on the synthesis procedure, a variety of powders can be obtained with differences in term of thickness, lateral size or defect concentrations. GNP are usually composed of 10 layers of graphene or more and the thickness of the nanoplatelet can vary from 1 to 3 nm. However, commercial GNP are a mix of monolayer and few layers graphene and graphite (Figure I-10). Therefore, GNP structure should be considered as an intermediate between graphene and graphite.

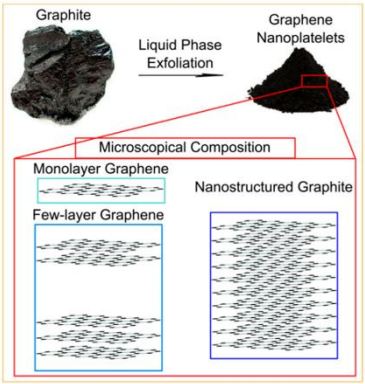

Figure I-10: Composition of graphene nanoplatelets (adapted from [186])

I.6.5 Intrinsic defects

Usually, defects within a carbon structure are considered as something that must be avoided because it can alter the electrical conductivity or its mechanical strength[189]. Nevertheless, defects have shown some interests in adsorption[190] or catalysis field. Indeed, defects can adsorb and form covalent bonds with a transition metal that lead to a better tethering of metal nanoparticles and decrease particles migration and sintering[191]. Intrinsic defects can be identified as single vacancies, multiple vacancies or dislocation-like defects.

The single vacancy results from one missing atom in the lattice whereas multiple vacancies can occur when several atoms are missing and single vacancies coalesce as a result of defects migration. When a vacancy is created, three dangling bonds are left behind that can rearrange in non-hexagonal rings like pentagons (Figure I-11). This results in a lowered amount of dangling bonds and thus a higher stability[192]. Hexagonal rings can also rearrange without any loss or win of atoms. The simplest of these rearrangements is called the Stone-Wales defect: four hexagons are transformed in two pentagons and two heptagons by a simple C-C rotation[193].

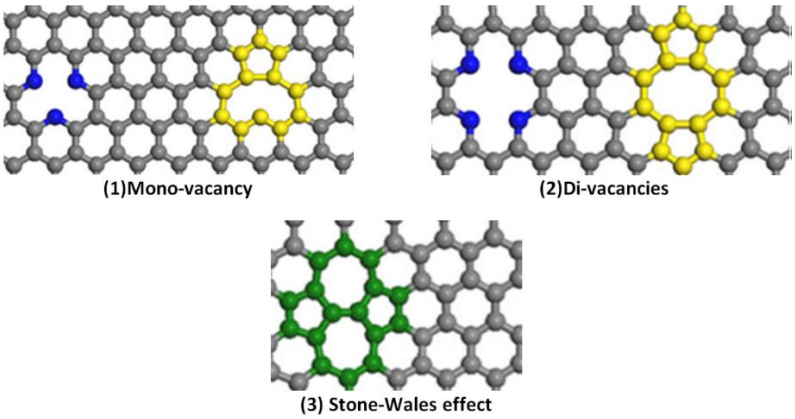

Figure I-11: Representation of (1) mono-vacancy, (2) di-vacancies and (3) Stone-Wales defect in an aromatic carbon structure (adapted from [190])

Dislocation-like defects are existing when two graphene layers from different orientations are interacting with each other. There are two possibilities to explain this boundary between two graphene sheets: either a direct bonding is occurring at the interface of the two graphene sheets (Figure I-12 a and b) or one sheet is overlapping another to form a bilayer area with no covalent bond but held together by interlayer van der Waals forces (Figure I-12 c and d)[194].

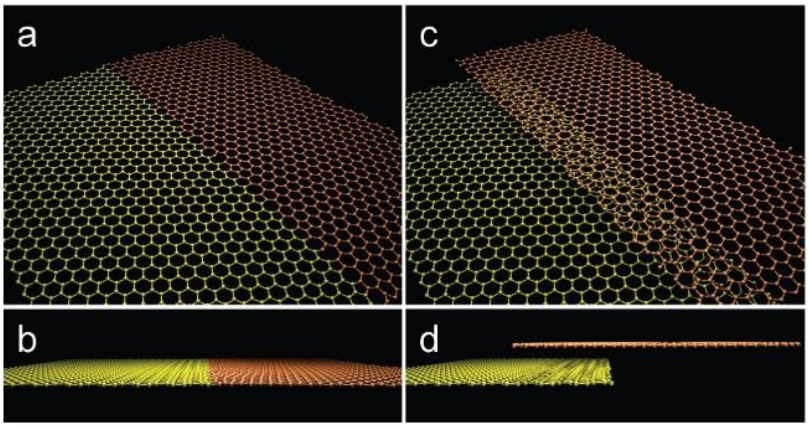

Figure I-12: Representation of two ways of graphene sheets connection; a) Atomic bonding at the interface; b) Side view of the bonding at the interface; c) Overlapping of two graphene sheets; d) Side view of the overlapping (adapted from [194])

Finally, carbon atoms at the edges of the graphene sheets are not coordinated as carbons in the inner structure. Therefore they possess high electronic density and can be free or passivated by hydrogen or oxygen atoms in an arm-chair or zigzag orientation[195]. The zigzag sites are carbene-like and the arm-chair sites are carbyne-like (Figure I-13).

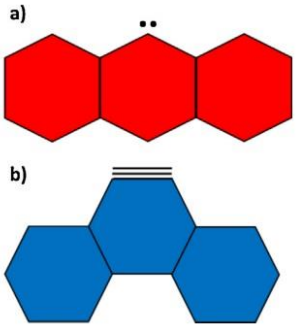

Figure I-13: Schematic of a) zigzag (carbene-like) and b) arm-chair (carbyne-like) edge configurations at the graphene edge (adapted from [195])

I.6.6 Extrinsic defects: Functionalization

Extrinsic defects are defined as surface functional groups and can usually be generated by functionalization of carbon materials, at the positions where there are defects in the structure (most of the time at the edges of the material). They can be introduced post-synthetically or arise from the production method (for example during activation of AC, during liquid-phase exfoliation for graphene and purification of CNT/CNF). In addition, some hetero-atoms might remain as impurities from the raw material used as carbon source.

Introduction of heteroatoms and functions can influence the carbon material properties[168]. For carbon materials used as catalytic support, functional groups can enhance the dispersion of metallic nanoparticles and improve their activity. Moreover it can also change the hydrophilicity of the carbon material: hydrophilic functions will improve the dispersion of carbon materials in protic solvents such as water. Most of the functional groups with heteroatoms that can be encountered in carbon materials are containing oxygen, nitrogen or sulfur.

Oxygen functions are the most common functions that can be present in carbon materials (Scheme I-9). They can be obtained after

oxidation of carbon materials. A lot of oxidants with different conditions can be applied and will impact the type of oxygen functions that can be formed. The most common ones are O_2, O_3, HNO_3, H_2O_2, H_2SO_4 and $KMnO_4$[196]. The type of oxygen functions will also depend on the type of carbon materials. Defectuous carbon materials will be easier to functionalize than clean carbon materials with low amount of defects. Oxygen functions are usually acidic functions and their introduction on a carbon material will increase its Brønsted acidity.

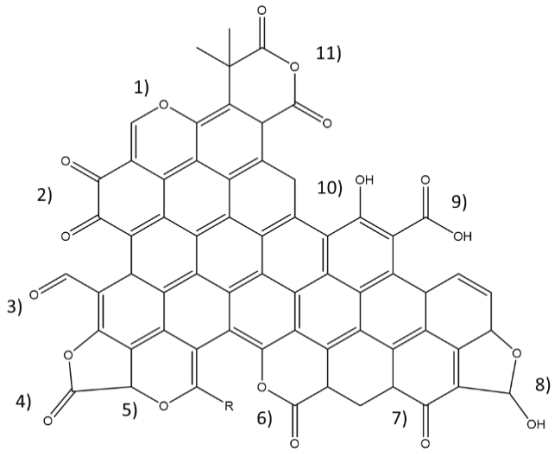

Scheme I-8: Oxygen functions within carbon materials: 1) ether, 2) quinone, 3) aldehyde, 4) lactone, 5) chromene, 6) pyrone, 7) carbonyl, 8) lactol, 9) carboxylic acid, 10) phenol, 11) carboxylic anhydride (adapted from [195])

Nitrogen functions can be incorporated within carbon materials by using gas like ammonia or in liquid phase by impregnation of nitrogen compounds such as urea or melamine (Scheme I-10)[195].

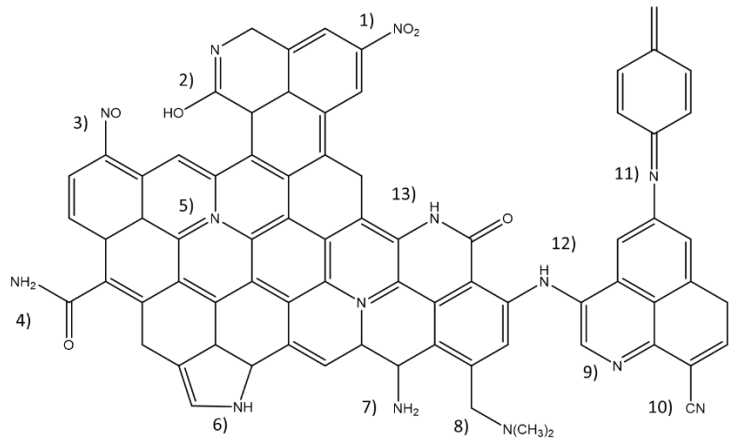

Scheme I-9: Nitrogen functions within carbon materials: 1) nitro group, 2) pyridone, 3) nitrosyl group, 4) amide, 5) quaternary amine, 6) pyrroline, 7) primary amine, 8) tertiary amine, 9) pyridine, 10) nitrile, 11) imine, 12) secondary amine, 13) lactam (adapted from [195])

After the functionalization, the type of nitrogen functions can be tuned by heat treatment under inert atmosphere. As the support is heated, imide, lactams and amide structures are transformed into pyrrole and pyridine. In addition, amines tend to be more substituted from primary to tertiary and quaternary. In short, nitrogen atoms enter within the carbon material structure and start to replace carbon atoms. This replacement of carbon by nitrogen changes the total number of electrons in the system without disturbing the inner structure as nitrogen and carbon atoms have similar radius[195]. Therefore, spin density and charge distribution of the neighboring carbon atoms are affected[197]. This effect can be valuable in improving metal nanoparticles tethering and have electronic influence on them. Moreover, nitrogen functions, which are mostly basic functions, can also increase the Brønsted basicity of the carbon material.

I.6.7 Carbon materials characterization

Characterization tools are primordial when carbon solids are involved as materials. As the nanocarbons syntheses techniques are still not efficient enough to produce perfectly defined and pure samples, characterization of pristine materials must be carried out. Moreover, after any functionalization step of carbon materials or deposition of metal nanoparticles onto them, identification and quantification of functions or nanoparticles require characterization techniques to get the full picture of the hybrid materials obtained. The most often used characterization methods are gathered in Table I-4 together with the main information they can deliver [198].

Table I-4: Most common methods used for carbon materials characterization (adapted from [198])

Analytical technique		Information
Spectroscopy	Fourier transformed infrared (FTIR)	Nature of functional groups
	UV-Vis-near infrared	Degree of functionalization
	X-ray photoelectron spectroscopy (XPS)	Surface elemental composition
	Raman spectroscopy	Amount of carbon impurities, diameter and number of layers
Thermal analysis	Thermogravimetric analysis (TGA)	Purity, thermal stability and degree of functionalization
	Differential scanning calorimetry (DSC)	Purity, thermal stability and degree of functionalization
Microscopy	Transmission electron microscopy (TEM)	Diameter, length, purity and size of metallic nanoparticles
	Scanning electron microscopy (SEM)	Purity
	Scanning tunneling microscopy (STM)	Degree of functionalization
Others	X-ray diffraction (XRD)	Crystallinity and presence of metallic nanoparticles
	Secondary ion mass spectrometry (SIMS)	Nature of functional groups
	Boehm titration	Amount and nature of acidic or basic sites

I.7 Objectives and methodology

I.7.1 Objectives

As it has been demonstrated in the previous sections, non-edible biomass valorization into chemicals and fuels is a very important and crucial research field for the future. One of the most useful molecule that can be obtained by biomass transformation is sorbitol. It is a chemical platform and can also be used itself for many applications. Sorbitol can be produced from the hydrogenolysis of cellulose. This whole transformation requires two types of catalysts: an acidic catalyst to improve the hydrolysis and a noble metal site for enhancing the hydrogenation. Usually, the two reactions are carried out consecutively or the two catalysts are used together in a one-pot reaction. Since many years, bifunctional catalysts with both active sites on the same support have been studied in order to improve the sorbitol production. This work is following a three points strategy: studying both hydrogenation and hydrolysis steps separately before trying to make a bifunctional catalyst that is producing sorbitol directly from cellulose.

The first goal is to study the hydrogenation of glucose into sorbitol. This reaction is catalyzed by noble metal catalysts and especially by ruthenium. Therefore, Ru nanoparticles supported on carbon materials will be synthesized as catalysts for the hydrogenation. The objective is to find conditions that favor sorbitol selectivity but with the possibility to compare results between them and observe the effect of different materials characteristics, to establish fundamental structure-activity relationships. Thus, optimization of Ru nanoparticles size in this reaction is required as well as finding reaction conditions that are not giving total conversion and complete selectivity in sorbitol.

Nitrogen doping of the carbon materials will be studied because of the ability of nitrogen to promote Ru activity and enhance nanoparticles

distribution. This secondary aspect within the first goal will be studied on the hydrogenolysis of cellobiose into sorbitol to assess the impact of the support modification at a bigger picture level. Moreover, nitrogen functions are known to be basic functions and their possible impact on cellobiose hydrolysis must be taken into account and studied.

The second objective of this thesis is to study the hydrolysis of cellobiose into glucose. Cellobiose is used as the simplest model of cellulose. As depicted in the previous sections, hydrolysis of cellulose is one of the biggest challenge for its transformation because of its high crystallinity and its huge degree of polymerization. Moreover cellulose is insoluble in water making its hydrolysis very difficult to realize. Therefore, efficient acidic catalysts are required to improve the hydrolysis. Homogeneous acids are used in industrial processes to perform the hydrolysis but numerous drawbacks are accompanying them. The use of heterogeneous solid acids, especially modified carbon materials, is very interesting to overcome these problems. Generally, acidic carbon materials are obtained by using concentrated H_2SO_4 in harsh conditions to incorporate sulfonic functions. However, these conditions can structurally damage carbon supports and the incorporated sulfonic functions are not stable and can easily leach. Therefore, functionalization of carbon materials with covalently bonded sulfonic functions that will be stable during hydrolysis reaction is primordial. Synthesis of such catalysts and assessment of their activity in cellobiose hydrolysis is the second goal of this work.

The third and final goal of this work is the synthesis of efficient bifunctional catalysts, that will surpass mere Ru/C catalyst, to produce sorbitol from cellulose. Indeed, having both active sites on the same support is always more interesting for industrial applications and fundamental studies as well. Synthesis of bifunctional catalysts with both sulfonic

functions and Ru nanoparticles is a huge challenge because of the known cross-poisoning between these two active sites. Optimization of the ratio between the two active sites will be decisive in order to limit cross-poisoning and hopefully show a synergetic effect between sulfonic functions and Ru nanoparticles. The bifunctional catalysts will be first assessed for cellobiose hydrogenolysis into sorbitol before moving step by step to more complicated substrates such as starch and insoluble cellulose.

I.7.2 Strategy

The methodology used for this work is following the same structure than the objectives. The two first **Chapters (II and III)** dedicated to the results will tackle the first goal of the project: the study of the hydrogenation reaction. **Chapter IV** will target the second goal of this work and discuss the hydrolysis of cellobiose into glucose. Finally, the final objective that is the synthesis of bifunctional catalyst will be covered in **Chapter V**. The thesis structure is schematized in Figure I-5.

The **Chapter II** of this manuscript deals with synthesizing Ru/C catalysts for the hydrogenation of glucose into sorbitol. Carbon nanofibers will be chosen first as a model support because of their stabilization effect that manage to keep nanoparticles small even after high temperature treatment. Two others carbon supports will also be studied: AC and GNP. By adapting synthesis methods and heat treatments, several sizes of Ru nanoparticles will be obtained selectively and the optimal size for the hydrogenation of glucose into sorbitol will be determined. Reaction conditions such as temperature, H_2 pressure, reaction time or Ru loading will be varied in order to find adequate conditions window to be able to compare our results efficiently. These preliminary results will be the starting point of the Chapter V where bifunctional catalysts will be elaborated.

The doping of carbon materials with nitrogen atoms will be studied in **Chapter III**. Two methods will be used to incorporate nitrogen atoms within the carbon materials lattice: one using urea adsorption and the other with ethylenediamine that will react covalently on the carbon surface. For both methods, a thermal treatment is needed to allow nitrogen atoms to insert within the carbon structure. Incorporated nitrogen sites are basic functions and can be analyzed by several methods. Boehm titration and CO_2-TPD will determine the amount and the strength of those basic functions on the carbon materials. XPS analyses will allow us to know which type of nitrogen functions are present on the carbon materials, by analyzing the position (binding energy) of the nitrogen peak. Several carbon materials (AC, CNF, CB and GNP) will be doped with nitrogen and compared. Ru nanoparticles will be deposited on the N-doped carbon supports with the same method than presented in Chapter II and considering the optimal size determined previously. These catalysts will be tested in the hydrogenolysis of cellobiose into sorbitol. As hydrogenation of glucose into sorbitol has been studied in Chapter II, the purpose here is to zoom out to a more challenging substrate. The reaction pathway will be determined by kinetic studies and the impact of nitrogen on Ru activity will be assessed.

Chapter IV will treat the use of acidic catalysts for the hydrolysis of cellobiose into glucose. In order to have acidic catalysts, carbon materials will be functionalized thanks to a diazonium coupling reaction. This reaction will graft benzyl sulfonic functions, which are acidic functions, on the surface of the carbon materials. These sulfonic functions should be more stable than the ones added with concentrated H_2SO_4 as it is done generally in the literature. Boehm titration and NH_3-TPD will give information about the number and the strength of these acidic groups. XPS analyses will confirm the presence of sulfonic moieties. These new acidic carbon materials will be

tested in the hydrolysis of cellobiose into sorbitol and the stability of the catalysts will be assessed by recyclability tests.

Eventually, the **Chapter V** will be focused on the synthesis of bifunctional catalysts for the direct production of sorbitol from cellulose/cellobiose. The methodology to obtain bifunctional catalysts is to deposit Ru nanoparticles on functionalized carbon supports. The main challenge of this synthesis is to preserve the integrity of both active sites. Bifunctional catalysts using the deposition method developed in Chapter II will be studied in the first part of Chapter V. However, these methods employed for depositing Ru nanoparticles involved basic media that could deactivate sulfonic functions on the functionalized carbons. In consequence, to overcome this deactivation problem, later in this Chapter, preformed RuO_2 will be synthesized and deposited on the functionalized supports. Synthesis of these RuO_2 nanoparticles will be adjusted to target the optimal size as determined in Chapter II. As cross-poisoning between sulfonic functions and Ru can occur, optimization of the ratio between the two active sites will be realized in order to have the most efficient catalyst. These bifunctional catalysts will be characterized by XPS (oxidation state of Ru and presence of sulfonic functions), XRD (presence of Ru and nanoparticles size), TEM (nanoparticles distribution and size) and EDX (elements mapping on the carbon support). These so-obtained bifunctional catalysts will be first tested in the hydrogenolysis of cellobiose into sorbitol to highlight possible synergetic effect between sulfonic functions and Ru. Bifunctional catalysts that surpass the performance of monofunctional catalyst (Ru/C) will be evaluated in the hydrogenolysis of more sophisticated substrates: starch and microcrystalline cellulose. Starch is more challenging than cellobiose but is still soluble in water. However, microcrystalline cellulose in not soluble in water making the consecutive reactions more difficult to occur, as it will

involve a solid/solid catalyst/substrate contact. As mentioned in the previous sections, pretreatment of cellulose is often required to make it more accessible and reactive. Catalytic reactions will be performed with and without ball-milling of the cellulose to point out the impact of this pretreatment. Ball-milling of both cellulose and catalyst together before the reaction will be also evaluated as it has been proven that it can enhance the catalytic performances. As the ultimate goal of this thesis is to have an efficient bifunctional catalyst that produces sorbitol from cellulose, reaction conditions with this catalyst will be varied to increase sorbitol yield. Finally, comparisons with literature will situate our results among other bifunctional catalysts and allow benchmarking.

This manuscript will end with a general conclusion and some suggestions for future work (**Chapter VI**), followed by an experimental part (**Chapter VII**) and supplementary data.

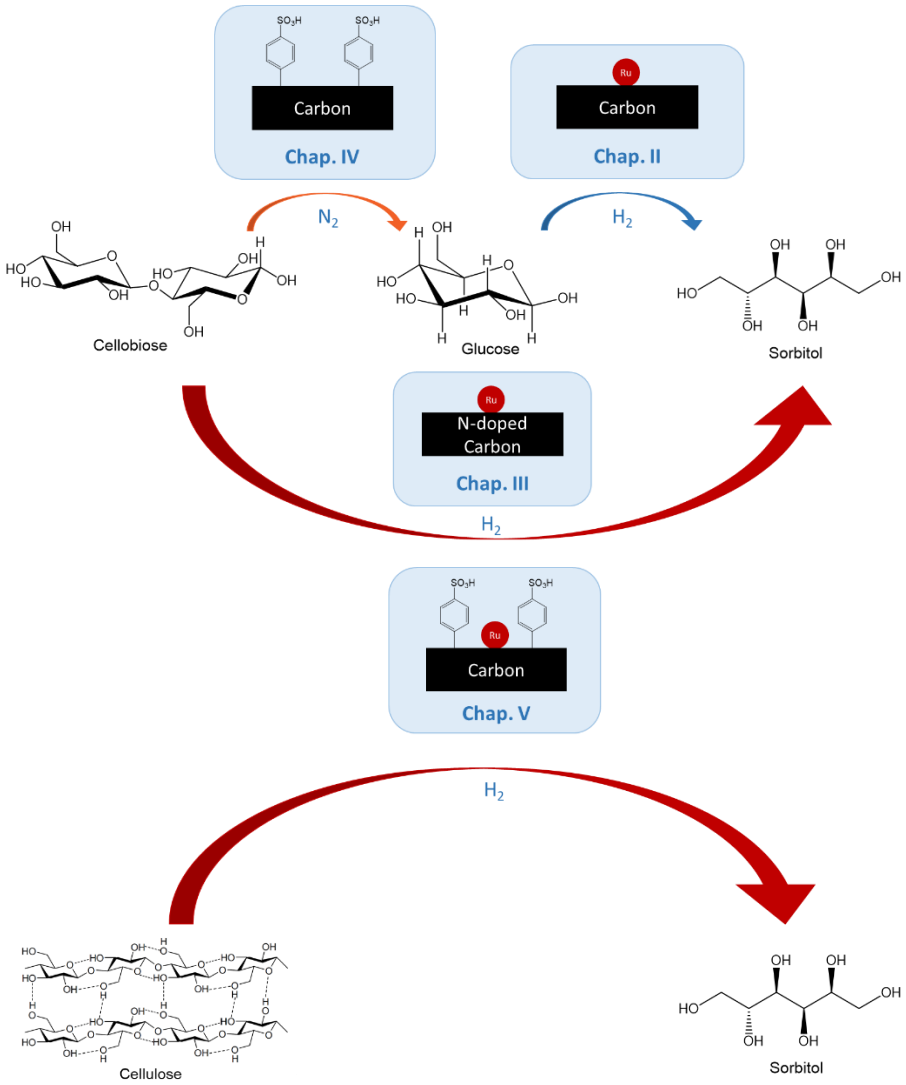

Figure I-5: Thesis map

References

[1] BP, *Stat. Rev. World Energy* **2021**, *70*.

[2] R. Parajuli, T. Dalgaard, U. Jørgensen, A. P. S. Adamsen, M. T. Knudsen, M. Birkved, M. Gylling, J. K. Schjørring, *Renew. Sustain. Energy Rev.* **2015**, *43*, 244–263.

[3] K. Bartholdy, *BP Statistical Review of World Energy*, **2019**.

[4] A. M. Ruppert, K. Weinberg, R. Palkovits, *Angew. Chemie - Int. Ed.* **2012**, *51*, 2564–2601.

[5] G. W. Huber, S. Iborra, A. Corma, *Chem. Rev.* **2006**, *106*, 4044–4098.

[6] J. C. Escobar, E. S. Lora, O. J. Venturini, E. E. Yáñez, E. F. Castillo, O. Almazan, *Renew. Sustain. Energy Rev.* **2009**, *13*, 1275–1287.

[7] I. Ntaikou, G. Antonopoulou, G. Lyberatos, *Waste and Biomass Valorization* **2010**, *1*, 21–39.

[8] K. Dutta, A. Daverey, J. G. Lin, *Renew. Energy* **2014**, *69*, 114–122.

[9] H. A. Baloch, S. Nizamuddin, M. T. H. Siddiqui, S. Riaz, A. S. Jatoi, D. K. Dumbre, N. M. Mubarak, M. P. Srinivasan, G. J. Griffin, *J. Environ. Chem. Eng.* **2018**, *6*, 5101–5118.

[10] Y. Chisti, *Biotechnol. Adv.* **2007**, *25*, 294–306.

[11] J. N. Rosenberg, G. A. Oyler, L. Wilkinson, M. J. Betenbaugh, *Curr. Opin. Biotechnol.* **2008**, *19*, 430–436.

[12] Q. Hu, M. Sommerfeld, E. Jarvis, M. Ghirardi, M. Posewitz, M. Seibert, A. Darzins, *Plant J.* **2008**, *54*, 621–639.

[13] M. Sarra, T. Rouissi, S. K. Brar, J. F. Blais, *Platf. Chem. Biorefinery* **2016**, 55–76.

[14] J. Lü, C. Sheahan, P. Fu, *Energy Environ. Sci.* **2011**, *4*, 2451–2466.

[15] M. S. K. Triantafyllidis, A. Lappas, *The Role of Catalysis for the Sustainable Production of Bio-Fuels and Bio-Chemicals*, **2013**.

[16] P. Zugenmaier, *Prog. Polym. Sci.* **2001**, *26*, 1341–1417.

[17] A. . O'Sullivan, *Cellulose* **1997**, *4*, 173–207.

[18] H. Wang, G. Gurau, R. D. Rogers, *Chem. Soc. Rev.* **2012**, *41*, 1519–1537.

[19] H. V. Scheller, P. Ulvskov, *Annu. Rev. Plant Biol.* **2010**, *61*, 263–289.

[20] K. Kulasinski, S. Keten, S. V. Churakov, D. Derome, J. Carmeliet, *Cellulose* **2014**, *21*, 1103–1116.

[21] T. Koshijima, T. Watanabe, *Association Between Lignin and Carbohydrates in Wood and Other Plant Tissues*, Springer Berlin Heidelberg, Berlin, Heidelberg, **2003**.

[22] V. K. Ponnusamy, D. D. Nguyen, J. Dharmaraja, S. Shobana, J. R. Banu, R. G. Saratale, S. W. Chang, G. Kumar, *Bioresour. Technol.* **2019**, *271*, 462–472.

[23] V. Menon, M. Rao, *Prog. Energy Combust. Sci.* **2012**, *38*, 522–550.

[24] R. Kumar, C. E. Wyman, *Aqueous Pretreat. Plant Biomass Biol. Chem. Convers. to Fuels Chem.* **2013**, 281–310.

[25] A. T. W. M. Hendriks, G. Zeeman, *Bioresour. Technol.* **2009**, *100*, 10–18.

[26] P. Bhama Iyer, S. Sreenivasan, P. K. Chidambareswaran, N. B. Patil, *Text. Res. J.* **1984**, *54*, 732–735.

[27] Y. H. P. Zhang, L. R. Lynd, *Biotechnol. Bioeng.* **2004**, *88*, 797–824.

[28] Q. Zhang, M. Benoit, K. De Oliveira Vigier, J. Barrault, G. Jégou, M. Philippe, F. Jérôme, *Green Chem.* **2013**, *15*, 963–969.

[29] L. P. Ramos, M. M. Nazhad, J. N. Saddler, *Enzyme Microb. Technol.* **1993**, *15*, 821–831.

[30] E. L. Springer, J. F. Harris, *Ind. Eng. Chem. Prod. Res. Dev.* **1985**, *24*, 485–489.

[31] A. Berlin, M. Balakshin, N. Gilkes, J. Kadla, V. Maximenko, S. Kubo, J. Saddler, *J. Biotechnol.* **2006**, *125*, 198–209.

[32] S. Haghighi Mood, A. Hossein Golfeshan, M. Tabatabaei, G. Salehi Jouzani, G. H. Najafi, M. Gholami, M. Ardjmand, *Renew. Sustain. Energy Rev.* **2013**, *27*, 77–93.

[33] M. H. Sipponen, S. Laakso, S. Baumberger, *Ind. Crops Prod.* **2014**, *61*, 130–136.

[34] A. S. A. Da Silva, H. Inoue, T. Endo, S. Yano, E. P. S. Bon, *Bioresour. Technol.* **2010**, *101*, 7402–7409.

[35] N. Meine, R. Rinaldi, F. Schüth, *ChemSusChem* **2012**, *5*, 1449–1454.

[36] J. Hilgert, N. Meine, R. Rinaldi, F. Schüth, *Energy Environ. Sci.* **2013**, *6*, 92–96.

[37] M. Yabushita, H. Kobayashi, K. Hara, A. Fukuoka, *Catal. Sci. Technol.* **2014**, *4*, 2312–2317.

[38] S. Banik, S. Bandyopadhyay, S. Ganguly, *Bioresour. Technol.* **2003**, *87*, 155–159.

[39] O. Merino-Pérez, R. Martínez-Palou, J. Labidi, R. Luque, **2015**, 197–224.

[40] V. Chaturvedi, P. Verma, *3 Biotech* **2013**, *3*, 415–431.

[41] J. S. Bak, *Biotechnol. Reports* **2014**, *4*, 30–33.

[42] E. Betiku, O. A. Adetunji, T. V. Ojumu, B. O. Solomon, *Brazilian J. Chem. Eng.* **2009**, *26*, 251–255.

[43] M. J. Bussemaker, D. Zhang, *Ind. Eng. Chem. Res.* **2013**, *52*, 3563–3580.

[44] A. Iskalieva, B. M. Yimmou, P. R. Gogate, M. Horvath, P. G. Horvath, L. Csoka, *Ultrason. Sonochem.* **2012**, *19*, 984–993.

[45] Y. Sun, J. Cheng, *Bioresour. Technol.* **2002**, *83*, 1–11.

[46] W. R. Grous, A. O. Converse, H. E. Grethlein, *Enzyme Microb. Technol.* **1986**, *8*, 274–

280.

[47] P. Kumar, D. M. Barrett, M. J. Delwiche, P. Stroeve, *Ind. Eng. Chem. Res.* **2009**, *48*, 3713–3729.

[48] B. Bals, C. Wedding, V. Balan, E. Sendich, B. Dale, *Bioresour. Technol.* **2011**, *102*, 1277–1283.

[49] J. Y.-T. K. Ming-Ju Chen, Kreuter, *J. Anat.* **1996**, *189 (Pt 3*, 503–505.

[50] S. P. S. Chundawat, B. S. Donohoe, L. Da Costa Sousa, T. Elder, U. P. Agarwal, F. Lu, J. Ralph, M. E. Himmel, V. Balan, B. E. Dale, *Energy Environ. Sci.* **2011**, *4*, 973–984.

[51] M. T. Holtzapple, J. E. Lundeen, R. Sturgis, J. E. Lewis, B. E. Dale, *Appl. Biochem. Biotechnol.* **1992**, *34–35*, 5–21.

[52] C. J. Biermann, *Handbook of Pulping and Papermaking*, Elsevier Science, **1996**.

[53] A. M. J. Kootstra, H. H. Beeftink, E. L. Scott, J. P. M. Sanders, *Biotechnol. Biofuels* **2009**, *2*, 1–14.

[54] M. J. Taherzadeh, K. Karimi, *Int. J. Mol. Sci.* **2008**, *9*, 1621–1651.

[55] P. Alvira, E. Tomás-Pejó, M. Ballesteros, M. J. Negro, *Bioresour. Technol.* **2010**, *101*, 4851–4861.

[56] D. Ding, J. Xi, J. Wang, X. Liu, G. Lu, Y. Wang, *Green Chem.* **2015**, *17*, 4037–4044.

[57] R. Palkovits, K. Tajvidi, J. Procelewska, R. Rinaldi, A. Ruppert, *Green Chem.* **2010**, *12*, 972–978.

[58] S. Van de Vyver, J. Geboers, P. A. Jacobs, B. F. Sels, *ChemCatChem* **2011**, *3*, 82–94.

[59] H. Kobayashi, A. Fukuoka, *Green Chem.* **2013**, *15*, 1740.

[60] X. Li, T. H. Kim, N. P. Nghiem, *Bioresour. Technol.* **2010**, *101*, 5910–5916.

[61] M. Balat, H. Balat, C. Öz, *Prog. Energy Combust. Sci.* **2008**, *34*, 551–573.

[62] C. Wan, Y. Zhou, Y. Li, *Bioresour. Technol.* **2011**, *102*, 6254–6259.

[63] J. Xu, J. J. Cheng, *Bioresour. Technol.* **2011**, *102*, 3861–3868.

[64] F. Carvalheiro, L. C. Duarte, F. M. Gírio, *J. Sci. Ind. Res. (India).* **2008**, *67*, 849–864.

[65] Y. J. Lee, C. H. Chung, D. F. Day, *Bioresour. Technol.* **2009**, *100*, 935–941.

[66] J. M. Gould, *Biotechnol. Bioeng.* **1984**, *26*, 46–52.

[67] R. S. Ramirez, M. Holtzapple, N. Piamonte, in *Aqueous Pretreat. Plant Biomass Biol. Chem. Convers. to Fuels Chem.*, John Wiley & Sons, Ltd, Chichester, UK, **2013**, pp. 145–167.

[68] M. Balat, *Energy Convers. Manag.* **2011**, *52*, 858–875.

[69] A. S. Schmidt, A. B. Thomsen, *Bioresour. Technol.* **1998**, *64*, 139–151.

[70] Y. D. Singh, K. B. Satapathy, *Int. J. Eng. Technol.* **2018**, *15*, 17–43.

[71] P. Sannigrahi, A. J. Ragauskas, *Aqueous Pretreat. Plant Biomass Biol. Chem. Convers. to Fuels Chem.* **2013**, 201–222.

[72] J. Wildschut, A. T. Smit, J. H. Reith, W. J. J. Huijgen, *Bioresour. Technol.* **2013**, *135*, 58–66.

[73] X. Zhao, K. Cheng, D. Liu, *Appl. Microbiol. Biotechnol.* **2009**, *82*, 815–827.

[74] W. J. J. Huijgen, A. T. Smit, P. J. de Wild, H. den Uil, *Bioresour. Technol.* **2012**, *114*, 389–398.

[75] J. Zakzeski, P. C. A. Bruijnincx, A. L. Jongerius, B. M. Weckhuysen, *Chem. Rev.* **2010**, *110*, 3552–3599.

[76] F. Sun, H. Chen, *Bioresour. Technol.* **2008**, *99*, 5474–5479.

[77] T. Heinze, T. Liebert, *Prog. Polym. Sci.* **2001**, *26*, 1689–1762.

[78] T. Heinze, A. Koschella, *Polímeros* **2005**, *15*, 84–90.

[79] A. Brandt, J. Gräsvik, J. P. Hallett, T. Welton, *Green Chem.* **2013**, *15*, 550.

[80] D. C. Dibble, C. Li, L. Sun, A. George, A. Cheng, Ö. P. Çetinkol, P. Benke, B. M. Holmes, S. Singh, B. A. Simmons, *Green Chem.* **2011**, *13*, 3255–3264.

[81] G. Cheng, P. Varanasi, C. Li, H. Liu, Y. B. Melnichenko, B. A. Simmons, M. S. Kent, S. Singh, *Biomacromolecules* **2011**, *12*, 933–941.

[82] H. Olivier-Bourbigou, L. Magna, D. Morvan, *Appl. Catal. A Gen.* **2010**, *373*, 1–56.

[83] A. M. Socha, R. Parthasarathi, J. Shi, S. Pattathil, D. Whyte, M. Bergeron, A. George, K. Tran, V. Stavila, S. Venkatachalam, M. G. Hahn, B. A. Simmons, S. Singh, *Proc. Natl. Acad. Sci. U. S. A.* **2014**, *111*, 3587–3595.

[84] P. Singh, A. Suman, P. Tiwari, N. Arya, A. Gaur, A. K. Shrivastava, *World J. Microbiol. Biotechnol.* **2008**, *24*, 667–673.

[85] P. Béguin, J.-P. Aubert, *FEMS Microbiol. Rev.* **1994**, *13*, 25–58.

[86] C. Wan, Y. Li, *Bioresour. Technol.* **2010**, *101*, 6398–6403.

[87] J. Shi, R. R. Sharma-Shivappa, M. Chinn, N. Howell, *Biomass and Bioenergy* **2009**, *33*, 88–96.

[88] C. E. Wyman, B. E. Dale, R. T. Elander, M. Holtzapple, M. R. Ladisch, Y. Y. Lee, *Bioresour. Technol.* **2005**, *96*, 1959–1966.

[89] D. G. Olson, J. E. McBride, A. Joe Shaw, L. R. Lynd, *Curr. Opin. Biotechnol.* **2012**, *23*, 396–405.

[90] F. Santos, P. Eichler, J. H. De Queiroz, F. Gomes, *Production of Second-Generation Ethanol from Sugarcane*, Elsevier Inc., **2019**.

[91] K. Olofsson, M. Bertilsson, G. Lidén, *Biotechnol. Biofuels* **2008**, *1*, 1–14.

[92] K. Öhgren, R. Bura, G. Lesnicki, J. Saddler, G. Zacchi, *Process Biochem.* **2007**, *42*, 834–839.

[93] T. Renders, S. Van Den Bosch, S. F. Koelewijn, W. Schutyser, B. F. Sels, *Energy Environ. Sci.* **2017**, *10*, 1551–1557.

[94] M. V. Galkin, J. S. M. Samec, *ChemSusChem* **2014**, *7*, 2154–2158.

[95] S. Van Den Bosch, W. Schutyser, R. Vanholme, T. Driessen, S. F. Koelewijn, T. Renders, B. De Meester, W. J. J. Huijgen, W. Dehaen, C. M. Courtin, B. Lagrain, W. Boerjan, B. F. Sels, *Energy Environ. Sci.* **2015**, *8*, 1748–1763.

[96] V. E. Tarabanko, K. L. Kaygorodov, E. A. Skiba, N. Tarabanko, Y. V. Chelbina, O. V. Baybakova, B. N. Kuznetsov, L. Djakovitch, *J. Wood Chem. Technol.* **2017**, *37*, 43–51.

[97] X. Wu, X. Fan, S. Xie, J. Lin, J. Cheng, Q. Zhang, L. Chen, Y. Wang, *Nat. Catal.* **2018**, *1*, 772–780.

[98] W. Deng, L. Yan, B. Wang, Q. Zhang, H. Song, S. Wang, Q. Zhang, Y. Wang, *Angew. Chemie - Int. Ed.* **2021**, *60*, 4712–4719.

[99] S. G. Wettstein, D. Martin Alonso, E. I. Gürbüz, J. A. Dumesic, *Curr. Opin. Chem. Eng.* **2012**, *1*, 218–224.

[100] R. Rinaldi, F. Schüth, *ChemSusChem* **2009**, *2*, 1096–1107.

[101] A. S. Amarasekara, B. Wiredu, *Ind. Eng. Chem. Res.* **2015**, *54*, 824–831.

[102] V. Popa, V. Irina, *Biomass as Renewable Raw Material to Obtain Bioproducts of High-Tech Value*, **2018**.

[103] C. Tagusagawa, A. Takagaki, A. Iguchi, K. Takanabe, J. N. Kondo, K. Ebitani, S. Hayashi, T. Tatsumi, K. Domen, *Angew. Chemie - Int. Ed.* **2010**, *49*, 1128–1132.

[104] C. Tagusagawa, A. Takagaki, A. Iguchi, K. Takanabe, J. N. Kondo, K. Ebitani, T. Tatsumi, K. Domen, *Chem. Mater.* **2010**, *22*, 3072–3078.

[105] J. N. Kondo, T. Yamashita, K. Nakajima, D. Lu, M. Hara, K. Domen, *J. Mater. Chem.* **2005**, *15*, 2035–2040.

[106] A. Takagaki, C. Tagusagawa, K. Domen, *Chem. Commun.* **2008**, 5363–5365.

[107] F. Zhang, X. Deng, Z. Fang, H. Zeng, X. Tian, J. A. Kozinski, *Petrochemical Technol.* **2011**, *40*, 43–48.

[108] J. Roggenbuck, H. Schäfer, T. Tsoncheva, C. Minchev, J. Hanss, M. Tiemann, *Microporous Mesoporous Mater.* **2007**, *101*, 335–341.

[109] Z. H. Lin, C. J. Guan, X. L. Feng, C. X. Zhao, *J. Mol. Catal. A Chem.* **2006**, *247*, 19–26.

[110] M. T. Sanz, R. Murga, S. Beltrán, J. L. Cabezas, J. Coca, *Ind. Eng. Chem. Res.* **2002**, *41*, 512–517.

[111] N. Hartler, K. Hyllengren, *J. Polym. Sci.* **1962**, *56*, 425–434.

[112] Z. Zhang, Z. K. Zhao, *Carbohydr. Res.* **2009**, *344*, 2069–2072.

[113] R. Rinaldi, R. Palkovits, F. Schüth, *Angew. Chemie - Int. Ed.* **2008**, *47*, 8047–8050.

[114] S. J. Kim, A. A. Dwiatmoko, J. W. Choi, Y. W. Suh, D. J. Suh, M. Oh, *Bioresour. Technol.* **2010**, *101*, 8273–8279.

[115] N. Salman, C. H. Rüscher, J. C. Buhl, W. Lutz, H. Toufar, M. Stöcker, *Microporous Mesoporous Mater.* **2006**, *90*, 339–346.

[116] T. Chen, C. Xiong, Y. Tao, *Molecules* **2018**, *23*, 1–10.

[117] A. Hou, X. Wang, L. Wu, *Carbohydr. Polym.* **2008**, *74*, 934–937.

[118] L. Zhou, M. Shi, Q. Cai, L. Wu, X. Hu, X. Yang, C. Chen, J. Xu, *Microporous Mesoporous Mater.* **2013**, *169*, 54–59.

[119] B. C. Gagea, Y. Lorgouilloux, Y. Altintas, P. A. Jacobs, J. A. Martens, *J. Catal.* **2009**, *265*, 99–108.

[120] F. Guo, Z. Fang, C. C. Xu, R. L. Smith, *Prog. Energy Combust. Sci.* **2012**, *38*, 672–690.

[121] A. E. Pramono, A. Zulfia, J. W. Soedarsono, *J. Mater. Sci. Eng.* **2011**, *5*, 12–19.

[122] E. T. Lu, S. G. Love, *Nature* **2005**, *438*, 177–178.

[123] L. Gan, J. Zhu, L. Lv, *Cellulose* **2017**, *24*, 5327–5339.

[124] S. Suganuma, K. Nakajima, M. Kitano, D. Yamaguchi, H. Kato, S. Hayashi, M. Hara, *J. Am. Chem. Soc.* **2008**, *130*, 12787–12793.

[125] A. V. Nakhate, G. D. Yadav, *ACS Sustain. Chem. Eng.* **2016**, *4*, 1963–1973.

[126] S. Suganuma, K. Nakajima, M. Kitano, D. Yamaguchi, H. Kato, S. Hayashi, M. Hara, *Solid State Sci.* **2010**, *12*, 1029–1034.

[127] D. M. Lai, L. Deng, Q. X. Guo, Y. Fu, *Energy Environ. Sci.* **2011**, *4*, 3552–3557.

[128] F. Shen, T. Guo, C. Bai, M. Qiu, X. Qi, *Fuel Process. Technol.* **2018**, *169*, 244–247.

[129] D. R. Stellwagen, F. Van Der Klis, D. S. Van Es, K. P. De Jong, J. H. Bitter, *ChemSusChem* **2013**, *6*, 1668–1672.

[130] J. M. A. R. Almeida, L. Da Vià, P. Demma Carà, Y. Carvalho, P. N. Romano, J. A. O. Peña, L. Smith, E. F. Sousa-Aguiar, J. A. Lopez-Sanchez, *Catal. Today* **2017**, *279*, 187–193.

[131] A. Onda, T. Ochi, K. Yanagisawa, *Green Chem.* **2008**, *10*, 1033–1037.

[132] T. A. Werpy, J. E. Holladay, J. F. White, *Top Value Added Chemicals From Biomass: I. Results of Screening for Potential Candidates from Sugars and Synthesis Gas*, Richland, WA, **2004**.

[133] IMARC, *Sorbitol Market: Global Industry Trends, Share, Size, Growth, Opportunity & Forecast 2021-2026*, **2021**.

[134] R. Otomo, T. Yokoi, T. Tatsumi, *Appl. Catal. A Gen.* **2015**, *505*, 28–35.

[135] B. Zada, M. Chen, C. Chen, L. Yan, Q. Xu, W. Li, Q. Guo, Y. Fu, *Sci. China Chem.* **2017**, *60*, 853–869.

[136] R. M. Gohil, *Polym. Eng. Sci.* **2009**, *49*, 544–553.

[137] X. Feng, A. J. East, W. B. Hammond, Y. Zhang, M. Jaffe, *Polym. Adv. Technol.* **2011**, *22*, 139–150.

[138] Y. Li, Y. Liao, X. Cao, T. Wang, L. Ma, J. Long, Q. Liu, Y. Xua, *Biomass and Bioenergy* **2015**, *74*, 148–161.

[139] L. Ye, X. Duan, H. Lin, Y. Yuan, *Catal. Today* **2012**, *183*, 65–71.

[140] I. Murillo Leo, M. López Granados, J. L. G. Fierro, R. Mariscal, *Appl. Catal. B Environ.* **2016**, *185*, 141–149.

[141] J. Sun, H. Liu, *Catal. Today* **2014**, *234*, 75–82.

[142] I. M. Leo, M. L. Granados, J. L. G. Fierro, R. Mariscal, *Cuihua Xuebao/Chinese J. Catal.* **2014**, *35*, 614–621.

[143] X. Guo, H. Dong, B. Li, L. Dong, X. Mu, X. Chen, *J. Mol. Catal. A Chem.* **2017**, *426*, 79–87.

[144] H. Schiweck, A. Bär, R. Vogel, E. Schwarz, M. Kunz, in *Ullmann's Encycl. Ind. Chem.*, Wiley-VCH Verlag GmbH & Co. KGaA, Weinheim, Germany, **2000**.

[145] A. Nezzal, L. Aerts, M. Verspaille, G. Henderickx, A. Redl, *J. Cryst. Growth* **2009**, *311*, 3863–3870.

[146] N. Koizumi, M. Fujii, R. Ninomiya, Y. Inoue, T. Kagawa, T. Tsukamoto, *Chemosphere* **1983**, *12*, 117–124.

[147] T. Sugisawa, T. Miyazaki, T. Hoshino, *Biosci. Biotechnol. Biochem.* **2005**, *69*, 659–662.

[148] G. Pappenberger, H. P. Hohmann, *Adv. Biochem. Eng. Biotechnol.* **2013**, *143*, 143–188.

[149] P. Gallezot, P. J. Cerino, B. Blanc, G. Flèche, P. Fuertes, *J. Catal.* **1994**, *146*, 93–102.

[150] B. Kusserow, S. Schimpf, P. Claus, *Adv. Synth. Catal.* **2003**, *345*, 289–299.

[151] S. Schimpf, C. Louis, P. Claus, *Appl. Catal. A Gen.* **2007**, *318*, 45–53.

[152] H. Li, W. Wang, J. Fa Deng, *J. Catal.* **2000**, *191*, 257–260.

[153] K. Van Gorp, E. Boerman, C. V. Cavenaghi, P. H. Berben, *Catal. Today* **1999**, *52*, 349–361.

[154] B. W. Hoffer, E. Crezee, P. R. M. Mooijman, A. D. Van Langeveld, F. Kapteijn, J. A. Moulijn, *Catal. Today* **2003**, *79–80*, 35–41.

[155] E. Crezee, B. W. Hoffer, R. J. Berger, M. Makkee, F. Kapteijn, J. A. Moulijn, *Appl. Catal.*

A Gen. **2003**, *251*, 1–17.

[156] J. Geboers, S. Van de Vyver, K. Carpentier, P. Jacobs, B. Sels, *Chem. Commun.* **2011**, *47*, 5590–5592.

[157] J. W. Han, H. Lee, *Catal. Commun.* **2012**, *19*, 115–118.

[158] Z. Li, Y. Liu, C. Liu, S. Wu, W. Wei, *Bioresour. Technol.* **2019**, *274*, 190–197.

[159] I. A. Ignatyev, C. Van Doorslaer, P. G. N. Mertens, K. Binnemans, D. E. De Vos, *ChemSusChem* **2010**, *3*, 91–96.

[160] Z. Yinghuai, E. Widjaja, S. L. P. Sia, W. Zhan, K. Carpenter, J. A. Maguire, N. S. Hosmane, M. F. Hawthorne, *J. Am. Chem. Soc.* **2007**, *129*, 6507–6512.

[161] J. Zhang, J. Li, S.-B. Wu, Y. Liu, *Ind. Eng. Chem. Res.* **2013**, *52*, 11799–11815.

[162] W. Deng, M. Liu, X. Tan, Q. Zhang, Y. Wang, *J. Catal.* **2010**, *271*, 22–32.

[163] L. Negahdar, J. U. Oltmanns, S. Palkovits, R. Palkovits, *Appl. Catal. B Environ.* **2014**, *147*, 677–683.

[164] D. Wang, W. Niu, M. Tan, M. Wu, X. Zheng, Y. Li, N. Tsubaki, *ChemSusChem* **2014**, *7*, 1398–1406.

[165] M. Liu, W. Deng, Q. Zhang, Y. Wang, Y. Wang, *Chem. Commun.* **2011**, *47*, 9717–9719.

[166] V. Georgakilas, J. A. Perman, J. Tucek, R. Zboril, *Chem. Rev.* **2015**, *115*, 4744–4822.

[167] A. K. Geim, K. S. Novoselov, *Nat. Mater.* **2007**, *6*, 183–191.

[168] H. Marsh, F. Rodríguez-Reinoso, in *Act. Carbon* (Ed.: Elsevier), Elsevier, **2006**, pp. 13–86.

[169] A. Ahmadpour, D. D. Do, *Carbon N. Y.* **1996**, *34*, 471–479.

[170] R. D. Heidenreich, W. M. Hess, L. L. Ban, *J. Appl. Crystallogr.* **1968**, *1*, 1–19.

[171] S. Khodabakhshi, P. F. Fulvio, E. Andreoli, *Carbon N. Y.* **2020**, *162*, 604–649.

[172] J.-B. Donnet, *Carbon Black: Science and Technology, Second Edition*, **1993**.

[173] M. R. Snowdon, A. K. Mohanty, M. Misra, *ACS Sustain. Chem. Eng.* **2014**, *2*, 1257–1263.

[174] J. D. Martínez, N. Cardona-Uribe, R. Murillo, T. García, J. M. López, *Waste Manag.* **2019**, *85*, 574–584.

[175] L. Wang, X. Wang, B. Zou, X. Ma, Y. Qu, C. Rong, Y. Li, Y. Su, Z. Wang, *Bioresour. Technol.* **2011**, *102*, 8220–8224.

[176] L. Fulcheri, F. Fabry, S. Takali, V. Rohani, *Plasma Chem. Plasma Process.* **2015**, *35*, 565–585.

[177] D. D. L. Chung, *Carbon Fibers, Nanofibers and Nanotubes*, **2017**.

[178] F. Silvearv, P. Larsson, S. L. T. Jones, R. Ahuja, J. A. Larsson, *J. Mater. Chem. C* **2015**, *3*,

3422–3427.

[179] M. Meyyappan, L. Delzeit, A. Cassell, D. Hash, *Plasma Sources Sci. Technol.* **2003**, *12*, 205–216.

[180] N. M. Rodriguez, *J. Mater. Res.* **1993**, *8*, 3233–3250.

[181] X. Shui, C. A. Frysz, D. D. L. Chung, *Carbon N. Y.* **1995**, *33*, 1681–1698.

[182] A. V. Melechko, K. L. Klein, J. D. Fowlkes, D. K. Hensley, I. A. Merkulov, T. E. McKnight, P. D. Rack, J. A. Horton, M. L. Simpson, *J. Appl. Phys.* **2007**, *102*, 074314.

[183] I. Martin-Gullon, J. Vera, J. A. Conesa, J. L. González, C. Merino, *Carbon N. Y.* **2006**, *44*, 1572–1580.

[184] B. Ribeiro, E. C. Botelho, M. L. Costa, C. F. Bandeira, *Polimeros* **2017**, *27*, 247–255.

[185] H. C. Lee, W.-W. Liu, S.-P. Chai, A. R. Mohamed, C. W. Lai, C.-S. Khe, C. H. Voon, U. Hashim, N. M. S. Hidayah, *Procedia Chem.* **2016**, *19*, 916–921.

[186] P. Cataldi, A. Athanassiou, I. Bayer, *Appl. Sci.* **2018**, *8*, 1438.

[187] R. J. Young, I. A. Kinloch, L. Gong, K. S. Novoselov, *Compos. Sci. Technol.* **2012**, *72*, 1459–1476.

[188] A. E. Del Rio Castillo, V. Pellegrini, A. Ansaldo, F. Ricciardella, H. Sun, L. Marasco, J. Buha, Z. Dang, L. Gagliani, E. Lago, N. Curreli, S. Gentiluomo, F. Palazon, M. Prato, R. Oropesa-Nuñez, P. S. Toth, E. Mantero, M. Crugliano, A. Gamucci, A. Tomadin, M. Polini, F. Bonaccorso, *Mater. Horizons* **2018**, *5*, 890–904.

[189] J. M. Hilding, E. A. Grulke, *J. Phys. Chem. B* **2004**, *108*, 13688–13695.

[190] H. Terrones, R. Lv, M. Terrones, M. S. Dresselhaus, *Reports Prog. Phys.* **2012**, *75*, 062501.

[191] F. Banhart, J. Kotakoski, A. V. Krasheninnikov, *ACS Nano* **2011**, *5*, 26–41.

[192] S. Berber, A. Oshiyama, *Phys. B Condens. Matter* **2006**, *376–377*, 272–275.

[193] H. F. Bettinger, *J. Phys. Chem. B* **2005**, *109*, 6922–6924.

[194] A. W. Robertson, A. Bachmatiuk, Y. A. Wu, F. Schäffel, B. Rellinghaus, B. Büchner, M. H. Rümmeli, J. H. Warner, *ACS Nano* **2011**, *5*, 6610–6618.

[195] M. R. Axet, O. Dechy-Cabaret, J. Durand, M. Gouygou, P. Serp, *Coord. Chem. Rev.* **2016**, *308*, 236–345.

[196] A. Stein, Z. Wang, M. A. Fierke, *Adv. Mater.* **2009**, *21*, 265–293.

[197] D. Wei, Y. Liu, Y. Wang, H. Zhang, L. Huang, G. Yu, *Nano Lett.* **2009**, *9*, 1752–1758.

[198] P. Singh, S. Campidelli, S. Giordani, D. Bonifazi, A. Bianco, M. Prato, *Chem. Soc. Rev.* **2009**, *38*, 2214–2230.

Chapter II

Hydrogenation of glucose into sorbitol: preliminary study with Ru/CNF catalysts

As mentioned in the introduction, the transformation of cellulose into sorbitol is composed of two different steps: a hydrolysis and a hydrogenation reactions. The first part of this project deals with the second step, namely the hydrogenation of glucose into sorbitol. Catalysts composed of Ru nanoparticles supported on carbon materials are investigated for the production of sorbitol from glucose. The purpose of this chapter is not to maximize sorbitol yield. Indeed, selectivity is more important than yield. In addition, reactions conditions are studied in order to find an operational window that allows comparison between different catalysts. In a second part, optimal Ru nanoparticles size is determined for this reaction, which will be useful for the next chapters.

II.1 Ru nanoparticles supported on CNF: first samples

In order to find the optimal features needed for the hydrogenation of glucose into sorbitol, several catalysts have been prepared on carbon nanofibers (LHT and LHT-OX types). The 'OX' type corresponds to nanofibers that have been oxidized by the manufacturer (Applied Sciences Inc., USA). Two deposition-precipitation methods have been used as described in the Experimental section (Chap. VII).

The method that was used for preparing catalysts with 1 and 3 wt. % of Ru on LHT and LHT-OX is the following: the $RuCl_3$ precursor is rapidly precipitated into $Ru(OH)_3$ by sodium carbonate before being reduced by $NaBH_4$. This method will be called "$NaBH_4$ method" for the rest of this work. As these two synthesis steps are very fast, the Ru nanoparticles are not well dispersed on the carbon support. Moreover the nanoparticles have a wide range of sizes (from 1 nm to 10 nm). This has been confirmed by the TEM images on both samples (Figure II-1), with no notable differences between LHT and LHT-OX supports. Indeed some of the nanofibers are decorated by a lot of nanoparticles while others have just a small number of nanoparticles on their surfaces.

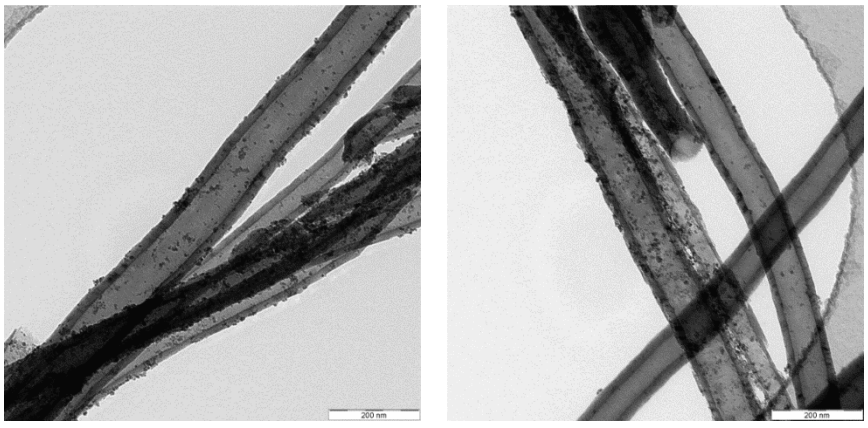

Figure II-1: TEM images of Ru / LHT (on the left) and Ru / LHT-OX (on the right) samples synthesized by the $NaBH_4$ method

II.2 Catalytic tests experimental conditions study

These first unoptimized catalytic materials have been used to study the catalytic conditions by modifying each factor one at a time, in order to determine their influence on selectivity and yield, the former being more important to us than the latter. It should be noted that all the parameters are interconnected so a full statistical analysis using Design-of-Experiment (DoE) methods would be necessary for global optimization. However, the goal here is to find reactions conditions that permit comparison between several catalysts and not to maximize the yield. As substrate and catalysts will change further in this work, a full optimization of the reactions conditions at this point is not necessary. Firstly, duration of the catalytic reaction has been studied (Table II-1). Confidence intervals have been calculated when the same catalytic test has been carried out at least two times, a table with the repeatability is shown in the supporting information (S1 in SI).

Table II-1: Hydrogenation of glucose (1 g) into sorbitol at 160°C and 50 bar of H_2 with Ru (3 wt. %) / LHT-OX (20 mg of catalyst); (Ru / glucose molar ratio = 1 / 935); The estimated confidence interval on glucose conversion and sorbitol selectivity is 7 %

Time (h)	Conversion (%)	Sorbitol selectivity (%)	Yield in sorbitol (%)
2	84	71	60
4.5	98	72	71
6.5	100	65	65
24	100	51	51

Obviously, as the time of the reaction increases, the conversion of glucose is getting higher and reaches 100 % after 6.5h. However, the selectivity in sorbitol is decreasing with time. Indeed it is known that catalysts with Ru as active phase can further transform sorbitol into side products, such as sorbitan, isosorbide[1] or glycols[2]. A too long reaction time will favorize the side reactions at this temperature. A list of molecules that have

been injected in HPLC and that can be ruled out from possible side products can be found in supporting information (S2 in SI).

Secondly, the influence of the temperature was studied, and results obtained can be found in Table II-2.

Table II-2: Hydrogenation of glucose (1 g) into sorbitol at 50 bar of H_2 during 2h with Ru (3 wt. %) / LHT-OX (20 mg of catalyst); (Ru / glucose molar ratio = 1 / 935); The estimated confidence interval on glucose conversion and sorbitol selectivity is 7 %

Temperature (°C)	Conversion (%)	Sorbitol selectivity (%)	Yield in sorbitol (%)
130	30	98	29
140	55	95	52
150	78	87	68
160	84	71	60

A double effect of the temperature influence can be observed. When the temperature is higher the conversion is increasing because glucose can react faster. But this enhancement of the reaction rate is also happening for the side reactions and a decrease of the selectivity in sorbitol is the direct consequence of this effect. Therefore a compromise will need to be found.
The third important factor for this hydrogenation reaction is the H_2 pressure (Table II-3).

Table II-3: Hydrogenation of glucose (1 g) into sorbitol at 160°C during 2h with Ru (3 wt. %) / LHT-OX (20 mg of catalyst); (Ru / glucose molar ratio = 1 / 935); The estimated confidence interval on glucose conversion and sorbitol selectivity is 7 %

H_2 pressure (bar)	Conversion (%)	Sorbitol selectivity (%)	Yield in sorbitol (%)
20	62	57	35
30	77	67	52
40	78	72	56
50	84	71	60

The impact of the H_2 pressure on the reaction is less important than for the temperature but an increase in both conversion and selectivity in

sorbitol can be noticed with higher H_2 pressure. With higher pressure, more H_2 will be solubilized in water[3] and then more H_2 available for the hydrogenation. However, due to the experimental error, results obtained for 30, 40 and 50 bars of H_2 can be considered similar. Therefore, 30 bar of H_2 has been chosen for the following experiments as it will consume less H_2 for the same result.

The last parameter that has been investigated is the quantity of Ru on the support. Four catalysts have been tested: 1 wt. % of Ru and 3 wt. % of Ru on both LHT and LHT-OX supports (Table II-4).

Table II-4: Hydrogenation of glucose (1 g) into sorbitol at 160°C and 50 bar of H_2 during 2h with Ru on CNF catalysts presenting different mass loadings (20 mg of catalyst); (Ru / glucose molar ratio = 1 / 935 for 3 wt. % and 1 / 2805 for 1 wt. % catalysts, respectively); The estimated confidence interval on glucose conversion and sorbitol selectivity is 7 %

Catalyst	Conversion (%)	Sorbitol selectivity (%)	Yield in sorbitol (%)
Ru (1 wt. %) / LHT	58	48	28
Ru (1 wt. %) / LHT-OX	69	66	46
Ru (3 wt. %) / LHT	84	71	60
Ru (3 wt. %) / LHT-OX	85	77	65

Both conversion and selectivity in sorbitol are positively impacted by the increase in Ru amount on the carbon support. Indeed it is obvious that when there is more Ru available, the reaction will be done faster. It is also important to highlight the better results for the catalysts supported on LHT-OX instead of LHT. The comparison between these two supports will be done in more depth in the next section.

In conclusion, the first synthesized catalysts have allowed us to study the catalytic testing experimental conditions of this catalytic reaction. The following conditions have been chosen for the next part of this study: 140 °C, 30 bar of H_2 and 2 hours of reaction time, as a compromise between the

influences of these various parameters. These conditions will limit side-products formation and will give lower conversion making comparison between catalysts easier.

II.3 Nanoparticles size optimization

After exploring the catalytic testing conditions, optimization of the synthesis of the catalysts is still needed as it has been shown that a poor dispersion with various particle sizes had been obtained with the $NaBH_4$ method. A 'softer' synthesis has been chosen where first the $RuCl_3$ is precipitated on the carbon support by urea degradation at 120 °C [4]. This urea degradation is occurring slowly and allows a good dispersion of the $Ru(OH)_3$ species on all the support surface. Then, sodium formate is added to reduce the Ru. This second method, that will be called "urea method" in the rest of this chapter, has been applied on both LHT and LHT-OX supports. In both cases, an excellent dispersion is obtained and very small nanoparticles size, around 1 nm, are visualized by TEM (see Figures II-2 (a) and II-3 (a)). Several TEM images have been taken for each sample and the images shown in Figures II-2 and II-3 are representative of each catalyst.

A post-treatment at different temperatures under H_2/Ar (5/95) mix was carried out to promote controlled coalescence and obtain nanoparticles of different sizes. This treatment has been conducted at 600 °C, 900 °C and 1200 °C. The four catalysts supported on LHT have been observed by TEM (Figure II-2). Without any heating, the nanoparticles have an average size of less than 1 nm (standard deviation of 0.4 nm) (Fig. II-2 (a)). After thermal treatment at 600 °C, the size is growing to 1-2 nm (standard deviation of 0.6 nm) (Fig. II-2(b)). At 900 °C, nanoparticles between 2 and 5 nm have been obtained (standard deviation of 1.0 nm) (Fig. II-2(c)). Finally at 1200 °C, the

nanoparticles size ranges from 5 nm to 10 nm (standard deviation of 1.8 nm) (Fig. II-2(d)).

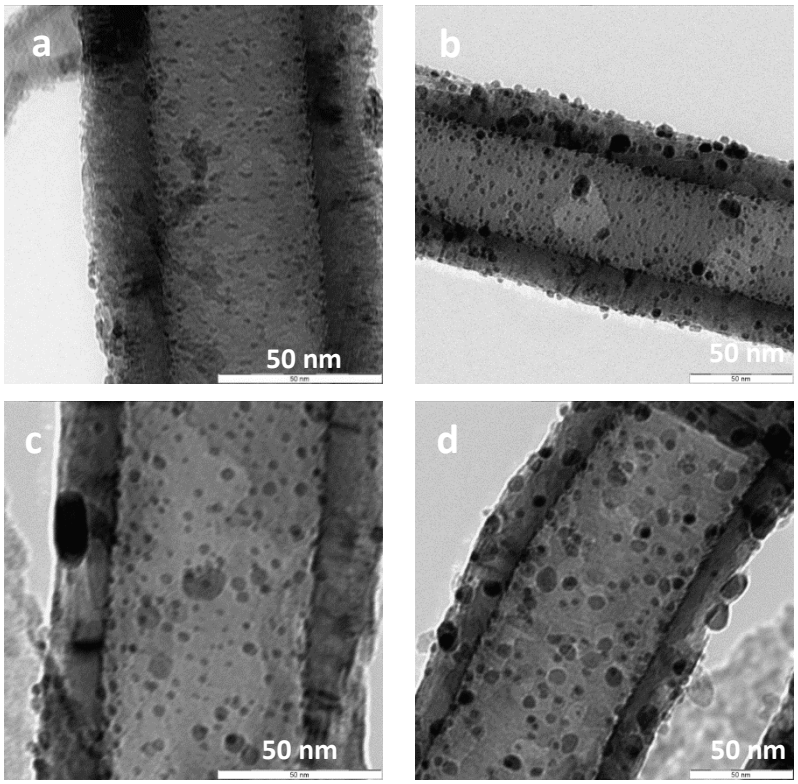

Figure II-2: TEM images of Ru (3 wt. %) / LHT samples synthesized by the urea method: a) without post-treatment; b) heat-treatment at 600 °C; c) heat-treatment at 900 °C; d) heat-treatment at 1200 °C

The same methodology has been conducted on LHT-OX and the four catalysts obtained are presented in Figure II-3. Without any heating, the nanoparticles also have an average size of less than 1 nm (standard deviation of 0.3 nm) (Fig. II-3 (a)). After thermal treatment at 600 °C, the nanoparticles size is included between 1 and 2 nm (standard deviation of 0.5 nm) (Fig. II-3 (b)). At 900 °C nanoparticles between 2 and 5 nm (standard deviation of 1.1 nm) have been observed (Fig. II-3 (c)). Finally at 1200 °C,

nanoparticles from 5 nm to 10 nm (standard deviation of 1.6 nm) have been obtained (Fig. II-3 (d)).

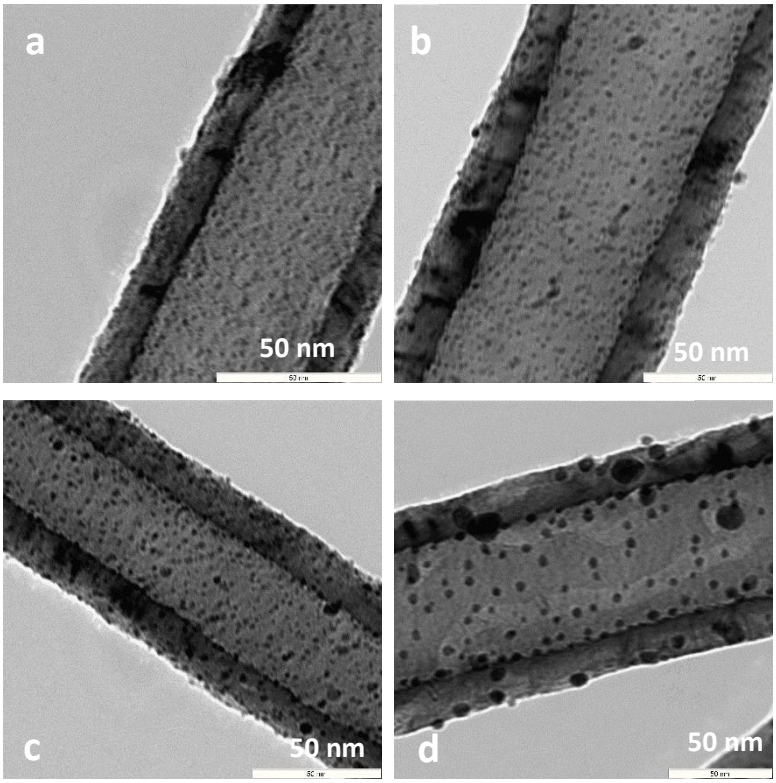

Figure II-3: TEM images of Ru (3 wt. %) / LHT-OX samples synthesized by the urea method: a) without post-treatment; b) heat-treatment at 600 °C; c) heat-treatment at 900 °C; d) heat-treatment at 1200 °C

It is interesting to note that these carbon nanofibers stabilize very well the nanoparticles. Indeed, even at high temperature, sintering is low and relatively small nanoparticles are kept and, more importantly, remain nicely distributed over the entire carbon surface. It is known that Ru has not a strong tendency of growing into large particles. But in the literature, Ru nanoparticles of over 10 nm are obtained after a heat-treatment at only 500 °C can be found[5]. The fact that the same size is obtained after a treatment at 1200 °C shows that the CNFs are decreasing the sintering

phenomena. This is probably due to the effect of the edges of carbon planes present on their surfaces, which can act as 'pincers' for metal nanoparticles[6]. The path taken by the big nanoparticles during their coalescence can be tracked on the TEM images (Figure II-3(d)).

All these catalysts have been characterized by XPS (Table II-5). For catalysts supported on both LHT and LHT-OX the same decrease of Ru/C atomic ratio, when comparing samples with increasing heat-treatment, is observed. Indeed, as the Ru nanoparticles size increases, not all the Ru is analyzed by XPS anymore, because the analysis depth is around 6 nm. Indeed, in the case of carbon support it can be calculated that 95 % of the signal is coming from the first 6 nm of the sample[7] (more details can be found in the Experimental section, Chap. VII). Moreover, the Ru/C ratio is systematically higher when considering samples prepared at the same temperature, for the catalysts supported on LHT-OX, which confirms that LHT-OX seems to stabilize small nanoparticles more than LHT. Finally, the position of the Ru peak is shifted from 463.5 eV to 461.5 eV after heating under the H_2/Ar (5/95) mix. It means that there is an effective reduction of the Ru during the heat-treatment and that the sodium formate used during the synthesis is not strong enough because Ru is still oxidized at the end (at least on the surface).

Table II-5: Ru/C atomic ratios measured by XPS and results from the hydrogenation of glucose into sorbitol at 140 °C under 30 bar of H_2 during 2 h with 20 mg of catalyst (Ru 3 wt. %) and 1 g of glucose; (Ru / glucose molar ratio = 1 / 935); The estimated confidence interval on glucose conversion and sorbitol selectivity is 7 %

Catalyst	Thermal treatment	Ru/C at. ratio (XPS)	Glucose conversion (%)	Selectivity in sorbitol (%)	Yield in sorbitol (%)
Blank	/	/	**9**	**41**	**4**
LHT	/	/	**10**	**15**	**2**
Ru / LHT	/	0.0086	**40**	**80**	**32**
Ru / LHT	600 °C	0.0043	**33**	**38**	**13**
Ru / LHT	900 °C	0.0021	**12**	**81**	**10**
Ru / LHT	1200 °C	0.0034	**4**	**80**	**3**
LHT-OX	/	/	**14**	**23**	**3**
Ru / LHT-OX	/	0.0213	**57**	**78**	**44**
Ru / LHT-OX	600 °C	0.0078	**74**	**84**	**62**
Ru / LHT-OX	900 °C	0.0060	**62**	**83**	**51**
Ru / LHT-OX	1200 °C	0.0038	**14**	**41**	**6**

These catalysts have been tested in the hydrogenation of glucose into sorbitol. The results are presented in Table II-5. First, it can be observed that Ru is improving both conversion and selectivity towards sorbitol even when it is not reduced before the reaction; indeed Ru can be reduced in situ during the catalytic test by the H_2 atmosphere. This is concluded based on comparisons with blank test (without any catalyst) and tests involving the bare supports. Second, it can be noticed that the oxidized nanofibers are better supports than the non-oxidized ones. For all nanoparticles sizes, Ru is more active when it is deposited on oxidized nanofibers (LHT-OX). Finally, the conversion is different depending on the nanoparticles size and the maximum of sorbitol yield is obtained with Ru/LHT-OX reduced at 600 °C. It means that small nanoparticles are more active for the hydrogenation of

glucose into sorbitol and that the optimal nanoparticles size is around 1-2 nm. It can be observed that there is no link between the activity and the O amount measured by XPS within the samples (Figure II-4). Moreover, it is surprising to see that the oxygen atomic percentage is not always decreasing when temperature of the treatment is increasing. Experimental error seems to be consequent for these XPS analyses, at least for several samples. Nevertheless, the differences of yield can be attributed solely to the different nanoparticles sizes and not to the removal of some oxygenated functions during heat-treatment.

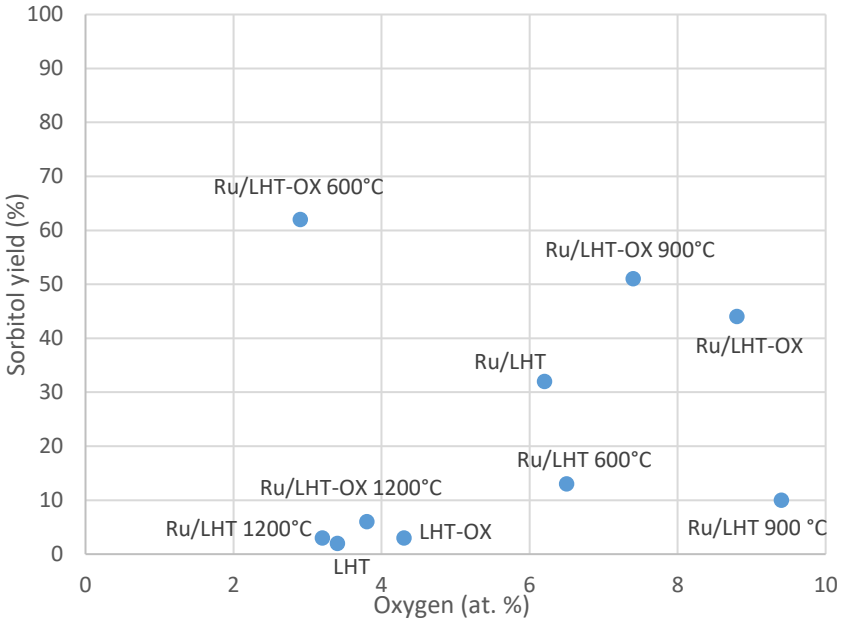

Figure II-4: Yield in sorbitol as a function of oxygen atomic percentage determined by XPS for each catalyst supported on LHT and LHT-OX

The same methodology was applied to the two other carbonaceous supports considered later in this work, namely activated coal (AC) and graphene nanoplatelets (GNP-C750). Ru was deposited on the solid surface and then heat-treated at different temperatures (TEM images are presented

in Figure II-5). The Ru nanoparticles are less visible due to the nature of those supports and the low contrast given by their thickness. It can nevertheless be observed that sintering is higher on GNP-C750 than on AC and CNF. The optimal nanoparticles size of 1-2 nm has been obtained at 600 °C on AC and at 400 °C on GNP (against 600 °C on CNF). Larger nanoparticles can be noticed on GNP after heat-treatment at 600 °C (between 5 and 10 nm). These results have been corroborated by catalytic tests performed at 160 °C under H_2 during 2h. Sorbitol yields of 28 %, 27 % and 0 % have been respectively obtained for Ru/AC heat-treated at 600 °C, Ru/GNP heat-treated at 400 °C and at 600 °C. Comparison with results displayed in Table II-5 is not ideal because the reaction temperature is not the same. Nevertheless, this highlights once more the stabilizing effect of AC and CNFs on the Ru nanoparticles, and the optimal nanoparticles sizes for this reaction.

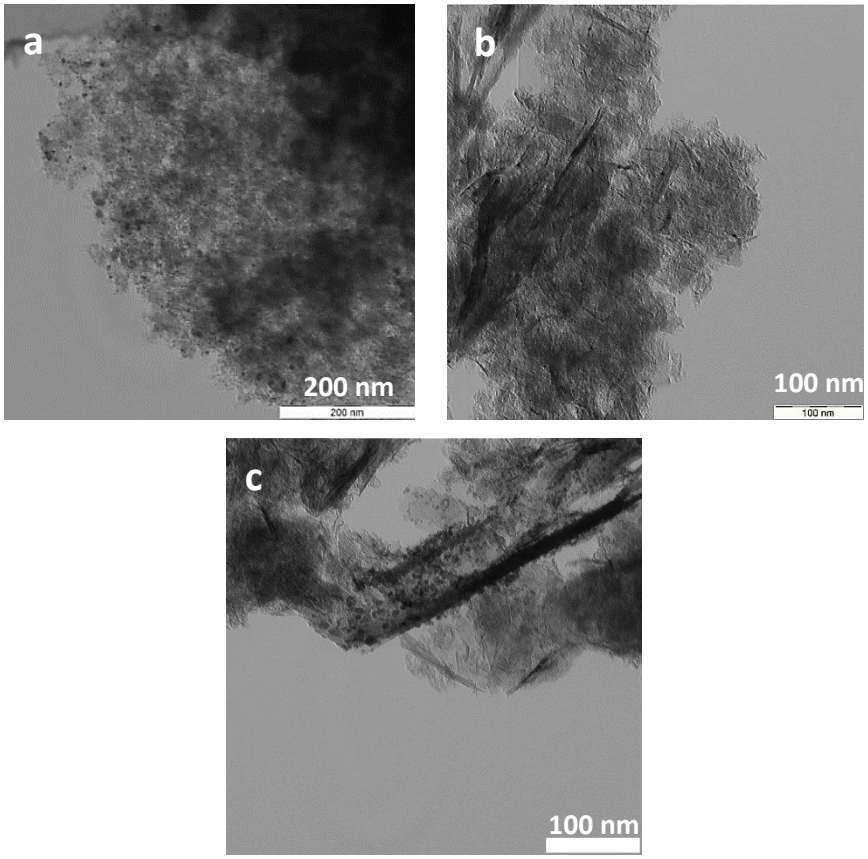

Figure II-5: TEM images of Ru nanoparticles deposited by the urea method on (a) AC and heated at 600 °C; on (b) GNP (C750) and heated at 400 °C and on (c) GNP (C750) and heated at 600 °C

Comparison of the best result obtained for sorbitol production from glucose with our Ru (3 wt. %) / LHT-OX catalyst with literature data can be found in Table II-6. Globally, all catalysts found in literature are displaying excellent glucose conversion and excellent sorbitol selectivity with reaction conditions that are quite similar to ours. However, a huge difference can be found when looking at the catalyst / glucose mass ratio. The quantity of catalyst introduced in our work is very low compared to glucose mass. This can explain the lower sorbitol yield in our work. However, when sorbitol production is normalized per gram of catalyst, it is observed that our catalyst is displaying one of the highest sorbitol production rate. Nevertheless, as said before, the reaction conditions in this chapter have been chosen to be able to compare our catalysts and not to maximize the sorbitol yield.

Table II-6: Comparison of hydrogenation of glucose into sorbitol from literature reports and our work (last line)

Catalyst	Catalyst / Glucose mass ratio	H_2 Pressure (bar)	Temperature (° C)	Time (h)	Glucose conversion (%)	Selectivity in sorbitol (%)	Yield in sorbitol (%)	Mol of sorbitol / g of catalyst	Ref.
Ru (1 wt. %) / ZSM-5	1 / 25	40	120	2	99	99	99	0.1374	[8]
Ni (40 wt. %) / ZSM-5	1 / 2	40	240	4	99	77	76	0.0084	[9]
Ru (4 wt. %) / SiO_2	1 / 1.68	25	120	0.42	90	100	90	0.0084	[10]
Ru (4 wt. %) / TiO_2	1 / 1.68	25	120	0.33	91	100	91	0.0085	[10]
Ru (5 wt. %) / AC	1 / 2.1	25	120	0.17	95	100	95	0.0111	[10]
Ru (3 wt. %) / AC	1 / 2.33	16	180	3	100	89	89	0.0115	[11]
Pt (3 wt. %) / AC	1 / 2.33	16	180	3	97	91	88	0.0114	[11]
Ru (1 wt. %) / HY zeolite	1 / 40	55	120	2	100	99	99	0.2198	[12]
Ru (5 wt. %) / SiO_2	1 / 10	30	120	2	99	84	83	0.0461	[13]
Ru (5 wt. %) / polymer	1 / 20	55	100	1	69	98	68	0.0755	[14]
Ru (5 wt. %) / C (cassava dregs)	1 / 10	30	120	2	100	98	98	0.0544	[15]
Ru (3 wt. %) / CNF	1 / 50	30	140	2	74	84	62	0.1721	Our work

II.4 Conclusion

Two methods of Ru/CNF catalyst preparation have been studied in this chapter. The $NaBH_4$ method has given poor dispersion with very variable nanoparticles sizes while the urea method has given very good dispersion of small nanoparticles, around 1 nm in diameter. Parameters for the catalytic reaction have been studied one by one in order to observe which factor influences sorbitol selectivity and in which direction. High temperature and long reaction time must be avoided to keep a high selectivity in sorbitol. Moreover, reaction conditions suitable for comparisons between catalysts have been chosen: 140 °C under 30 bar of H_2 during 2 h. These conditions are not giving full glucose conversion with complete sorbitol selectivity and permit to see differences between catalysts. Optimization of reaction conditions to maximize sorbitol productivity will be performed later in this work when final substrates and catalysts will be studied in detail.

The optimal nanoparticles size has been also investigated and it was shown that small nanoparticles between 1 and 2 nm are the most efficient for the hydrogenation of glucose into sorbitol. The CNF supports and especially the LHT-OX have shown high stabilization of the nanoparticles. Indeed, even at 1200 °C, the Ru nanoparticles have grown to only 10 nm in diameter. Finally, the urea method has been applied to two other carbon supports, namely AC and GNP. The GNP has stabilized the nanoparticles less than the LHT-OX and a temperature of 400 °C was sufficient to obtain nanoparticles between 1 and 2 nm on this support. Higher temperature led to larger and less active Ru nanoparticles. However AC seems to stabilize nanoparticles the same way as LHT-OX does: a heat-treatment at 600 °C has also given nanoparticles of 1-2 nm. This first study about Ru nanoparticles supported on carbon supports will be the starting point of the next chapter

dedicated to the N-doping of carbon materials and its effect on catalyst preparation and performance.

References

[1] J. Zhang, J. Li, S.-B. Wu, Y. Liu, *Ind. Eng. Chem. Res.* **2013**, *52*, 11799–11815.

[2] I. M. Leo, M. L. Granados, J. L. G. Fierro, R. Mariscal, *Cuihua Xuebao/Chinese J. Catal.* **2014**, *35*, 614–621.

[3] C. Ziparo, A. Giannasi, L. Ulivi, M. Zoppi, *Int. J. Hydrogen Energy* **2011**, *36*, 7951–7955.

[4] T. Haynes, V. Dubois, S. Hermans, *Appl. Catal. A Gen.* **2017**, *542*, 47–54.

[5] W. Deng, M. Liu, X. Tan, Q. Zhang, Y. Wang, *J. Catal.* **2010**, *271*, 22–32.

[6] S. Hermans, J. Sloan, D. S. Shephard, B. F. G. Johnson, M. L. H. Green, *Chem. Commun.* **2002**, *2*, 276–277.

[7] M. J. Genet, C. C. Dupont-Gillain, P. G. Rouxhet, in *Med. Appl. Colloids* (Ed.: E. Matijevic), Springer New York, New York, NY, **2008**, pp. 177-307 (Chap 5).

[8] X. Guo, X. Wang, J. Guan, X. Chen, Z. Qin, X. Mu, M. Xian, *Cuihua Xuebao/Chinese J. Catal.* **2014**, *35*, 733–740.

[9] G. Liang, L. He, H. Cheng, W. Li, X. Li, C. Zhang, Y. Yu, F. Zhao, *J. Catal.* **2014**, *309*, 468–476.

[10] A. Romero, E. Alonso, Á. Sastre, A. Nieto-Márquez, *Microporous Mesoporous Mater.* **2016**, *224*, 1–8.

[11] P. A. Lazaridis, S. Karakoulia, A. Delimitis, S. M. Coman, V. I. Parvulescu, K. S. Triantafyllidis, *Catal. Today* **2015**, *257*, 281–290.

[12] D. K. Mishra, A. A. Dabbawala, J. J. Park, S. H. Jhung, J. S. Hwang, *Catal. Today* **2014**, *232*, 99–107.

[13] J. Zhang, L. Lin, J. Zhang, J. Shi, *Carbohydr. Res.* **2011**, *346*, 1327–1332.

[14] A. A. Dabbawala, D. K. Mishra, J. S. Hwang, *Catal. Today* **2016**, *265*, 163–173.

[15] Z. Li, Y. Liu, S. Wu, *BioResources* **2018**, *13*, 1278–1288.

Chapter III

N-doped carbon materials as supports for Ru nanoparticles

In this Chapter, nitrogen doping of carbon materials is studied. This incorporation is carried out by using nitrogen-rich precursors such as urea or ethylenediamine that are impregnated onto carbonaceous solids followed by heat treatment. The newly formed nitrogen functions are mainly characterized by Boehm titration and XPS in order to assess their nature and their number. The purpose of this nitrogen doping is to enhance the Ru/C catalysts by improving Ru nanoparticles dispersion and promoting the Ru activity. The activity of these catalysts on N-doped carbon materials are investigated in this Chapter by transforming cellobiose directly into sorbitol.

III.1 N-doped carbon materials synthesis

Carbon materials modification by nitrogen doping has been widely studied in recent years. Nitrogen doping can induce n-type electronic modifications of the carbon structure[1]. Therefore, it can enhance Ru activity for hydrogenation reactions. Moreover, nitrogen incorporation can increase basicity of the carbon materials and could have a positive effect on cellobiose or cellulose hydrolysis. The main goal of this Chapter is to study the influence of N-doping on hydrogenation activity of Ru nanoparticles.

The incorporation of nitrogen atoms within the carbon lattice of different carbon materials has been carried out with two methods. The first one has been called “urea impregnation”. The idea was to mix urea and the carbon material in same quantities (1 g of each for example) in a solvent. After solvent evaporation, the urea molecules adsorb preferentially on the surface of the solid forming weaker (electrostatic or van der Waals) interactions or stronger covalent bonds with the oxygenated functions. Finally a heat treatment was applied to decompose the adsorbed urea and introduce nitrogen atom within the carbon structure.

This method has been applied onto three different supports: activated coal (AC), carbon nanofibers (LHT-OX) and carbon black (CB). Results for the N-functionalization of those carbon materials are displayed in Table III-1. XPS analyses have been carried out to confirm whether nitrogen atoms are indeed incorporated in the carbon materials. The N/C atomic ratios for the samples that have not been submitted to heat-treatment is high, indicating that urea had been deposited as expected. As soon as the heat treatment has been applied, the N/C ratio drops drastically to a value close to the pristine material. This indicates that all the urea is decomposed even at low temperature, highlighting the weak interactions between urea and the carbon material. Boehm titrations for the basic functions have been

also conducted on the different carbon materials. Indeed as nitrogen should be introduced within the carbon lattice, basic functions such as pyridine, pyrrole or amines would appear (see Scheme I-10 in General Introduction, Chap. I) and the basicity of the carbon material would increase. This basic character can be determined by such back-titration method. The quantification of the basic sites can inform us on the amount of nitrogen incorporated in the carbon materials, and give a hint on the type of functionalities, as aromatic N-heterocycles are stronger bases than dangling aliphatic amines for example.

Table III-1: Basicity from Boehm titration and atomic ratios determined by XPS for the pristine and the N-functionalized supports; The estimated confidence interval on basicity is 10 %

Carbon	Thermal treatment (°C)	O/C atomic ratio (XPS)	N/C atomic ratio (XPS)	Basicity (mmol/100g)
AC	/	0.041	0.003	24
AC + adsorbed urea	/	0.080	0.040	/
AC + adsorbed urea	500	0.030	0.008	46
AC + adsorbed urea	900	0.014	0.008	43
Oxidized AC	/	0.135	0.006	5
Oxidized AC + adsorbed urea	500	0.073	0.042	30
LHT-OX	/	0.035	0.002	9
LHT-OX+ adsorbed urea	500	0.004	n.d.	10
CB	/	0.043	0.005	3
CB + adsorbed urea	500	0.016	n.d.	0

n.d. = non detected

The support that has not endured the heat treatment has not been titrated as the urea that was physisorbed on the surface of the carbon would simply desorb in the titrating aqueous medium. Basicity has doubled for the AC samples heat-treated at 500 °C and 900 °C compared to the starting

material. It indicates that the functionalization is successful even if the nitrogen at. % measured by XPS is really low. As the urea molecules could also react specifically with surface oxygenated functions (Scheme III-1), resulting in an increased incorporation, AC sample has been oxidized as well prior to urea impregnation (see Experimental Section). However, direct reaction between urea and the oxygenated functions is difficult and most urea will be mainly adsorbed on the carbon surface. In the case of oxidized AC, a drop of basicity can be witnessed after oxidation which is carried out with HNO_3. After urea adsorption, an increase of basicity can be observed and this increase is similar to the increase observed for non-oxidized AC. Moreover, the N/C ratio measured by XPS on oxidized AC is higher after the urea impregnation, indicating that the functionalization is also effective on oxidized AC (same increase of 20 mmol / 100 g of basicity).

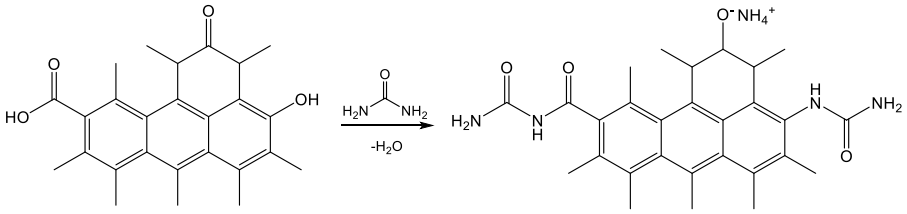

Scheme III-1: Possible reactions between urea and carbon oxygenated surface groups

Results for the functionalization of LHT-OX and CB have been disappointed as the basicity did not increase and no nitrogen was detected by XPS.

As the “urea impregnation” method did not show good results, it was not investigated further. However, a second functionalization method has been studied, using ethylenediamine (EDA). The first step is a nitric acid oxidation to promote carboxylic acid groups formation on the surface of the carbon support. These carboxylic acid groups are subsequently transformed

into acyl chlorides. Then, the chlorine is replaced by EDA (Scheme III-2). Finally, the heat treatment will decompose EDA and incorporate the nitrogen atoms within the carbon supports lattice. The final samples after the heat-treatment will be named "N-doped" followed by the type of carbons for the rest of this chapter.

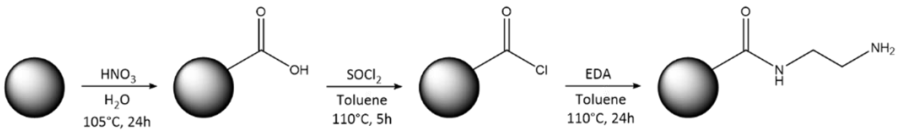

Scheme III-2: Functionalization of carbon materials with ethylenediamine

Three types of carbon supports were treated this way: carbon nanofibers (LHT-OX), activated coal (AC) and graphene nanoplatelets (GNP-C750 which will be named GNP in this chapter).

These functionalized materials have been characterized by Boehm titration and XPS (O/C and N/C ratios) at each step of their preparation (Table III-2). LHT-OX could not be oxidized further with HNO_3, as it is already the oxidized form of LHT nanofibers. It can be seen (Table III-2) that the O/C ratio measured by XPS was not increased after the oxidation of LHT-OX whereas it has been highly improved after oxidation of AC and GNP.

Obviously, nitric acid treatment causes a decrease in basicity measured by titration. It can be noticed that, in the next step, the incorporation of EDA is increasing nitrogen content and basicity of the carbons. After the heat-treatment, these dangling amine functions will mainly be destroyed and a small portion of the nitrogen will be inserted in the structure of the carbon support and form nitrogenated heterocycles. This is witnessed by the decrease of N/C ratio. The increase of basicity after heat-treatment for AC can be explained also by the decomposition of oxygenated functions that creates active sites at the edges of carbon material which will attract oxygen, when exposed to air, to form basic functions such as

chromene and pyrone [2]. Moreover, heat-treatment can also create more defects on AC surface and increase its basicity by producing dangling bonds at the edges of carbon surface, as explained in section I.6.5 in the Introduction[3].

Table III-2: Basicity from Boehm titration and atomic ratios determined by XPS for the pristine materials and the supports functionalized by the EDA method; The estimated confidence interval on basicity is 10 %

Carbon	Thermal treatment (°C)	O/C atomic ratio (XPS)	N/C atomic ratio (XPS)	Basicity (mmol/100g)
LHT-OX	/	0.035	0.002	0
Oxidized LHT-OX	/	0.020	0.002	0
EDA-LHT-OX	/	0.026	0.017	10
N-doped LHT-OX	700	0.018	0.008	0
AC	/	0.041	0.003	24
Oxidized AC	/	0.135	0.006	5
EDA-oxidized AC	/	0.160	0.111	46
N-doped oxidized AC	900	0.055	0.035	91
GNP	/	0.063	0.000	31
EDA-GNP	/	0.051	0.043	102
N-doped GNP	900	0.025	0.008	61
Oxidized GNP	/	0.258	0.004	0
EDA-oxidized GNP	/	0.095	0.077	167
N-doped oxidized GNP	900	0.018	0.014	81

It is also pointed out that pre-oxidized GNP are more N-functionalized than the pristine GNP even though GNP display more O-group than the other supports at the start (Boehm acidity for pristine GNP: 228 mmol/100g). The final basicity and the amount of nitrogen are both higher for the pre-oxidized material. This is explained by the need for carboxylic acid functions to attach the EDA on the support (Scheme III-2).

The amount of nitrogen on the surface of the functionalized carbons determined by XPS analyses is varying the same way than the basicity determined by Boehm titration (Figure III-1), confirming the link between these two factors and the incorporation of nitrogen. Strikingly, the final sample of CNF has incorporated very low levels of N and displayed no basicity. This carbon support was therefore discarded for the following steps.

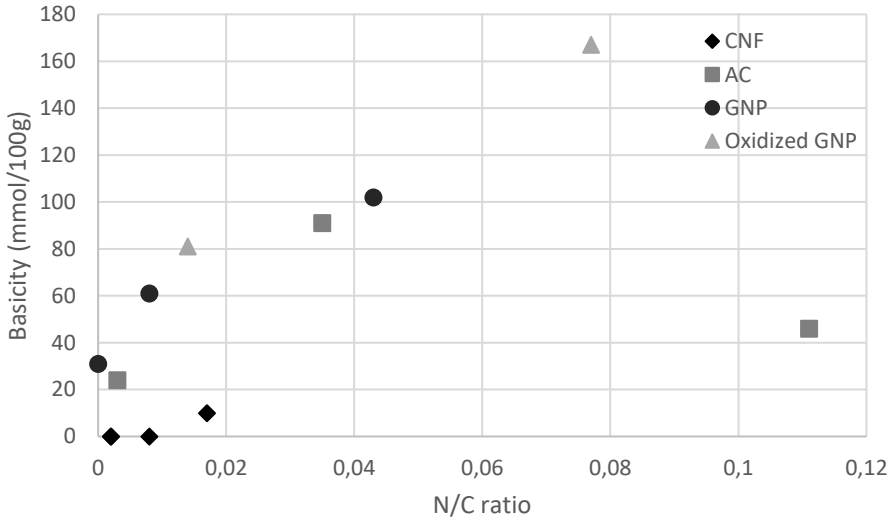

Figure III-1: Basicity determined by Boehm titration as a function of N/C ratio obtained by XPS

Depending on the type of nitrogen functions present on the support, nitrogen peaks (N1s) obtained by XPS analyses will appear at different binding energies. After grafting EDA but before heat-treatment, a majority of terminal amine functions (NH_2 peak at 400 eV) are present, as expected. After the heat treatment, nitrogen enters within the carbon structure and functions such as pyridine or pyrrole appear, as confirmed by increase of the peak at 398.6 eV in the XPS spectrum of N-doped GNP and N-doped AC (Figure III-2). This peak arises from a family of functions (pyridine/pyrrole) because of the impossibility to decompose more the nitrogen peak to separate finely all types of nitrogen functions. It is therefore possible to

quantify the amount of pyridine/pyrrole functions versus amine functions. Before heat-treatment, almost 80 % of amines functions are present. After heat treatment, less total amount of nitrogen can be observed but the ratio between amine functions and pyridine/pyrrole functions is around 50/50 (in at. %). This indicates that the heat-treatment is promoting formation of pyridine/pyrrole functions which is interesting because these functions are more stable and stronger basic sites than amine functions.

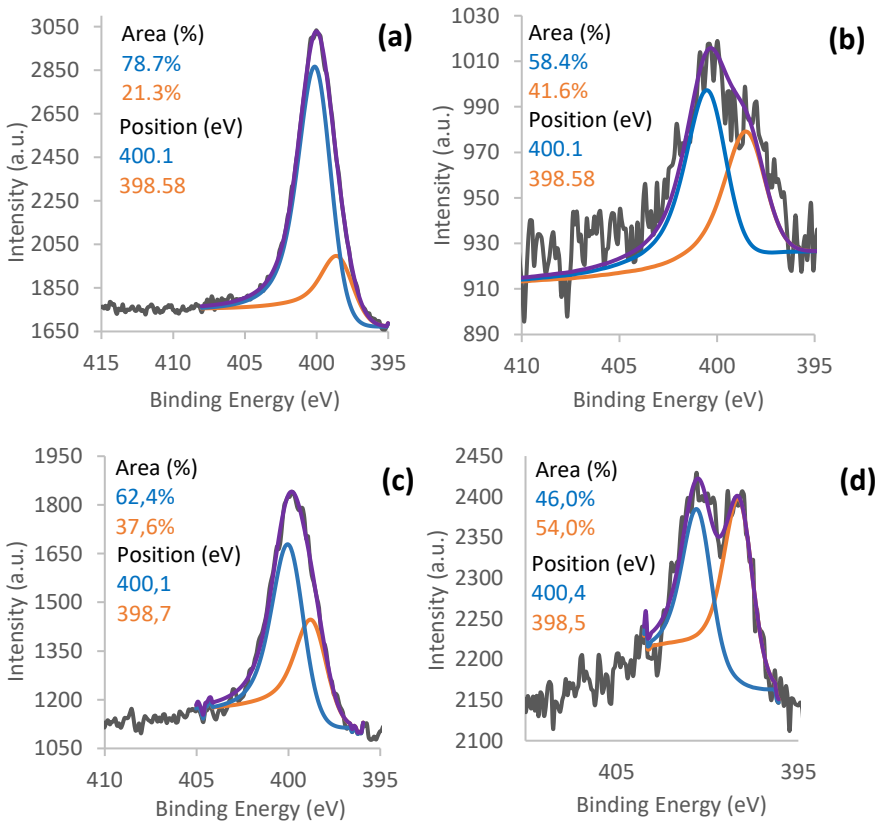

Figure III-2: N1s peaks (in blue: amine; in orange: pyridine/pyrrole) from XPS analyses of (a) N-doped GNP before heat-treatment (b) N-doped GNP after heat treatment at 900 °C (c) N-doped AC (non-oxidized) before heat-treatment (d) N-doped AC (non-oxidized) after heat-treatment at 900 °C

CO_2-TPD analyses have been carried out on the N-doped supports to confirm the presence of basic sites. The TPD analyses for the N-doped AC are

presented in Figure III-3. TPD analyses for the N-doped GNPs can be found in the supporting information (S3 in SI). For the N-doped activated coal, the basicity amounts to 63 mmol/100g if the first CO_2 desorption peak is considered (starting at 200 °C) together with the main contribution at 750 °C. It is interesting to link this measure to the result obtained by Boehm titration on the same sample (Table III-2). Both results are in the same order of magnitude but slightly different (63 vs 91). For GNPs, the difference is more pronounced (21 vs 81) with also a higher figure for basicity measured by Boehm titration. It is important to point out that the amount of CO_2 desorbed variates with the temperature at which the saturation is carried out [4].

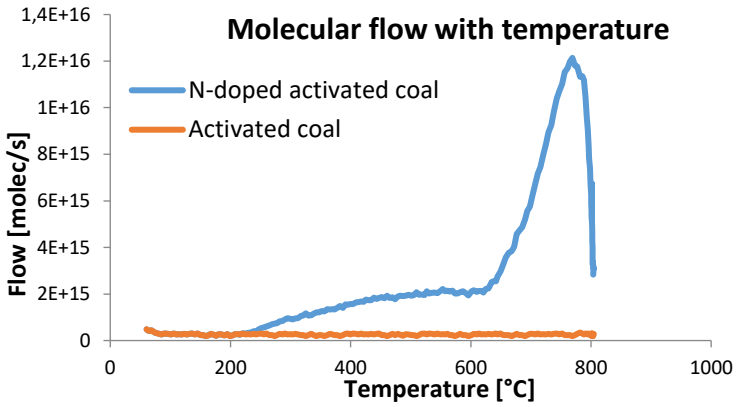

Figure III-3: Molecular flow of CO_2 as a function of the temperature for activated coal and N-doped activated coal

At 50 °C, even the weakest sites adsorb the probe molecule that will then be quantified during the desorption. This slight difference could also come from the hypothesis that one CO_2 molecule was adsorbed on each basic site whereas the reality might be that two close basic sites adsorb only one molecule, underestimating the number of basic sites determined by TPD. In addition, the main peak seems to extend above 800 °C, which could not be measured with our instrument. This difference in basicity can also be the result of the short pre-treatment of samples required for TPD analyses. As a

decrease of basicity by XPS and Boehm titration has already been noticed after the heat treatment of EDA-AC or EDA-GNP, this pre-treatment at 850°C could also have the same impact but the type of functions should not be much different. Nevertheless, it can be firmly concluded that the sample contains basic sites that are stable at temperatures up to 200 °C. A higher stability is not needed as biomass transformation is carried out in water and thus never exceeds this limit.

III.2 Ru nanoparticles deposition on N-doped carbon supports

N-doped carbon materials were then used as supports for Ru nanoparticles. The nitrogen within the structure should help to reach good dispersion and a better tethering of the metal nanoparticles. The Ru nanoparticles were deposited on the supports with the deposition/precipitation method, as described in the experimental section and implemented on supports at each step of the N-functionalization. The optimal Ru nanoparticles size of 1-2 nm, as determined in Chapter II, has been targeted for these catalysts. ICP analyses have confirmed that between 2.6 and 2.9 wt. % of Ru were deposited on the supports (Table III-3). As 3 wt. % of Ru was targeted, these analyses have confirmed that this deposition method is effective and that only small quantities of Ru are lost during the process.

Table III-3: Amount of deposited Ru on AC catalysts measured by ICP analyses

Catalyst	Ru (wt. %)
Ru/AC	2.6
Ru/EDA-AC	2.9
Ru/N-doped AC	2.6

It is shown that the heat treatment used for reducing Ru nanoparticles has a slight influence on the nitrogen content and the types of nitrogen functions present in the final activated materials. It can be seen that the ratio of pyridine/pyrrole functions over amine functions is getting a bit higher after Ru deposition (Figure III-4). Indeed, the change in the type of nitrogen functions present is also depending on the duration of the heat treatment. As the N-doped carbon supports had already been heated beforehand up to 900 °C, the further treatment at 600 °C for Ru reduction will influence the nitrogen functions less dramatically than if it was the sole heat-treatment. This change in the composition of nitrogen functions would have been more substantial if the second heat treatment was done at a higher temperature than the first one.

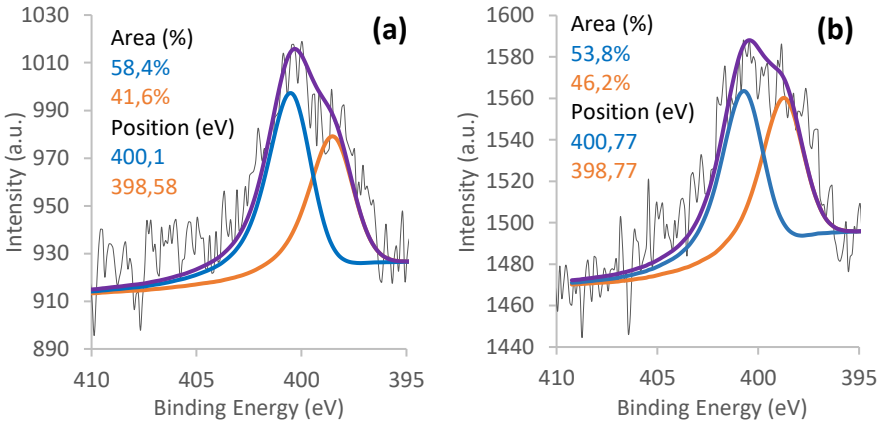

Figure III-4: N1s peaks (in blue: amine; in orange: pyridine/pyrrole) from XPS analyses of (a) N-doped GNP after heat treatment at 900°C (b) N-doped GNP after heat treatment at 900°C with deposited Ru nanoparticles reduced at 600°C

Heat treatment for the reduction of Ru nanoparticles has been optimized for each support in order to obtain a Ru nanoparticle size of 1-2 nm. The catalysts on N-doped activated coal have been heated at 600 °C under Ar/H_2 (95/5) whereas the catalysts on N-doped GNP have been heated at 400 °C under Ar/H_2 (95/5). TEM images of these catalysts are presented in Figure III-5. It can be noticed here that the Ru nanoparticles are better dispersed on the N-doped materials than on the pristine support (see Chapter II) showing the positive impact of the nitrogen presence within the lattice. All catalysts were analyzed by XPS (S4 in SI) and the position of the $Ru_{3p3/2}$ peak indicated that metallic Ru is always obtained after the heat treatment under Ar/H_2.

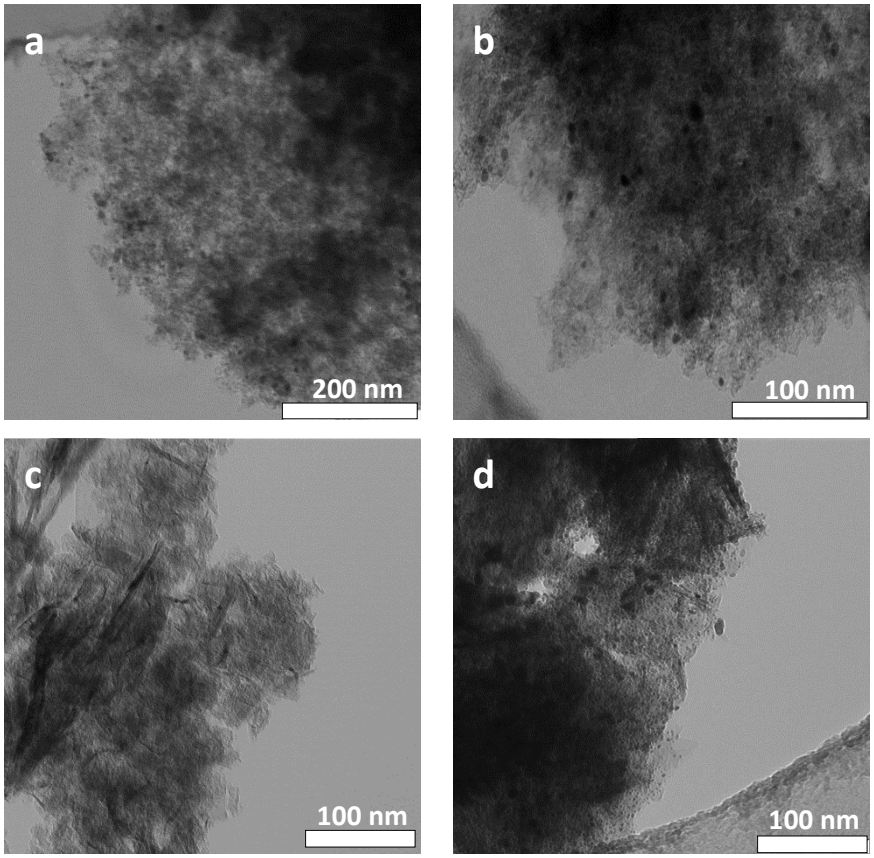

Figure III-5: TEM images of Ru nanoparticles on a) pristine AC; b) N-doped AC; c) pristine GNP; d) N-doped GNP

The catalysts composed of Ru deposited on AC and GNP without and with nitrogen doping were also characterized by XRD (Figure III-6). The peaks around 26° and 43° correspond to the graphitic domains (002 and 100 reflections, respectively) of the AC and the GNP carbonaceous materials [5], [6], [7]. The peak at 44° matches with metallic Ru [8]. There is no meaningful difference between the Ru/pristine AC and the Ru/N-doped AC. However, the Ru peak is more visible in the case of Ru/N-doped GNP compared to the Ru/pristine GNP, even if the Ru loading (as measured by ICP for the AC, see above) is similar in all cases, indicating that the Ru nanoparticles are more crystalline when they are supported on N-doped

GNP. Indeed the presence of the nitrogen functions seem to play a role in the structuration of the nanoparticles, probably acting as a nucleation point. Scherrer equation has been used to determine Ru nanoparticles size from XRD data: 9 nm, 22 nm and 18 nm of diameter have been obtained respectively for Ru/N-doped GNP, Ru/N-doped AC and Ru/pristine AC materials. This is not what has been visualized on TEM images and this difference can be explained by the fact that the small Ru nanoparticles are not crystalline and do not contribute to the signals in XRD[9].

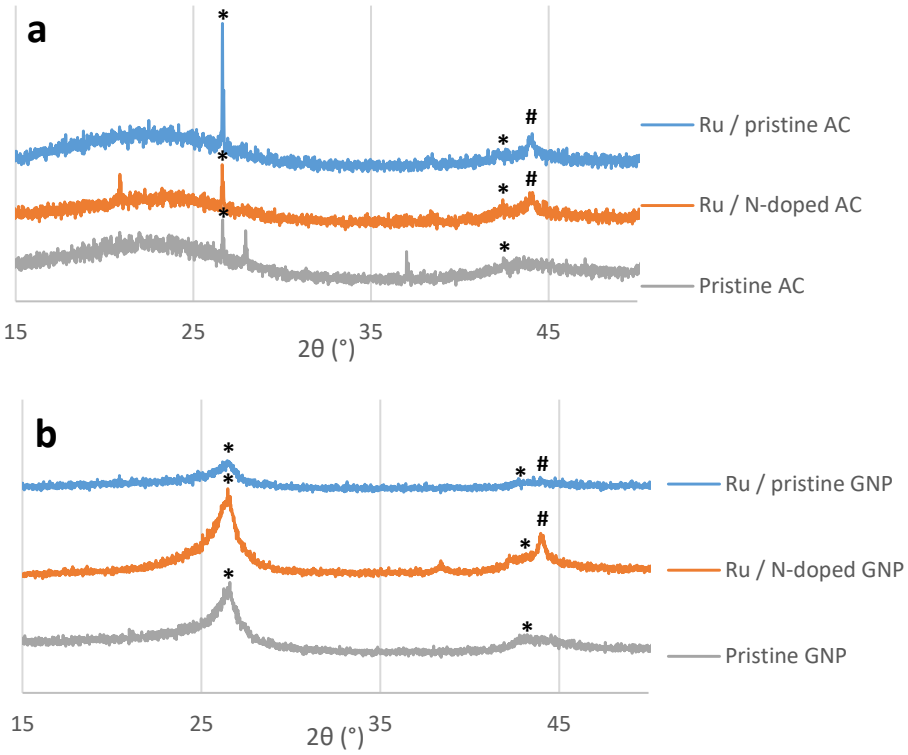

Figure III-6: XRD pattern for (a) pristine AC, Ru nanoparticles on AC and Ru nanoparticles on N-doped AC and for (b) pristine GNP, Ru nanoparticles on GNP and Ru nanoparticles on N-doped GNP. Asterisks denote peaks attributed to carbon phases and '#' denote Ru metal phase

Basicity of the Ru/N-doped GNP has been measured by Boehm titrations. The results can be found in Table III-4. The drop of basicity observed after the addition of Ru nanoparticles can be explained either by

the fact that Ru nanoparticles will block the access to some of the nitrogen functions or by the heat treatment implemented to reduce the Ru. Indeed, a decrease of basicity has also been observed after a heat treatment on EDA-GNP or EDA-oxidized GNP.

Table III-4: Basicity of the GNP before and after deposition of Ru nanoparticles; The estimated confidence interval on basicity is 10 %

Catalysts	Basicity (mmol/100g)
GNP	31
N-doped GNP	61
Ru / N-doped GNP	28
Oxidized GNP	0
N-doped oxidized GNP	81
Ru / N-doped oxidized GNP	35

III.3 Hydrogenation of cellobiose into sorbitol

In this section the goal was to assess the impact of nitrogen functions on the activity of Ru nanoparticles for the direct transformation of cellobiose into sorbitol. For this part of the work, the most promising catalysts among the materials synthesized in the previous sections are selected to assess their activity in this 2-step transformation. Kinetic curves have been built over 6 hours period for four representative catalysts (Figure III-7). As mentioned in the introduction (section I.5.1), two pathways are possible to obtain sorbitol from cellobiose. The same reaction pattern is observable in all cases. Indeed the preferential pathway is going through the hydrogenation of cellobiose into cellobitol before breaking this hydrogenated disaccharide into sorbitol/glucose (see Scheme I-8 in Introduction, Chap. I). After 1-2 hours, cellobitol production is reaching a peak before decreasing. Concomitantly, sorbitol production rises. A very peculiar observation is that nearly no glucose accumulation has been observed during the course of the reaction.

This means that as soon as the glucose is formed by cellobitol hydrolysis, it is hydrogenated into sorbitol. It is confirming, as mentioned in literature[10], that both hydrogenation reactions are faster than the two hydrolysis steps. Confidence intervals have been calculated when the same catalytic test has been carried out at least two times, a table with the repeatability is shown in the supporting information (S1 in SI).

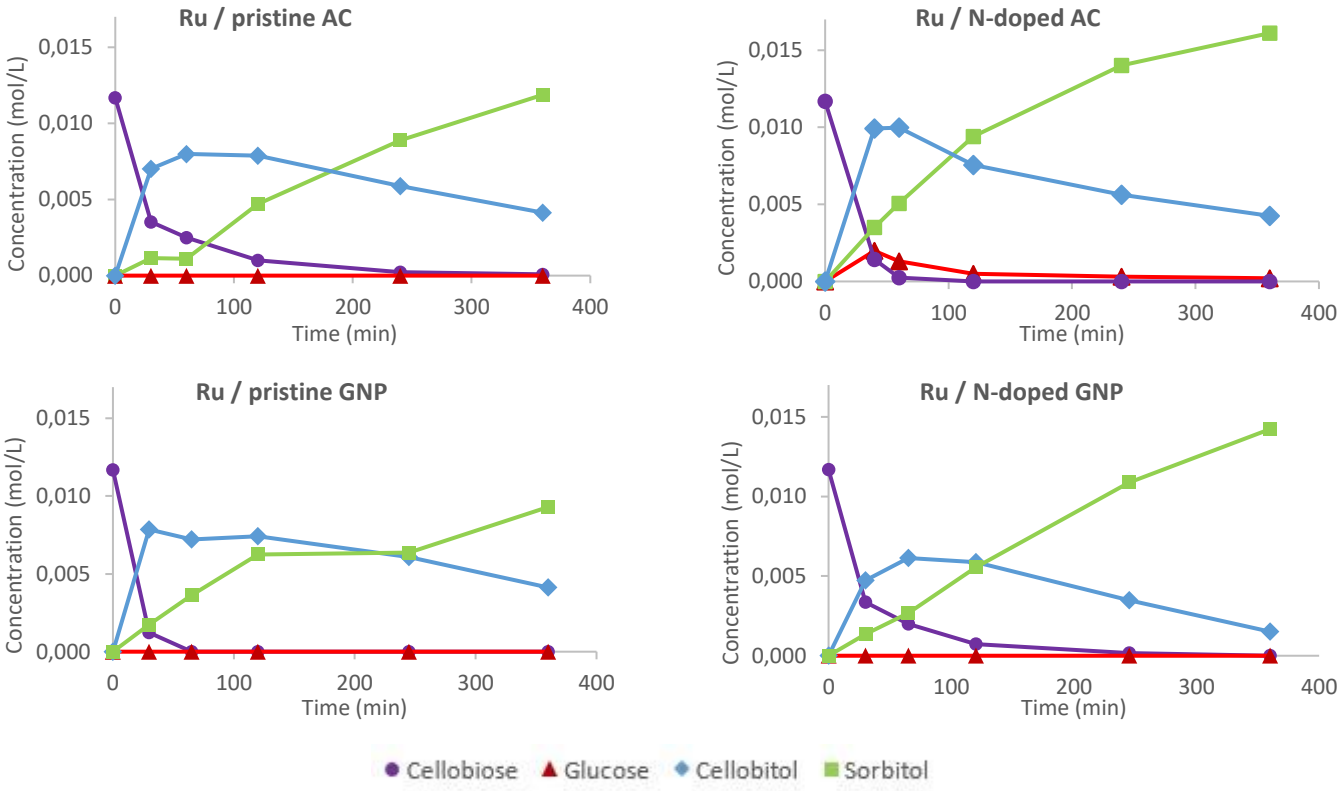

Figure III-7: Kinetic curves for the transformation of 1 g of cellobiose into sorbitol (testing conditions: 160°C; 30 bar H_2; 1700 rpm; 20 mg of catalyst); the lines connecting experimental points are only a visual aid and do not correspond to any mathematical model; The estimated confidence interval on each value is 5 %

As there are four transformations in total with consecutive and parallel reactions, the kinetic mathematical relationships are complicated to establish. Therefore, it is unfortunately too difficult to calculate the kinetic constants for each reaction in this complex network with the experimental data at hand here.

It can be noticed that both catalysts prepared on N-doped supports display better activity than the catalysts on non-functionalized supports (Table III-5). This is the proof that the nitrogen atoms incorporated in the lattice enhance the Ru nanoparticles activity.

Table III-5: Hydrogenation of cellobiose into sorbitol with pristine and N-doped AC and GNP: conversion of 1 g of cellobiose and selectivity into glucose, cellobitol and sorbitol and yield in sorbitol after 6 hours (160 °C; 1700 rpm; 30 bar H_2; 20 mg of catalyst); The estimated confidence interval on each value is 5 %

Catalyst	Conversion (%)	Selectivity in glucose (%)	Selectivity in cellobitol (%)	Selectivity in sorbitol (%)	Yield in sorbitol (%)
Ru / pristine AC	99	0	36	51	51
Ru / pristine GNP	100	0	35	40	40
Ru / N-doped AC	100	1	31	66	66
Ru / N-doped GNP	100	0	13	61	61

This can be explained first by the fact that the nitrogen atoms improved the dispersion of the Ru nanoparticles (see TEM images and discussion above). Second, they can also influence the spin density and the charge distribution, which have an impact on the Ru reactivity as already shown in the literature [11]. Unfortunately, any by-product apart from some traces of fructose (produced by isomerization of glucose) could be detected. It is known that isosorbide or levulinic acid could be obtained as products from degradation of sorbitol but their presence could not be confirmed with our HPLC system. A list of molecules that have been injected in HPLC and that can be ruled out from possible side products can be found in supporting

information (S2 in SI). Therefore, total organic content (TOC) analyses were performed and it was confirmed that the carbon balance at the end of the reaction in solution was respected (Table III-6).

Table III-6: TOC analyses of Ru / pristine GNP and Ru / N-doped GNP catalytic test filtrates

Catalyst	Concentration of carbon (mg/L)
Reference value (1 g of cellobiose into 120 mL)	1683
Ru / pristine GNP	1602
Ru / N-doped GNP	1640

Some catalytic tests have been performed with Ru nanoparticles on EDA GNP as support (Table III-7). In this case the nitrogen has not been incorporated into the carbon lattice and mainly ethylenediamine NH_2 dangling functions are present.

Table III-7: Hydrogenation of cellobiose into sorbitol without catalyst (blank), with N-doped GNP, EDA GNP and with a mixture of Ru/GNP and N-doped GNP: conversion of 1 g of cellobiose, selectivity into glucose, cellobitol and sorbitol and yield in sorbitol after 2 hours (160 °C; 1700 rpm; 30 bar H_2; 20 mg of catalyst); The estimated confidence interval on each value is 5 %

Catalyst	Conversion (%)	Selectivity in glucose (%)	Selectivity in cellobitol (%)	Selectivity in sorbitol (%)	Yield in sorbitol (%)
Blank	21	52	0	0	0
Ru / EDA GNP	70	0	57	11	8
Ru / N-doped GNP	95	6	50	29	28
Ru / GNP + N-doped GNP (mechanical mix)	100	0	64	22	22

These results show that this catalyst is less active than the bifunctional catalyst Ru / N-doped GNP. A mechanical mixture between Ru / GNP and N-doped GNP has also been tested. As this mixture is less active than the bifunctional catalyst, it proves that the Ru nanoparticles have to be

on the N-doped support to be promoted by the nitrogen functions. A simple proximity between the two type of solids is not enough to enhance the Ru activity.

Recyclability tests have been performed with the Ru/N-doped GNP catalyst to assess the stability of the catalyst over several runs. After each catalytic test, the catalyst was recovered and dried. It has then been reused for the next reaction. The results are shown in Table III-8 for a total of three consecutive catalytic tests. It can be observed that the conversion remains the same in all the different runs. The selectivity is slightly lower for the 2nd and the 3rd run. Despite this slight decrease of selectivity after the first reaction, the catalyst can be re-used for three runs without losing its activity.

Table III-8: Recyclability tests of the Ru/N-doped GNP; conversion of 1 g of cellobiose, selectivity and yield in sorbitol after 2 hours (160 °C; 1700 rpm; 30 bar H_2; 20 mg of catalyst); The estimated confidence interval on each value is 5 %

Catalyst	Conversion (%)	Selectivity in sorbitol (%)	Yield in sorbitol (%)
Ru/N-doped GNP 1st run	95	29	28
Ru/N-doped GNP 2nd run	95	23	22
Ru/N-doped GNP 3rd run	96	23	22

XPS analyses and TEM images have been carried out on the used catalyst (S5 and S6 in SI). These analyses have confirmed that the used catalyst has quite the same composition and morphology than the starting catalyst. XPS analyses have indicated that the nitrogen functions have the same nature than before the catalytic tests. TEM images have shown that Ru nanoparticles have the same size and the same dispersion on the support, confirming the stability of our bifunctional material.

Results for the transformation of cellobiose into sorbitol from the literature are gathered in Table III-9. Several catalysts from the literature are only giving high yield of cellobitol and low amounts of sorbitol, indicating that

the hydrolysis step is the limiting factor for sorbitol production. Only the catalysts in entries 3 and 5 are producing high yields of sorbitol. This can be explained by the fact that these catalysts are based on an acidic support that will catalyze the hydrolysis of cellobitol into sorbitol and glucose. The results obtained in our work are excellent if compared directly with these results from the literature. Indeed, with similar reaction conditions but lower catalyst / cellobiose mass ratio in our case, sorbitol yield is one of the most elevated in the Table. An industrial catalyst provided by Evonik has also been tested in our conditions as a reference from industries and the sorbitol yield obtained with it is lower that with our catalysts. Moreover, when sorbitol production is normalized by calculating sorbitol mol produced per gram of catalyst, it is striking that our catalysts are simply the best and giving excellent results for direct cellobiose transformation into sorbitol.

By improving the Ru hydrogenation ability, sorbitol formation from cellobiose has been promoted without requiring hydrolysis secondary active sites or the addition of inorganic acids in the solution. This opens the door to many applications for biomass valorization reactions that currently still depend on environmentally harmful substances.

Table III-9: Results for hydrogenolysis of cellobiose into cellobitol and sorbitol reported in the literature in comparison with our work (last two lines)

Entry	Catalyst	Catalyst / Cellobiose mass ratio	H_2 Pressure (bar)	Temp. (° C)	Time (h)	Cellobiose conversion (%)	Yield in cellobitol (%)	Yield in sorbitol (%)	Mol of sorbitol / g of catalyst	Ref.
1	Ru (5 wt. %) / C	1 / 12	40	150	5	100	80	7	0.0049	[12]
2	Ru (1 wt. %) / CNT	1 / 2	20	140	6	100	90	7	0.0008	[13]
3	Ru (1 wt. %) / $Cs_3PW_{12}O_{40}$	1 / 2	20	140	6	100	12	85	0.0099	[13]
4	Ru (1 wt. %) / HZSM-5	1 / 2	20	140	6	100	68	25	0.0029	[13]
5	Ru (3.2 wt. %) – PTA (16.7 wt. %) / MIL-100(Cr) [a]	1 / 1.7	20	160	10	100	n.a.	81	0.0080	[14]
6	Ru (5 wt. %) / RGO	1 / 3.4	50	190	3	100	n.a.	65	0.0129	[15]
7	Ru (5 wt. %) / Zr-SBA-15 (0.25)[b]	1 / 5	50	140	0.25	98	80	15	0.0044	[16]
8	Ru (5 wt. %) / C (industrial)	1 / 50	30	160	2	100	n.a.	25	0.0730	Our work
9	Ru (3 wt. %) / N-doped GNP	1 / 50	30	160	6	100	13	61	0.1782	Our work
10	Ru (3 wt. %) / N-doped AC	1 / 50	30	160	6	100	31	66	0.1928	Our work

[a] PTA = phosphotungstic acid
[b] (0.25) = Zr / Si molar ratio

III.4 Conclusion

Two different methods to incorporate nitrogen atoms within the lattice of the carbon sheets of different carbonaceous materials have been investigated. The urea method has been carried out on CNF, AC and CB carbons but it has not increased enough the surface N/C ratio and the basicity for the intended application. Therefore the functionalized materials obtained by this method have not been used for supporting Ru nanoparticles. The second method, the EDA method, has been conducted on CNF, AC and GNP. Only the AC and GNP have given good results because of the impossibility to further oxidize the CNF. These N-doped carbon materials have been analyzed by XPS, TPD and Boehm titration, which demonstrated successful modification, thereby increasing surface basicity and number of pyridine/pyrrole sites. These new supports were used to deposit Ru nanoparticles. TEM and XRD analyses have shown improvement of the deposition of Ru nanoparticles on N-doped carbon supports compared with the pristine ones. The nanoparticles are better dispersed and more crystalline.

These Ru/N-doped carbon catalysts have been tested for the direct 2-steps transformation of cellobiose into sorbitol. Kinetic curves for the full transformation have demonstrated that the first step is the hydrogenation of cellobiose into cellobitol and the second step is cellobitol hydrolysis into one molecule of sorbitol and one molecule of glucose that is directly transformed into sorbitol. This study clearly highlighted the better activity of the catalysts supported on N-doped carbon materials compared to pristine ones. Nitrogen within the structure of the support is improving the Ru nanoparticles activity. A more detailed kinetic study to understand better the whole mechanism of the reaction and to determine kinetic constants for each individual reaction step would be interesting to establish in the future.

Moreover, one of our best catalysts has been tested several times to assess its recyclability. It displayed high activity over several runs showing that neither the introduced nitrogen functions nor the Ru nanoparticles suffer from deactivation, as confirmed by XPS and TEM analyses. Finally, results obtained with our Ru / N-doped catalysts have been compared with the literature. Considering reaction conditions that have been used, excellent sorbitol productivity from cellobiose has been pointed outin our case.

References

[1] K. N. Wood, R. O'Hayre, S. Pylypenko, *Energy Environ. Sci.* **2014**, *7*, 1212–1249.

[2] J. A. Menéndez, J. Phillips, B. Xia, L. R. Radovic, *Langmuir* **1996**, *12*, 4404–4410.

[3] M. R. Axet, O. Dechy-Cabaret, J. Durand, M. Gouygou, P. Serp, *Coord. Chem. Rev.* **2016**, *308*, 236–345.

[4] C. Breyer, D. Reichert, J. Seidel, R. Hüttl, F. Mertens, S. Kureti, *Phys. Chem. Chem. Phys.* **2015**, *17*, 27011–27018.

[5] R. Siburian, H. Sihotang, S. Lumban Raja, M. Supeno, C. Simanjuntak, *Orient. J. Chem.* **2018**, *34*, 182–187.

[6] K. L. Routray, S. Saha, D. Behera, *Mater. Sci. Eng. B* **2020**, *257*, 114548.

[7] Z. Q. Li, C. J. Lu, Z. P. Xia, Y. Zhou, Z. Luo, *Carbon N. Y.* **2007**, *45*, 1686–1695.

[8] J. Z. Bloh, R. Dillert, D. W. Bahnemann, *Phys. Chem. Chem. Phys.* **2014**, *16*, 5833–5845.

[9] R. Wojcieszak, M. J. Genet, P. Eloy, P. Ruiz, E. M. Gaigneaux, *J. Phys. Chem. C* **2010**, *114*, 16677–16684.

[10] P. J. C. Hausoul, A. K. Beine, L. Neghadar, R. Palkovits, *Catal. Sci. Technol.* **2017**, *7*, 56–63.

[11] D. Wei, Y. Liu, Y. Wang, H. Zhang, L. Huang, G. Yu, *Nano Lett.* **2009**, *9*, 1752–1758.

[12] J. M. A. R. Almeida, L. Da Vià, P. Demma Carà, Y. Carvalho, P. N. Romano, J. A. O. Peña, L. Smith, E. F. Sousa-Aguiar, J. A. Lopez-Sanchez, *Catal. Today* **2017**, *279*, 187–193.

[13] M. Liu, W. Deng, Q. Zhang, Y. Wang, Y. Wang, *Chem. Commun.* **2011**, *47*, 9717–9719.

[14] J. Chen, S. Wang, J. Huang, L. Chen, L. Ma, X. Huang, *ChemSusChem* **2013**, *6*, 1545–1555.

[15] D. Wang, W. Niu, M. Tan, M. Wu, X. Zheng, Y. Li, N. Tsubaki, *ChemSusChem* **2014**, *7*, 1398–1406.

[16] Y. Niu, H. Wang, X. Zhu, Z. Song, X. Xie, X. Liu, J. Han, Q. Ge, *Microporous Mesoporous Mater.* **2014**, *198*, 215–222.

Chapter IV

Sulfonated carbon materials for cellobiose hydrolysis into glucose

As the previous two Chapters have shown that sorbitol can be obtained by hydrogenation of glucose or cellobiose, studying hydrolysis of cellobiose into glucose is the next logical step. Hydrolysis is usually catalyzed by homogenous or heterogenous acids. The aim of this Chapter is to study the acidic functionalization of several carbon materials and to assess their acidity by Boehm titration. The activity of these catalysts for the hydrolysis of cellobiose into glucose, as well as their recyclability will be investigated. Bases are also known to catalyze the hydrolysis of organic molecules. That is why a section of this Chapter is dedicated to the catalytic performance of N-doped carbon materials depicted in Chapter III in the same transformation.

IV.1 Carbon materials functionalization

Several carbon materials (LHT-OX, RGO, AC, MWCNT, CB, GNP-M15 and GNP-C750) have been functionalized by a diazonium coupling strategy in order to introduce sulfonic acid groups at their surfaces. First sulfanilic acid and isoamyl nitrite react together to form *in situ* a diazonium cation. After that step, a de-diazoniation reaction will couple the aryl sulfonic acid fragment on the carbon surface, *via* a strong covalent C-C bond with C atoms in the polyaromatic structure of the carbon material backbone (Scheme IV-1). This functionalization method is safer than common methods (involving sulfuric acid) for producing sulfonic functions on carbon materials and can easily be scaled up. Moreover, this method is gentle on the carbonaceous (nano-)material that keeps its mechanical strength.

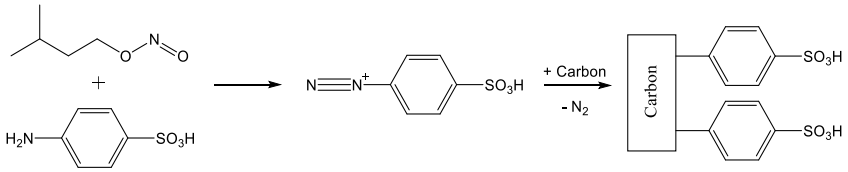

Scheme IV-1: Diazonium coupling on carbon materials for sulfonic acid grafting

A first observation is that the functionalized carbons become more hydrophilic and give better suspensions in aqueous medium than the starting carbons, which is an advantage for catalytic applications. Functionalized materials have been characterized by XPS and the spectra displayed a single S_{2p} peak, at 168.3 eV, which can be assigned to sulfonic functions [1]. All the selected carbon materials have been successfully functionalized and the XPS spectra of each sample, before and after functionalization, are presented in the Supporting Information (S7 in SI, Figures 4-10). Most carbon materials do not display any S_{2p} peak before functionalization except GNP M15 that has a S_{2p} peak around 164 eV which could be identified as thiol functions [2]. These

thiols functions might arise during synthesis of GNP M15. After functionalization, all carbon materials present a clear peak at 168.3 eV corresponding to sulfonic functions, as expected. The obtained S/C and N/C surface atomic ratios are presented in Table IV-1. It is observed that the S/C ratio is increasing strongly after functionalization, confirming the grafting of sulfonic functions. In addition, the N/C ratio is also rising after the reaction. This is due to some isoamyl nitrite that would have not reacted completely during the functionalization procedure and is still adsorbed on the carbon surface. This is confirmed by XPS analyses. Indeed, a nitrogen peak is appearing after the functionalization but it is not present anymore after catalytic test (S8 in SI, Figure 11). Moreover, the XPS results have shown that the carbon peak has not been altered (S8 SI, Figure 12). The integrity of the carbon support is intact after functionalization, as was expected from the choice of functionalization procedure.

The acidity of each catalyst was determined by Boehm titration (Table IV-1). For each different carbon, the acidity after functionalization is more important than before. The non-functionalized materials are presenting a low acidity, except the GNP that already possesses acidic functions[3]. Indeed, graphene nanoplatelets are produced by graphite exfoliation in acidic medium and are therefore heavily functionalized. The increase is more or less important depending on the type of carbon considered. It should be noted that the diazonium coupling reaction is grafting the sulfonic functions directly on the carbon aromatic rings. The amount of defects on the carbon should not influence the yield of this grafting reaction.

There is one exception: the GNP that keeps almost the same acidity after the sulfonic functions grafting. This can be explained by the huge amount of acidic groups already present on the surface at the start. This does

not mean that the functionalization is not occurring. Indeed, some of the starting acidic functions have been replaced by the sulfonic functions and this is confirmed by the XPS results showing an increase in the sulfur amount. Therefore, the acidity displayed by the GNPs is not coming only from the sulfonic functions but also from weaker O-only acidic functions.

Table IV-1: Catalysts acidity determined via Boehm titration; Atomic ratios determined by XPS analyses and specific surface areas measured by N_2 physisorption; The estimated confidence interval on acidity is 10 %

Sample	Specific area (S_{BET}, m^2/g)	Acidity (mmol/100 g)	S/C (%at. ratio)	N/C (%at. ratio)
LHT-OX	26	10	0.001	0.002
SO_3H/LHT-OX		50	0.019	0.015
RGO	600	73	0.002	0
SO_3H/RGO		126	0.021	0.004
AC	922	42	0	0.002
SO_3H/AC		145	0.042	0.058
MWCNT	257	14	0	0
SO_3H/MWCNT		189	0.018	0.004
CB	63	74	0	0.004
SO_3H/CB		121	0.025	0.041
GNP-M15	116	136	0.005	0
SO_3H/GNP-M15		125	0.014	0.024
GNP-C750	799	228	0	0
SO_3H/GNP-C750		211	0.030	0.044

The grafting disparities between some of the carbon solids may be linked to their specific surface areas, especially for CNF (LHT-OX) that displays a low surface area (26 m^2/g). By opposition, activated coal (AC), which has a high specific surface area (922 m^2/g), is showing a much higher acidity increase. Nevertheless, a perfectly linear relationship between BET surface area and the obtained acidity (or the S amount) was not observed (Figure IV-1). Indeed, there are other factors that can impact the effectiveness of the functionalization. The type of carbon surface is important, i.e. the amount of defects, the presence of an amorphous layer,

the number of sp2 carbon atoms etc., but also the amount of acid functions already present at the beginning. Moreover, the diazonium produced in situ might have some difficulties to access the internal surface due to microporosity in some materials. A peculiar point can be observed in the case of functionalized MWCNT, which displays high acidity with low specific surface area. As MWCNT surface is quite exempt of defects, it explains why this functionalization method is working well on it. This could indicate as well, by contrast, that CNF surface is not exempt of defects. This makes sense, considering that more graphene layers edges will be exposed on CNF than on CNT surfaces, the latter being considered as Russian dolls perfect cylindrical structures.

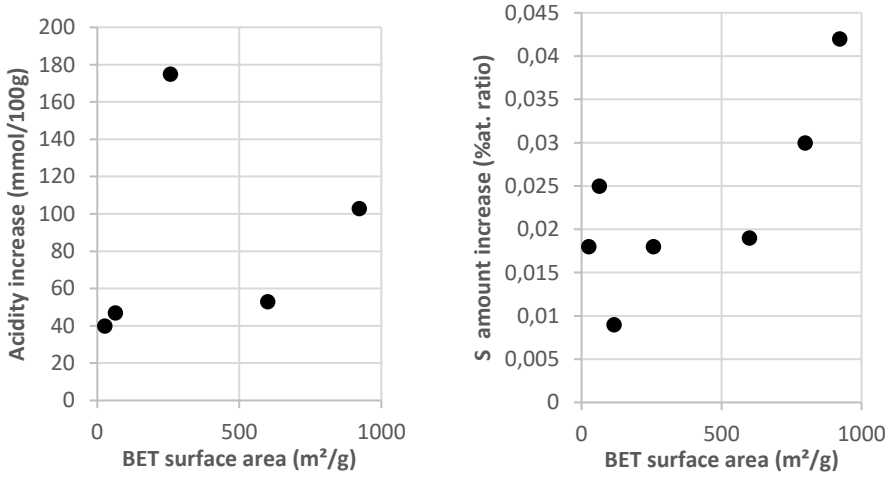

Figure IV-1: Acidity increase as a function of BET surface area (on the left); S amount increase measured by XPS as a function of BET surface area (on the right)

By looking at other catalysts synthesized by the same method in the literature, it can be seen that the acidity reported for nanofibers (52 or 63 mmol/100 g) [4] is similar to the SO_3H/LHT-OX catalyst synthesized in this work, which is the lowest value obtained here after functionalization. Moreover our best catalysts, especially the functionalized MWCNT that reaches 189 mmol/100 g starting from a mere 14 mmol/100 g acidity, possess higher acidity than reported sulfonated carbons (108 mmol/100 g) or acidic aluminosilicates (105 mmol/100 g) but not as much of course as commercial resin Amberlyst-15 (470 mmol/100 g) [4],[5],[6]. However, the sulfonic functions on our catalysts are more accessible and should display a better hydrolysis activity. A more detailed overview compiling acidic catalysts from the literature and their acidity values can be found in Table IV-2.

Table IV-2: Comparison of acidic catalysts found in the literature

Sample	Synthesis method	Acidity (mmol/100 g)
SO_3H/MWCNT (our catalyst)	Diazonium coupling method	189
SO_3H/LHT-OX (our catalyst)	Diazonium coupling method	50
Sulfonated carbon nanofibers [4]	H_2SO_4 at reflux	63
Sulfonated activated carbon [6]	H_2SO_4 at reflux	190
BC (bamboo carbonized) - SO_3H [6]	H_2SO_4 at reflux	198
Sulfonated carbon - SO_3H [6]	H_2SO_4 at reflux	215
CMK-3 (mesoporous carbon) - SO_3H [6]	H_2SO_4 at reflux	239
Sulfonated cellulose based amorphous carbon [4]	Diazonium coupling method	108
HY zeolite [6]	Ion-exchange	136
Aluminosilicates (H-beta; Si/Al = 13) [5]	Commercial	105
$HNbMoO_6$ [6]	Layered Nb oxide	190
Amberlyst-15 [5]	Commercial	470

TPD-NH_3 analyses have been performed to assess the strength of the acidic sites. Data are all presented in the Supporting Information (S9 in SI). It can be observed in the representative examples of Figure IV-2 that the functionalized LHT-OX presents the same curve than without functionalization (Fig. IV-2 (a)). It confirms the very low acidity of the functionalized material due to poor grafting of the sulfonic sites. The presence of two types of acidic functions can also be determined on the functionalized GNP-C750 (Fig. IV-2(b)). Indeed a peak around 180 °C (weak acids) can be noticed for the starting GNP-C750. After functionalization, this peak is still visible but a more intense peak appears at 300 °C. The first peak corresponds to the weak O-acidic functions already present on the starting carbon surface while the second peak can be identified as the sulfonic functions and can also be found on all the other functionalized materials. This peak from the sulfonic functions confirms the hypothesis that weak acids are replaced by the sulfonic acids in the case of M15 and C750 GNPs.

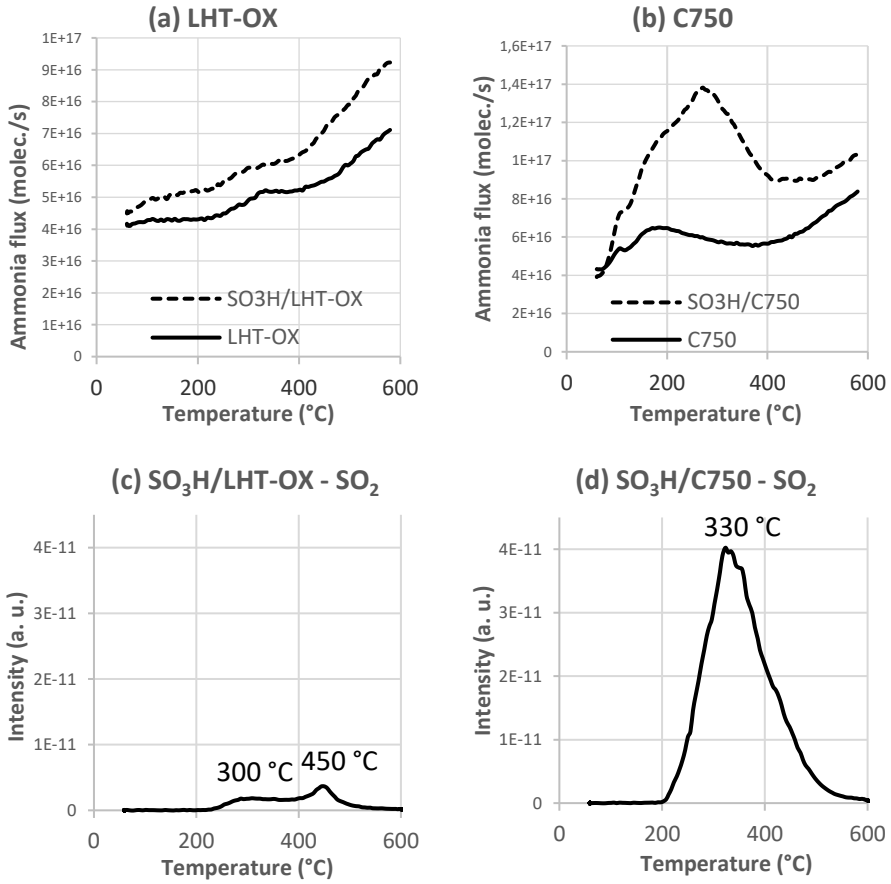

Figure IV-2: Ammonia desorption flux as a function of the temperature (a, b) and SO_2 flux followed by MS during the TPD analysis (c, d)

However, TPD analyses do not seem to be ideal for sulfonic acids characterization because of the sulfonic functions thermal degradation, as mentioned in the literature [7]. Indeed the SO_2 peak has been followed by MS during the TPD analyses and for each functionalized material a peak at 300 °C is observed (Figure IV-2 (c, d) and S10 in SI). This indicates that the sulfonic functions are degraded at this temperature. It means that the ammonia measured at 300 °C comes from the sulfonic functions degradation, rather than desorption from intact sites. If the sulfonic functions were stable at higher temperature, the ammonia desorption could possibly occur at higher

temperature. Therefore, the strength of these functions is certainly underestimated if concluding solely on the basis of the peak observed in TPD analyses and corresponding temperature. The sulfonic functions cannot reliably be characterized with this method, and Boehm titrations are found more pertinent.

IV.2 Hydrolysis of cellobiose into glucose

The sulfonated catalysts have been tested for the hydrolysis of cellobiose into glucose under mild conditions, namely under N_2 autogenic pressure, at 150 °C and 1700 rpm for 2h (Table IV-3). Confidence intervals have been calculated when the same catalytic test has been carried out at least two times, a table with the repeatability is shown in the supporting information (S1 in SI). Blank was carried out using the same testing conditions, as described in the experimental part, but without any catalyst. Globally, non-functionalized starting carbon materials are giving the same conversion than the blank, around 25 %. It confirms that the acidity determined by Boehm titration is due to weak acids, even with GNPs, that cannot catalyze the hydrolysis reaction. Indeed the observed conversion arises from the thermal cleavage of the glycosidic bond at this temperature. Functionalized catalysts are dramatically increasing the conversion up to a maximum of 94 % with the SO_3H/GNP-C750 graphene material. Sulfonic functions are controlling the hydrolysis pathway [8] and are improving the selectivity towards glucose to 95 % (*vs*. 57% in the 'blank' case). It is noteworthy that these figures (>90 % conversion and selectivity) were obtained in only 2 hours at 150 °C. Common side-products usually obtained from glucose such as levulinic acid or formic acid have not been observed here. Other products such as isosorbide cannot be completely ruled out as they are not identified with the HPLC column used in this work. A list of

molecules that have been injected in HPLC and that can be ruled out from possible side products can be found in supporting information (S2 in SI). Only some traces of fructose arising from isomerization of glucose have been identified. However, a total organic content (TOC) analysis has been carried out for each catalytic test and 100 mol. % of engaged carbon is always accounted for. It means that no other gaseous products are being formed.

Best results have been obtained with RGO, AC, MWCNT and GNP-C750 materials. As AC is the cheapest and most used carbon material for industrial applications, it has been chosen for the remainder of this chapter and for the fabrication of bifunctional catalysts presented in Chapter V.

Table IV-3: Conversion of cellobiose and selectivity in glucose (N_2 autogenic pressure; 150 °C; 2h; 1700 rpm; 1g of cellobiose; 300 mg of catalyst); The estimated confidence interval on cellobiose conversion and glucose selectivity is 4 %

Catalyst	Conversion (%)	Selectivity in glucose (%)
Blank (same conditions but without catalyst)	24	57
LHT-OX	19	87
SO_3H/LHT-OX	25	47
RGO	40	24
SO_3H/RGO	84	95
AC	31	82
SO_3H/AC	81	96
MWCNT	24	47
SO_3H/MWCNT	81	95
CB	20	52
SO_3H/CB	57	70
GNP-M15	23	64
SO_3H/GNP-M15	40	80
GNP-C750	29	57
SO_3H/GNP-C750	94	80

The catalysts that are displaying a poor acidity, such as the SO_3H/LHT-OX sample, do not improve the conversion at all. It can be assessed that there is a minimum amount of acid necessary to switch on the catalysis for the acidic hydrolysis. As shown in Figure IV-3, below 120 mmol/100g the conversion remains low. Beyond this threshold value, the catalysts show a good activity, as long as sulfonic functions are present. Unfortunately, there are no points between 50 and 100 mmol / 100 g to confirm this observation. Therefore, a linear tendency cannot be fully discarded.

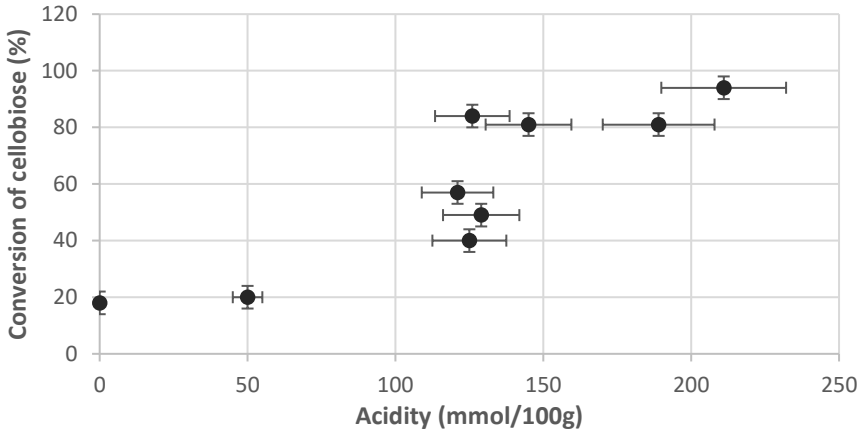

Figure IV-3: Conversion of cellobiose depending on the acidity of the catalyst

The quantity of catalyst used during the test also influences the activity. Several amounts of catalysts have been tested in the case of the SO_3H/AC material (Figure IV-4). When the amount of catalyst is too low (20 mg), the catalyst is not active and the conversion is the same as the blank. When the amount of catalyst is increased, the acidic hydrolysis is triggered and the conversion is higher. However the selectivity is excellent in all cases (much higher than the blank), independently of the amount of catalyst engaged. Preliminary tests have been conducted on cellulose fibers (Sigma, reference C6288, crystalline and high purity) and 20 % conversion (based on

cellulose weight loss at the end of test) was observed with our catalyst (SO_3H/AC) against only 10 % with a blank test.

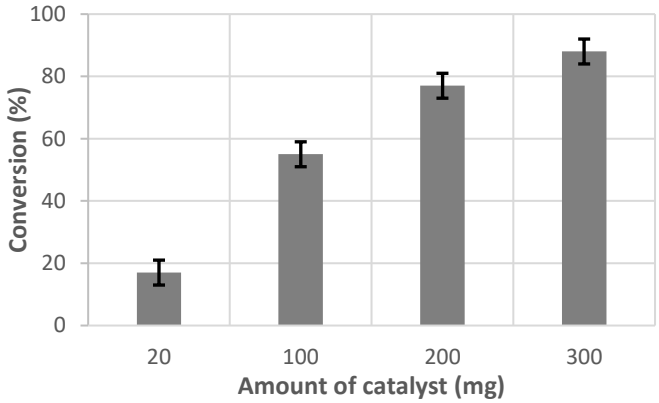

Figure IV-4: Conversion of cellobiose depending on the amount of catalyst (SO_3H/AC)

Recyclability tests have been carried out with SO_3H/AC and are shown on Figure IV-5. A slight decrease of the conversion from 81 % to 67 % is observed after the second run but the selectivity remains very high (97 %). After the third run the conversion decreases again to reach 50 % but stays quite stable for the next three runs. However, the selectivity is still reaching almost 100 %. The plateau reached after three runs shows a conversion far better than the blank. It is shown here that the sulfonic functions are very robust and remain on the carbon material despite the test conditions.

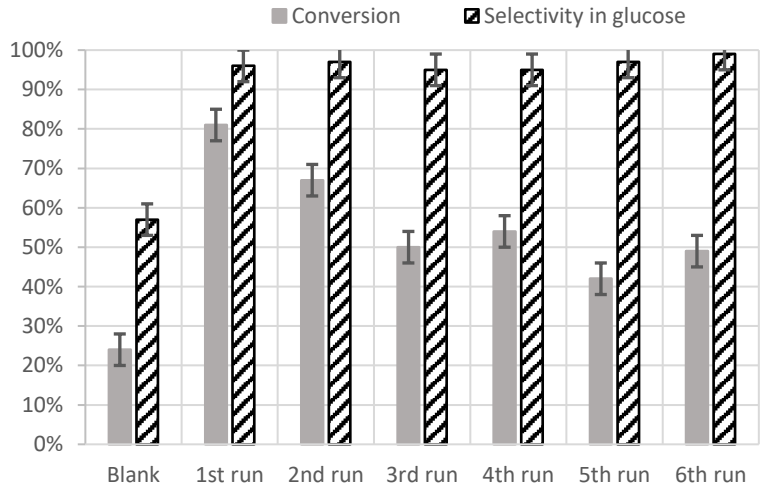

Figure IV-5: Recyclability of SO_3H/AC catalyst

The slight decrease of conversion can be incriminated to the removal of some unreacted sulfonic compounds that were just adsorbed on the carbon surface. Indeed the acidity of the catalyst after the sixth run is 129 mmol/100g for 145 mmol/100g before tests. Nevertheless, the selectivity into glucose stays high because of the presence of strong acid sulfonic functions, which are the active sites for this transformation, even after six runs. In order to confirm this effect, a pre-treatment in the same conditions as those of the catalytic tests but without cellobiose was performed on the catalyst. The acidity of the pre-treated catalyst is 116 mmol/100g and matches with the value obtained for the catalyst after six runs. Following the same trend than acidity, XPS analyses confirm that sulfonic functions are fewer but still present on the pre-treated catalyst and the catalyst after test (Figure IV-6). This demonstrates that the sulfonic groups are stable under the catalytic tests reaction conditions (130 °C and N_2 autogenic pressure (6 bar)). It is also observed that the position of the sulfur peak is not shifted. This means that the sulfonic functions are not reduced during the catalytic test eluding this possibility as a deactivation

phenomenon. Two other reasons for the slight drop in conversion observed in Figure IV-5 that might be cited are strong adsorption of reactants and/or products and coking. However, no significant weight increase of our catalyst has been observed after the test.

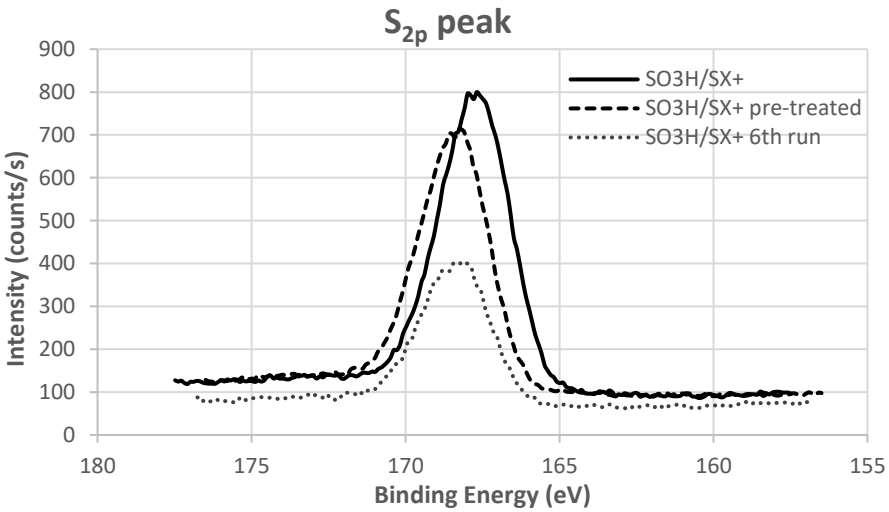

Figure IV-6: S_{2p} XPS peak for the functionalized AC before and after test and pre-treated catalyst

Moreover, the quantity of nitrogen (reactant molecules present N atoms) in the used or pre-treated catalysts is very small compared to the quantity on the freshly synthesized catalyst. Reactants that were stacked on the carbon material are washed away under these conditions. The acidic functions that are still grafted on the solid are robust and that is why they can be used many times. The conversion and the selectivity obtained with the pre-treated catalyst, respectively 51 % and 98 %, are the same than the plateau reached after three runs. These results show that our sulfonic functions grafted with the diazonium coupling procedure are much more stable than sulfonic functions generated by hot H_2SO_4 treatment[1],[9]. Therefore, the main interest of these catalysts is their recyclability. Highly

active and stable acidic catalysts suitable for biomass hydrolysis reaction at low temperature and within a short reaction time have been obtained.

IV.3 N-doped carbon materials as hydrolysis catalysts

In the previous section excellent results have been shown for the hydrolysis of cellobiose with our acidic catalysts. Nevertheless, hydrolysis in general is a chemical reaction that can also be catalyzed by basic functions. Given that the N-doped carbons that have been prepared contain basic functions (amine, pyridine, pyrrole, *etc.*), they might present an activity for the hydrolysis of the β-1,4-glycosidic bond. Acid sites are usually used to catalyze such transformation, but basic functions could also fulfill this role. Therefore, some catalytic tests on the hydrolysis of cellobiose into glucose under nitrogen in the absence of Ru or H_2 with the N-doped carbons have been carried out (Table IV-4).

Table IV-4: Hydrolysis of cellobiose into glucose (160 °C; 1700 rpm; N_2; 2 h); The estimated confidence interval on cellobiose conversion and glucose selectivity is 5 %

Catalyst	Conversion (%)	Selectivity in glucose (%)	Yield in glucose (%)
Blank (no catalyst)	42	70	29
AC pristine	43	60	26
N doped AC before heat treatment	33	61	20
N doped AC after heat treatment	38	59	22
GNP pristine	43	68	29
N doped GNP before heat treatment	57	33	19
N doped GNP after heat treatment	37	73	27
SO_3H on AC	86	86	74
SO_3H on GNP	93	84	78

It is shown that N-doped carbons (AC and GNP) with or without heat treatment do not improve the hydrolysis of cellobiose into glucose. Indeed the results obtained are not better than the catalytic test without any catalyst (blank). Only the N-doped GNP before heat treatment, with the dangling EDA, is slightly increasing the conversion but the selectivity towards glucose is lower. After the heat treatment, the N-doped GNP is giving the same results as the blank. The amount of basic functions on the carbon material should not be the issue, given that the molar ratio between cellobiose and basic functions is around 10 after heat treatment. The main explanation for this lack of activity is that the basic functions that have been introduced on the carbon supports are not adequate sites, given the mechanism [8], to catalyze the hydrolysis step. Therefore, it can be concluded that the nitrogen functions incorporated within the carbon supports will have no direct impact on the hydrolysis of cellobiose into glucose.

IV.4 Conclusion

Various (nano)carbon solids have been functionalized through a diazonium coupling reaction leading to strong acidic sulfonic functions grafted on their surface. Their presence has been confirmed by Boehm titration, XPS and TPD analyses. Hydrolysis of cellobiose into glucose under inert atmosphere in neutral water medium has been improved by all our functionalized catalysts, compared to a 'blank' with no catalyst, or the unfunctionalized carbon materials. A maximum of 84 % of conversion with 95 % of selectivity towards glucose has been obtained with the SO_3H/RGO catalyst. Moreover these results have been obtained at a low temperature (150 °C) in only 2h which is promising for hydrolysis of more robust substrate like cellulose for example. It has been discovered that below a certain amount of acidic functions no catalytic improvement is observed. In our

conditions, 120 mmol/100g of catalyst acidity is the minimum amount to trigger the hydrolysis activity. It has also been shown that our catalysts are recyclable. Indeed the performance of the SO_3H/AC catalyst after 6 runs is much better than the hydrolysis without any catalyst. Moreover the observed slight decrease of activity has been assigned to some reactants stacked on the carbon material that are washed away, while the sulfonic functions well-bound on the surface remain on it after tests. It is demonstrating the robustness of these functions in comparison with other functionalization methods such as carbon materials treatment with sulfuric acid that would also weaken the material mechanical properties. These functionalized carbons can further be used as supports for metallic nanoparticles in order to prepare bifunctional catalysts. The acidic functions will hydrolyze cellobiose into glucose while the metallic center can transform the glucose into high value molecules like sorbitol or HMF. Finally some tests have been conducted with our N-doped carbons as basic catalysts. Unfortunately it has been shown that, despite their basicity, they could not improve the hydrolysis of cellobiose into glucose.

As functionalized AC has given one of the best results for glucose production from cellobiose, this support has been chosen for the synthesis of bifunctional catalysts that will be described in Chapter V.

References

[1] Y. Wu, Z. Fu, D. Yin, Q. Xu, F. Liu, C. Lu, L. Mao, *Green Chem.* **2010**, *12*, 696–700.

[2] D. G. Castner, K. Hinds, D. W. Grainger, *Langmuir* **1996**, *12*, 5083–5086.

[3] XG Sciences Inc., "xGnP® Graphene Nanoplatelets - Grade C," **2018**.

[4] D. R. Stellwagen, F. Van Der Klis, D. S. Van Es, K. P. De Jong, J. H. Bitter, *ChemSusChem* **2013**, *6*, 1668–1672.

[5] A. Onda, T. Ochi, K. Yanagisawa, *Green Chem.* **2008**, *10*, 1033–1037.

[6] Y. B. Huang, Y. Fu, *Green Chem.* **2013**, *15*, 1095–1111.

[7] K. I. Shimizu, E. Hayashi, T. Hatamachi, T. Kodama, T. Higuchi, A. Satsuma, Y. Kitayama, *J. Catal.* **2005**, *231*, 131–138.

[8] G. W. Huber, S. Iborra, A. Corma, *Chem. Rev.* **2006**, *106*, 4044–4098.

[9] R. Zhong, B. F. Sels, *Appl. Catal. B Environ.* **2018**, *236*, 518–545.

Chapter V

Bifunctional catalysts for the direct transformation of cellobiose / cellulose into sorbitol

Chapter II and III have dealt with the deposition of Ru nanoparticles on carbon supports (without or with nitrogen doping) for the enhancement of the hydrogenation step, aiming at transforming efficiently glucose into sorbitol. Chapter IV has tackled the hydrolysis improvement with acidic catalysts, to obtain glucose from cellobiose or cellulose. In this last Chapter, bifunctional catalysts that combine both sulfonic functions and Ru nanoparticles on the same support will be studied in order to improve both hydrolysis and hydrogenation of cellobiose into sorbitol. Preliminary studies will be carried out with the LHT-OX support as Ru nanoparticles deposition had been investigated on this specific carbon in Chapter II. As acidic functionalization is more effective on AC, this support will later replace LHT-OX for the remainder of the Chapter. Moreover, Ru nanoparticles deposition method will be modified to limit deactivation of the sulfonic functions during the synthesis procedure. Indeed, we should avoid basic pH to keep the protonated acid sites. Optimization of sulfonic functions and Ru nanoparticles amounts will be described, as well as the characterization of each catalyst. Next, with the best bifunctional catalysts obtained, transformation of more challenging substrates such as starch into sorbitol will be investigated. Finally, the ultimate goal of this thesis which is the direct transformation of cellulose into sorbitol will be carried out.

V.1 Bifunctional catalysts: preliminary study

The synthesis of bifunctional catalysts with both sulfonic functions and Ru is a challenge because it is known that sulfur can strongly poison noble metals and especially Ru [1]. The order of the successive functionalization is important. Both orders have been tried out with either Ru nanoparticles deposition at first or sulfonic acid functionalization first. The LHT-OX (carbon nanofibers) has been chosen as support for these catalysts because of the preliminary study that has been carried out with it, modifying particles sizes to find an optimum, as described in Chapter II. The catalysts have been analyzed by XPS (Table V-1). The catalyst with sulfonic functionalization before the addition of Ru nanoparticles is named Ru - SO_3H / LHT-OX, while the opposite methodology gave the solid named SO_3H - Ru / LHT-OX. The Ru nanoparticles deposition method is the same as that was used in Chapter II and III (urea method) and the targeted nanoparticles size is between 1 and 2 nm. Sulfur content is lower when the sulfonic functionalization is done first. Indeed when Ru is deposited after the functionalization it will go preferentially on the sulfonic functions and will cover them, decreasing the sulfur signal in XPS measurements. Moreover the method of deposition for Ru nanoparticles is under basic conditions that will deactivate the sulfonic functions formerly anchored, which is not adequate for our catalytic application.

Table V-1: Element contents in monofunctional and bifunctional catalysts, determined by XPS

	SO_3H / LHT-OX	**Ru / LHT-OX**	**Ru - SO_3H / LHT-OX**	**SO_3H - Ru / LHT-OX**
Element	At. %	At. %	At. %	At. %
O 1s	11.9	7.1	16.9	18.2
Ru 3p	/	1.4	0.9	0.7
N 1s	1.2	0.9	0.8	1.1
C 1s	85.0	90.6	80.7	78.4
S 2p	1.9	/	0.6	1.6

The two bifunctional catalysts have been assessed in the transformation of cellobiose into sorbitol (Table V-2). Confidence intervals have been calculated when the same catalytic test has been carried out at least two times, a table with the repeatability is shown in the supporting information (S1 in SI). It is striking that both bifunctional catalysts are less selective in sorbitol than a mere ruthenium on carbon Ru / LHT-OX catalyst. For the Ru - SO_3H / LHT-OX solid, these results confirm what has been said about the deactivation of sulfonic functions. For the other bifunctional catalyst, SO_3H - Ru / LHT-OX, the lack of sorbitol selectivity can be explained by the poisoning of the Ru nanoparticles by the sulfonic functions. This poisoning effect seems to be even higher when the sulfonic functionalization is done in second position. Indeed during the functionalization process the sulfur will prefer to go on the Ru nanoparticles rather than react with the carbon support.

Table V-2: Hydrogenolysis of cellobiose with monofunctional and bifunctional catalysts; Cellobiose conversion, selectivity in glucose, cellobitol and sorbitol, yield in sorbitol (160 °C, 30 bar of H_2, 2h, 20 mg of catalyst with 3 wt. % of Ru); The estimated confidence interval on cellobiose conversion and selectivities is 3 %

Sample	Conversion (%)	Selectivity in glucose (%)	Selectivity in cellobitol (%)	Selectivity in sorbitol (%)	Yield in sorbitol (%)
Ru / LHT-OX	100	52	n.d.	23	23
Ru - SO_3H / LHT-OX	77	22	n.d.	9	7
SO_3H - Ru / LHT-OX	60	40	n.d.	4	2

These preliminary results have shown the difficulty of having active sulfonic functions and Ru nanoparticles on the same carbon support. In parallel to the bifunctional catalysts fabrication, optimization of carbon materials functionalization with sulfonic moieties has shown that LHT-OX is the least acid-functionalized carbon. Therefore, it has been decided for further optimization to change the support to AC because the sulfonic functionalization is very efficient on it and it is a cheap and industrially-relevant support. The main issue for producing bifunctional catalysts is to adjust the quantity of Ru and SO_3H functions. Indeed in Chapter III the Ru catalysts have been tested with only 20 mg of solid engaged in each test but the acidic catalysts, presented in Chapter IV, have been tested on 300 mg in each test. Catalytic tests have therefore been carried out with both quantities of bifunctional catalysts. Moreover, kinetic studies have been conducted to understand better how the reaction proceeds. The kinetics for the reactions using 20 mg or 300 mg of monofunctional or bifunctional catalysts supported on the active carbon (AC) are presented in Figure V-1.

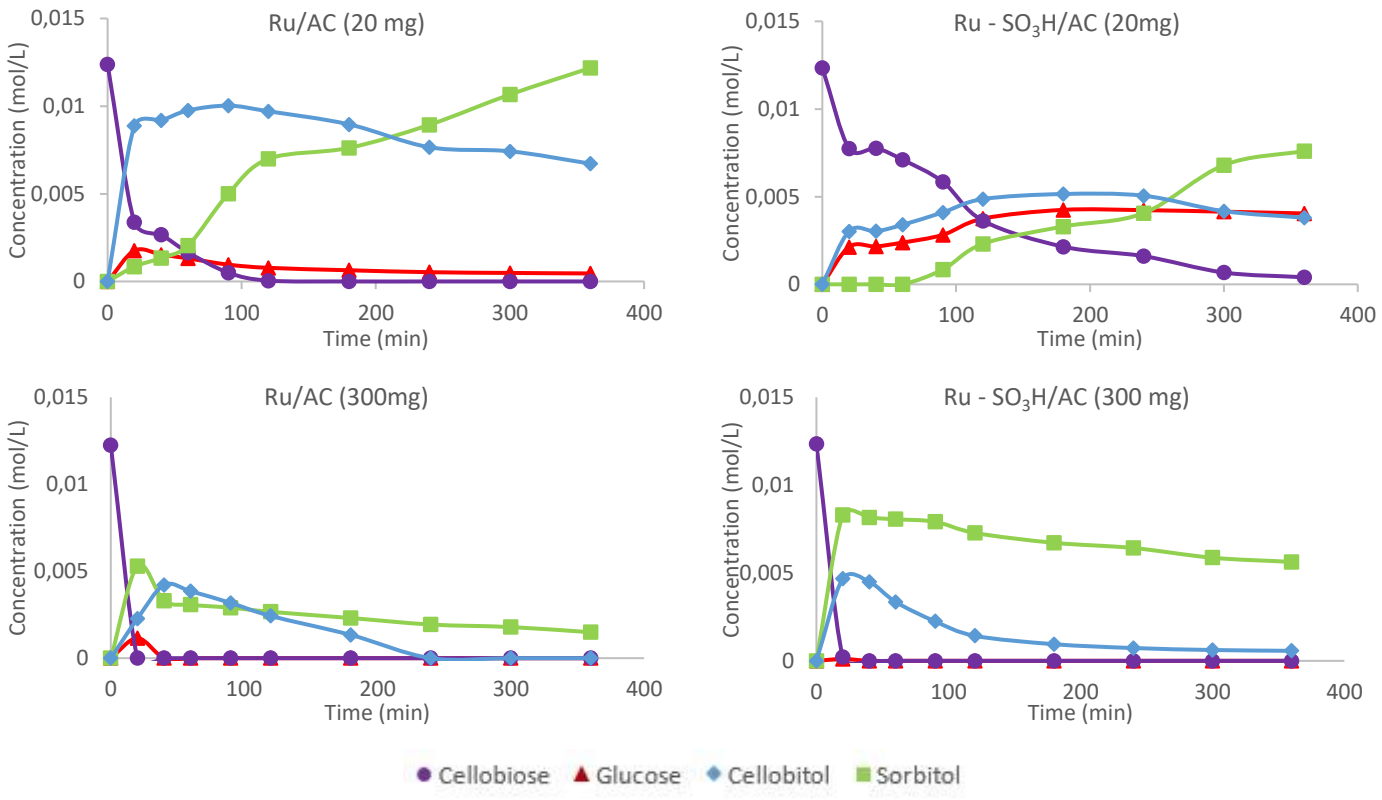

Figure V-1: Kinetic curves for the transformation of cellobiose into sorbitol (testing conditions: 160°C; 30 bar H_2; 1700 rpm)

When 20 mg of catalyst is used, the bifunctional catalyst is less active than the monofunctional one. It means that with low amount of catalyst the poisoning of Ru is too important and an increase in activity cannot be witnessed. It can also be noticed that for the bifunctional catalyst, both pathways are followed to produce sorbitol. Indeed there is a constant increase of both glucose and cellobitol during the reaction before levelling off. By looking at the two kinetic curves with 300 mg of catalyst, it can be seen that the bifunctional catalyst is producing more sorbitol than the monofunctional one. For the Ru/AC catalyst some sorbitol is quickly produced but after that it is decreasing with time. Indeed it is known that sorbitol can react further in presence of Ru catalyst (see Introduction, section I.5). As 300 mg of catalyst have been engaged, the Ru amount is so important that the sorbitol will quickly give side products. However with the bifunctional catalyst, a lower decrease of the sorbitol amounts during the reaction can be observed. The most likely hypothesis is that, as the Ru is poisoned by the SO_3H, it will be less active and then will degrade less the produced sorbitol. Moreover, sorbitol seems to be stabilized by the sulfonic functions as it can be seen that sorbitol is decreasing less with time, while the bifunctional catalyst is very active (100 % of cellobiose conversion after 20 minutes). Nevertheless, by looking at the amount of sorbitol produced during the reaction (in concentration on the y axis) it can be noticed that, when using 300 mg of catalyst, less sorbitol is produced than with 20 mg of the monofunctional catalyst. Having too much Ru engaged in the reaction is not a good option to obtain sorbitol. These results have shown that the optimal bifunctional catalyst is certainly between these two extreme conditions. That is why it has been decided for the next catalytic tests to reduce the temperature to 150 °C to limit the sorbitol degradation. It also has been chosen to use 150 mg of catalyst as a balance between the

conditions studied above and to work on optimizing the ratio between the Ru and the sulfonic acid amounts. As the Ru is quite expensive and knowing that it can easily degrade sorbitol into unwanted side-products, only 1 wt. % will be introduced in the catalysts as a starting point.

V.2 Optimization of the bifunctional catalyst

The bifunctional catalysts that has been studied in the previous section were synthesized with the impregnation method that can deactivate the sulfonic functions. Moreover the Ru was activated at 600 °C in a tubular oven which can also destroy some of the sulfonic functions. Therefore another method to deposit Ru nanoparticles has been chosen. This method is not using basic conditions and will not neutralize the sulfonic acid functions. The idea is to synthesize preformed RuO_2 nanoparticles that are then deposited on the carbon support. This synthesis method can be modulated (by varying experimental conditions) to target the Ru nanoparticles size between 1 and 2 nm that has been determined as optimal in Chapter II. It was also decided to first functionalize the carbon support with the sulfonic functions before adding the RuO_2 nanoparticles, to limit the poisoning of the nanoparticles. Rather than using a high temperature heat treatment under reductive atmosphere that could destroy the sulfonic functions anchored on the carbon support, the Ru will be reduced *in situ* by H_2 during the catalytic reaction and no pre-treatment was implemented for this series of catalysts. Catalytic tests have been carried out with monofunctional, either sulfonic functions alone or RuO_2 nanoparticles alone, and bifunctional catalysts (Table V-3).

Table V-3: Hydrogenolysis of cellobiose with monofunctional and bifunctional catalysts: Cellobiose conversion, selectivity in glucose, cellobitol and sorbitol, yield in sorbitol (150 °C, 30 bar of H_2, 2h, 150 mg of catalyst with 1 wt. % of Ru); The estimated confidence interval on cellobiose conversion and selectivities is 3 %

Catalyst	Cellobiose conversion (%)	Glucose selectivity (%)	Cellobitol selectivity (%)	Sorbitol selectivity (%)	Yield in sorbitol (%)
RuO_2 / AC	100	0	59	29	29
SO_3H / AC	61	86	0	0	0
RuO_2 - SO_3H / AC	65	84	0	2	1
RuO_2 / AC and SO_3H / AC [1]	84	81	0	2	2

[1] Mechanical mix between the two monofunctional catalysts

The hydrogenation pathway is favored with RuO_2 / AC catalyst which gave essentially cellobitol and sorbitol. The SO_3H / AC acid monofunctional catalyst gave high yield of glucose, as expected in the absence of Ru to catalyze the hydrogenation. Unfortunately, with the bifunctional catalyst, prepared exactly in the same way, sorbitol has not been obtained but very similar result than with the acidic catalyst without Ru has been observed. This means in this case that all the Ru is poisoned by the sulfur of the sulfonic functions. A test with the two monofunctional catalysts mechanically mixed has been carried out and the result is still similar to the SO_3H / AC. Even if the sulfonic functions are not on the same support, they manage to poison the Ru.

Several parameters have been studied to optimize the ratio between sulfur and ruthenium. In order to control the amount of sulfur for the preparation of bifunctional catalysts, the degradation of the sulfonic functions grafted on the carbon supports under heat-treatment (under N_2 atmosphere) was investigated (Table V-4). By increasing the heat-treatment temperature, a decrease of the O and S surface amounts is observed. While the acidity (determined by Boehm titration) is not decreasing at 200 °C, it is lower after treatment at 300 °C and 400 °C. This indicates that the sulfonic

functions present on the carbon materials are more destroyed when the temperature of the treatment increases.

Table V-4: Oxygen and sulfur contents determined by XPS and acidity from Boehm titration of the acidic catalyst without heat-treatment and heat-treated at 200 °C, 300 °C and 400 °C

Catalyst	O (at. %)	S (at. %)	Acidity (mmol/100g)
SO_3H / AC	12.95	3.66	145
SO_3H 200°C / AC	10.33	2.96	146
SO_3H 300°C / AC	7.53	1.51	115
SO_3H 400°C / AC	2.88	0.75	69

These new catalysts with varying acidities have been assessed in the hydrolysis of cellobiose into glucose under nitrogen atmosphere (Table V-5). As expected, the activity of these acidic catalysts decreased with the applied heat-treatment temperature. The low selectivity into glucose obtained with the catalysts heated at 300 °C and 400 °C is the same selectivity as obtained when the test is conducted without any catalyst (blank test). The sulfonic functions are no longer useful after these heat-treatments. It is confirming that the sulfonic functions are indeed present in lower amounts when the temperature of the heat treatment is increasing. Moreover it is in adequacy with the results described in Chapter III where it was shown that a minimum amount of SO_3H is needed to trigger the hydrolysis of cellobiose.

Table V-5: Hydrolysis of cellobiose: Cellobiose conversion, selectivity and yield in glucose (150°C, N_2, 2h, 150 mg of catalyst) obtained with acid catalysts heat-treated at different temperatures; The estimated confidence interval on cellobiose conversion and selectivities is 3 %

Catalyst	Cellobiose conversion (%)	Glucose selectivity (%)	Glucose yield (%)
Blank	22	43	9
SO_3H / AC	88	83	73
SO_3H 200°C / AC	47	79	37
SO_3H 300°C / AC	22	39	9
SO_3H 400°C / AC	22	35	8

These supports, possessing different amounts of sulfonic functions, have been used to prepare a set of new bifunctional catalysts by depositing RuO_2 nanoparticles. Hydrogenolysis of cellobiose has been tested for 2 h with these materials to investigate the impact of the Ru/S ratio on the performance of the catalysts (Table V-6).

Table V-6: Hydrogenolysis of cellobiose with bifunctional catalysts possessing different amounts of sulfonic functions: Cellobiose conversion, selectivity in glucose, cellobitol and sorbitol, yield in sorbitol (150 °C, 30 bar of H_2, 2h, 150 mg of catalyst with 1 wt. % of Ru); The estimated confidence interval on cellobiose conversion and selectivities is 3 %

Catalyst	Cellobiose conversion (%)	Glucose selectivity (%)	Cellobitol selectivity (%)	Sorbitol selectivity (%)	Sorbitol yield (%)
RuO_2 - SO_3H 200°C / AC	66	84	0	1	1
RuO_2 - SO_3H 300°C / AC	55	45	37	4	2
RuO_2 - SO_3H 400°C / AC	51	17	55	13	7

These results show that the pathway of the reaction is different depending on the ratio between Ru and sulfonic functions. When the sulfonic functions are treated at 200 °C, they are still present in high amounts and poisoning the Ru. Therefore, the hydrolysis of cellobiose into glucose is the main reaction and sorbitol is not produced. After treatment at 300 °C, sulfonic functions are degraded partially and both pathways are followed in

parallel. Glucose (hydrolysis product) and cellobitol (hydrogenation product) are produced simultaneously while sorbitol production stays really low due to the very short testing duration. The material pre-heated at 400 °C is producing more sorbitol while glucose selectivity is pretty low compared to cellobitol selectivity. It means that in this case the hydrogenation pathway is the major one. All these observations have been confirmed with kinetic studies with each of these catalysts (S11 in SI). After 24 h, it can be observed that the bifunctional catalysts pre-heated at 300 °C and 400 °C produced sorbitol while the pre-heated at 200 °C bifunctional catalyst barely managed to form some of it. The diminution of sulfonic functions allows the Ru to be less poisoned and the resulting bifunctional catalysts can produce sorbitol. However, the sorbitol production was not better than a monofunctional catalyst with only Ru deposited on the unmodified carbon support (see above in Table V-3). Therefore, other ways of enhancing the sorbitol productivity have been investigated.

In order to study a different method that could avoid the poisoning of Ru by the sulfur, consecutive reactions with both monofunctional catalysts have been carried out (Table V-7). Cellobiose conversion and sorbitol yield are always given with respect to the starting material even in the case of consecutive reactions. First hydrogenation using the RuO_2 / AC catalyst has been carried out and then the solution has been filtered out. Consecutively, the SO_3H / AC catalyst has been added to catalyze the hydrolysis. By doing so, a sorbitol yield of 46 % in 2 h has been obtained, which is far better than with any other catalyst tested so far. It is important to highlight the fact that when cellobitol is hydrolyzed, it gives one equivalent of glucose and one equivalent of sorbitol. If staged in this order, the two reactions cannot give 100 % of sorbitol because the glucose produced need to be further hydrogenated. If the two consecutive reactions are done in the opposite

order (first hydrolysis and then hydrogenation) it has to be noticed that the sorbitol yield was dramatically lower (11 %). It can be explained by the fact that during hydrolysis some sulfonic functions will leach and go into solution. Indeed sulfonic moieties were present in the solution as the pH went down from 5 to 3 after the hydrolysis step. Then, when the RuO_2 / AC is added for the second reaction, it is poisoned by sulfur from within the solution, decreasing the Ru activity.

Table V-7: Consecutive reactions with SO_3H / AC without and with a pre-treatment and RuO_2 / AC catalysts: Cellobiose conversion, selectivity in glucose, cellobitol and sorbitol, yield in sorbitol (150 °C, 30 bar of H_2 or autogenic pressure of N_2, 2h, 150 mg of catalyst with 1 wt. % of Ru); The estimated confidence interval on cellobiose conversion and selectivities is 3 %

Catalyst	Cellobiose conversion (%)	Glucose selectivity (%)	Cellobitol selectivity (%)	Sorbitol selectivity (%)	Sorbitol yield (%)
RuO_2 / AC for 2h under H_2	100	0	52	29	29
SO_3H / AC for 2h under N_2	100	6	30	46	46
SO_3H / AC for 2h under N_2	62	88	0	0	0
RuO_2 / AC for 2h under H_2	88	36	32	13	11
Pre-treated SO_3H / AC for 2h under N_2	51	98	0	0	0
RuO_2 / AC for 2h under H_2	100	10	27	37	37

As the sulfonic functions can leach and poison the Ru nanoparticles, a pre-treatment in the same conditions as the catalytic tests has been conducted to remove all labile functions and keep solely the sulfonic groups well grafted on the carbon support. Two consecutive reactions have been carried out with first the pre-treated SO_3H / AC catalyst and then with the RuO_2 / AC catalyst. Sorbitol yield at the end of the two consecutive reactions is significantly higher when the SO_3H / AC is pre-treated beforehand. This shows indeed that the pre-treatment can lower the quantity of labile sulfonic

functions that can poison the Ru nanoparticles. However, there is still a portion of sulfonic functions that inhibit the Ru. Indeed the obtained yield is not as good as when the two consecutive reactions were carried out in the opposite order.

Nevertheless, this pre-treatment on the sulfonic functions has been used to prepare new bifunctional catalysts that would suffer less from the poisoning of the Ru. This time the Ru/S ratio has been optimized by varying the amount of Ru. New catalysts with 1 wt.%, 3 wt.% and 5 wt.% of Ru have been synthesized. They have been assessed as catalysts in comparison with corresponding mono- and bifunctional catalysts without pre-treatment of SO_3H functions (Table V-8). The results obtained with the bifunctional catalyst loaded with 1 wt.% of Ru are similar to the bifunctional catalyst without any pre-treatment of the sulfonic functions. Indeed even if the amount of sulfonic functions decreases with the pre-treatment it is enough to totally inhibit the Ru active phase. For the monofunctional catalyst with 3 wt.% of Ru, it can be observed that the sorbitol yield is the same that the monofunctional catalyst with 1 wt.% Ru. Nevertheless, as the quantity of cellobitol is lower, the sorbitol yield should be higher. It means that sorbitol seems to react further or to suffer from degradation. The bifunctional catalyst with 3 wt.% of Ru is more active than the one with 1 wt.%. The apparition of cellobitol and sorbitol in the products can also be observed. It indicates that both pathways are followed and that both Ru nanoparticles and sulfonic functions are active at the same time. However, the sorbitol yield is still not higher than with the monofunctional catalyst. It is also observed that the bifunctional catalyst with 3 wt.% of Ru without pre-treatment of sulfonic functions displays lower yield of sorbitol. The monofunctional catalyst with 5 wt.% of Ru is giving higher yield of sorbitol which was expected as the Ru quantity is increasing. Finally, the bifunctional

catalyst with 5 wt.% is giving the best results. Indeed the sorbitol yield reaches 53 % in 2 h, indicating that a synergy between the two active sites is happening with this ratio between Ru and SO_3H functions (10 Ru atoms for 1 S atom based on XPS analysis). The sorbitol yield decreases drastically to 13 % when the SO_3H functions are not pre-treated. This highlights the importance of this pre-treatment in order to have an efficient bifunctional catalyst.

Table V-8: Hydrogenolysis of cellobiose with monofunctional and bifunctional catalysts with different Ru weight percentages and pre-treated supports: Cellobiose conversion, selectivity in glucose, cellobitol and sorbitol, yield in sorbitol (150 °C, 30 bar of H_2, 2h, 150 mg of catalyst); The estimated confidence interval on cellobiose conversion and selectivities is 3 %

Catalyst	Cellobiose conversion (%)	Glucose selectivity (%)	Cellobitol selectivity (%)	Sorbitol selectivity (%)	Sorbitol yield (%)
RuO_2 (1%) / AC	100	0	59	29	29
RuO_2 (1%) – SO_3H / AC	65	84	0	2	1
RuO_2 (1%) – pre-treated SO_3H / AC	61	80	0	2	1
RuO_2 (3%) / AC	100	4	34	30	30
RuO_2 (3%) – SO_3H / AC	77	43	36	11	8
RuO_2 (3%) – pre-treated SO_3H / AC	85	26	40	22	19
RuO_2 (5%) / AC	100	3	19	43	43
RuO_2 (5%) – SO_3H / AC	76	29	44	17	13
RuO_2 (5%) – pre-treated SO_3H / AC	100	6	29	53	53

Kinetic studies have been carried out on the monofunctional and bifunctional catalysts with 5 wt.% of Ru to highlight the differences between them (Figure V-2). It can be seen that the bifunctional catalyst is giving higher yield in sorbitol than the monofunctional catalyst during all the investigated timeframe.

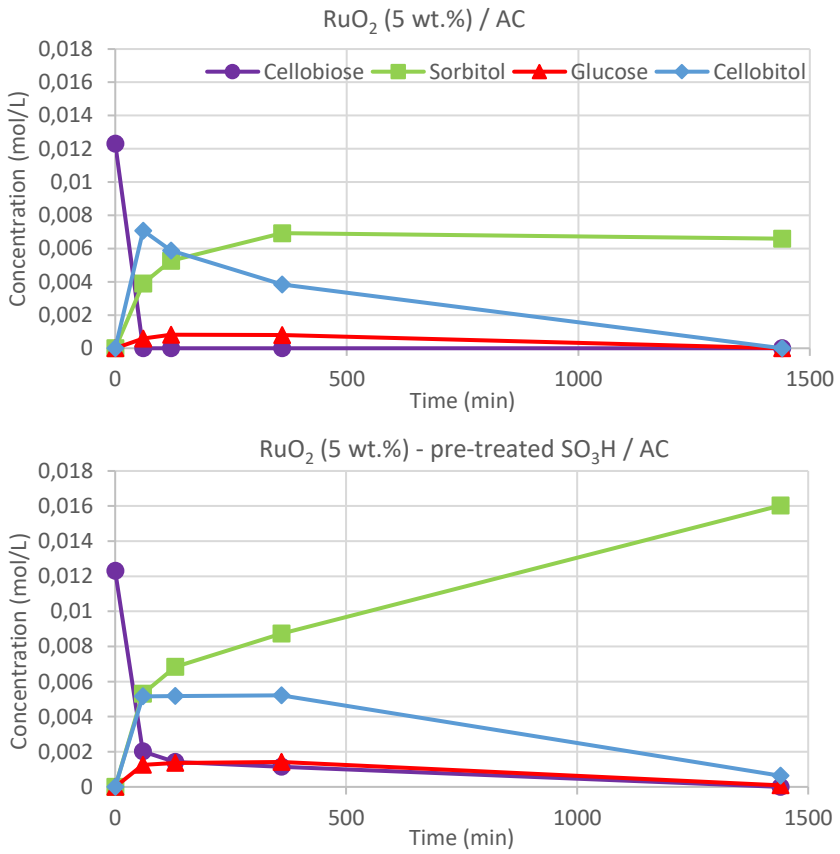

Figure V-2: Kinetic curves for the hydrogenolysis of cellobiose into sorbitol (testing conditions: 150°C, 30 bar of H_2, 24h, 150 mg of catalyst)

Conversion of cellobiose and selectivity/yield in sorbitol are presented in the Supplementary Information (S12 in SI). Sorbitol yield is the same after 6h and after 24h for the monofunctional catalyst whereas cellobitol is decreasing. It confirms our assumption that sorbitol is reacting further during the test. This is not happening with the bifunctional catalyst. The combination of SO_3H functions and Ru nanoparticles in this optimized ratio is stabilizing the sorbitol and preventing it from reacting further or degrading. This effect has been reported in the literature [2]. This explains the higher yield of sorbitol at the end of the reaction. The bifunctional catalyst is

not really more active than the monofunctional catalyst: indeed the conversion is lower at the beginning of the reaction with the RuO_2 - pre-treated SO_3H / AC catalyst, but it is stabilizing sorbitol which gives *in fine* a much higher yield. This effect is striking after 24 h of reaction with a yield of 11 % for the monofunctional catalyst against 79 % for the bifunctional catalyst.

Degradation of sorbitol with the RuO_2 / AC and the bifunctional catalyst has been further studied. Sorbitol (the product of the reaction) rather than cellobiose has been placed in the presence of the two catalysts in the same conditions as in the previous tests (Table V-9). These results show that the RuO_2 / AC can transform 50 % of the sorbitol under these conditions while the bifunctional catalyst has transformed only 7 % sorbitol within 2h. The presence of SO_3H functions highly stabilizes the sorbitol and prevents it from degradation. Unfortunately the products formed by the sorbitol degradation could not be identified with the HPLC column that is used. A list of molecules that have been injected in HPLC and that can be ruled out from possible side products can be found in supporting information (S2 in SI).

Table V-9: Degradation of sorbitol with monofunctional and bifunctional catalysts (150 °C, 30 bar of H_2, 2h, 150 mg of catalyst)

Catalyst	Sorbitol conversion (%)
RuO_2 (5%) / AC	50
RuO_2 (5%) – pre-treated SO_3H / AC	7

To optimize further the Ru/S ratio, modification of sulfur amount using the thermal pre-treatment as a tool for fine-tuning has been investigated with 5 wt.% of Ru loading (Table V-10). The bifunctional catalyst with sulfonic functions treated at 200 °C is giving the same amount of glucose than sorbitol. It means that there are still too many sulfonic groups and that Ru nanoparticles are poisoned. When the sulfonic functions are treated at

300 °C, results are quite the same that when the sulfonic functions are pre-treated in water. The bifunctional catalyst is better than the reference RuO_2 / AC, showing a synergy between the two types of active sites. After a heat-treatment at 400 °C, the bifunctional material displays a lower sorbitol selectivity. Indeed sulfonic functions are more degraded, leading to more active Ru nanoparticles and sorbitol degradation. The synergy between the two active sites is no longer observable.

Table V-10: Hydrogenolysis of cellobiose with bifunctional catalysts possessing sulfonic functions treated at different temperatures: Cellobiose conversion, selectivity in glucose, cellobitol and sorbitol, yield in sorbitol (150 °C, 30 bar of H_2, 2h, 150 mg of catalyst with 5 wt. % of Ru); The estimated confidence interval on cellobiose conversion and selectivities is 3 %

Catalyst	Cellobiose conversion (%)	Glucose selectivity (%)	Cellobitol selectivity (%)	Sorbitol selectivity (%)	Sorbitol yield (%)
RuO_2 (5 wt.%) - SO_3H 200°C / AC	100	26	31	21	21
RuO_2 (5 wt.%) - SO_3H 300°C / AC	100	0	40	47	47
RuO_2 (5 wt.%) - SO_3H 400°C / AC	100	0	47	38	38

Eventually, the recyclability of both monofunctional and the best bifunctional catalysts has been assessed. Five catalytic tests have been carried out with each catalyst (Figure V-3). Both catalysts suffer from deactivation after the first run but the impact is less important on the bifunctional catalyst than on the monofunctional catalyst. The activity is then stable over the next runs.

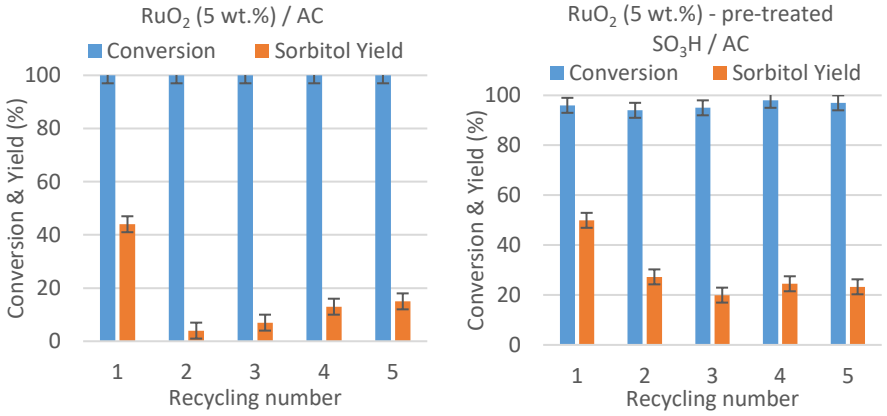

Figure V-3: Recycling tests with monofunctional RuO_2 / AC and bifunctional RuO_2 – pre-treated SO_3H / AC catalysts

XPS characterizations have been performed on the monofunctional and bifunctional catalysts before and after the catalytic tests. The results are presented in Table V-11 while the XPS narrow scans can be found in the SI (S13 in SI). Ru_{3d} (IV) amount is higher for the bifunctional catalyst than the monofunctional one before catalytic test. The same statement can be made for the catalysts with 3 wt.% of Ru (S14 in SI). The in situ activation of Ru in the reactor has been confirmed by these analyses. Indeed, as expected, the Ru(0) amount is drastically increasing after the catalytic tests. It is known that Ru can be reduced during the XPS analyses, explaining the small amount of Ru(0) in the catalysts before tests. It should be noted that not all the Ru(IV) has been reduced during the catalytic tests. Most likely, the core of the nanoparticles has not been reduced and only the surface has become Ru(0).

Table V-11: Atomic percentage of C_{1s} and Ru_{3d} from XPS analyses for monofunctional and bifunctional catalysts before and after five catalytic tests

Catalyst	C_{1s} (at. %)	Ru_{3d} (IV) (at. %)	Ru_{3d} (0) (at. %)
RuO_2 (5%) / AC	62.5	7.1	1.7
RuO_2 (5%) / AC after 5 runs	73.9	1.9	5.3
RuO_2 (5%) – pre-treated SO_3H / AC	52.7	8.3	1.5
RuO_2 (5%) – pre-treated SO_3H / AC after 5 runs	71.0	1.2	3.4

XRD analyses have also been conducted on these catalysts (Figure V-4). The wide peak between 12° and 28° comes from the carbon support (AC)[3]. The Ru peak is around 44° [4]. It is very low for the catalysts before reaction because it is essentially RuO_2. After reaction, Ru is reduced and the Ru peak increases because Ru(0) is crystalline. It is the case for the monofunctional catalyst but surprisingly it has not happened for the bifunctional catalyst. It seems that the presence of sulfonic functions interferes with the crystallinity of the Ru(0) domains.

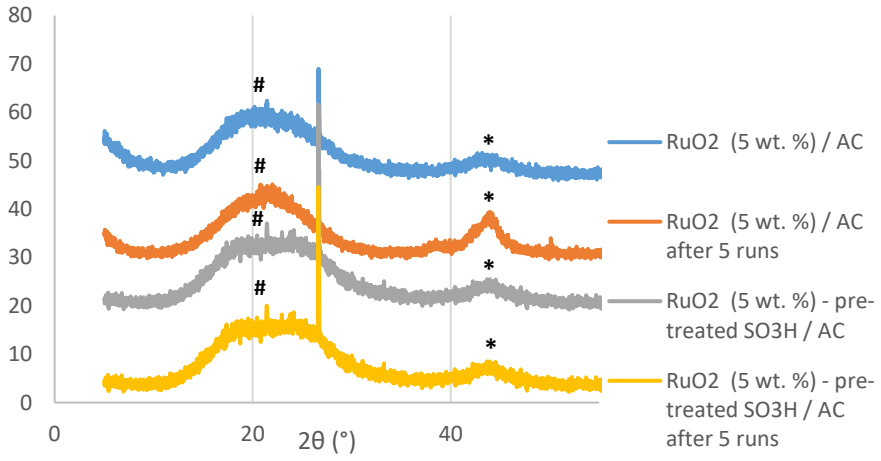

Figure V-4: XRD analyses of monofunctional and bifunctional catalysts before and after catalytic tests. Asterisks denote peaks attributed to the Ru metal phase and '#' denote carbon phase

HR-TEM images have been obtained for these four catalysts (Figure V-5). RuO_2 nanoparticles preparation method can be adapted to control their sizes and a nanoparticles size of 1-2 nm has been targeted here [5]. The images show that RuO_2 nanoparticles have a mean size around 1 nm, as expected. The distribution and the size of the nanoparticles are the same without or with sulfonic functions (compare Figure V-5 a and b). EDX mapping analyses have been performed and have confirmed the good dispersion of the Ru on the carbon support (S15 in SI). When the support is functionalized by the sulfonic functions, sulfur has been found everywhere on the carbon support. There is no specific area that could be identified where Ru and S are more present together. Catalysts, recovered after catalytic reaction (5 runs), have also been analyzed by HR-TEM (Figure V-5 c and d) and EDX (S15 in SI). TEM images have shown that Ru nanoparticles are still well dispersed on the support. However, due to the high temperature during the reaction a small increase of the nanoparticles size can be observed after catalyst recovery but the nanoparticles size is still between 1 and 2 nm. The presence of sulfur everywhere on the support for the bifunctional catalyst after 5 runs has been confirmed by EDX analyses.

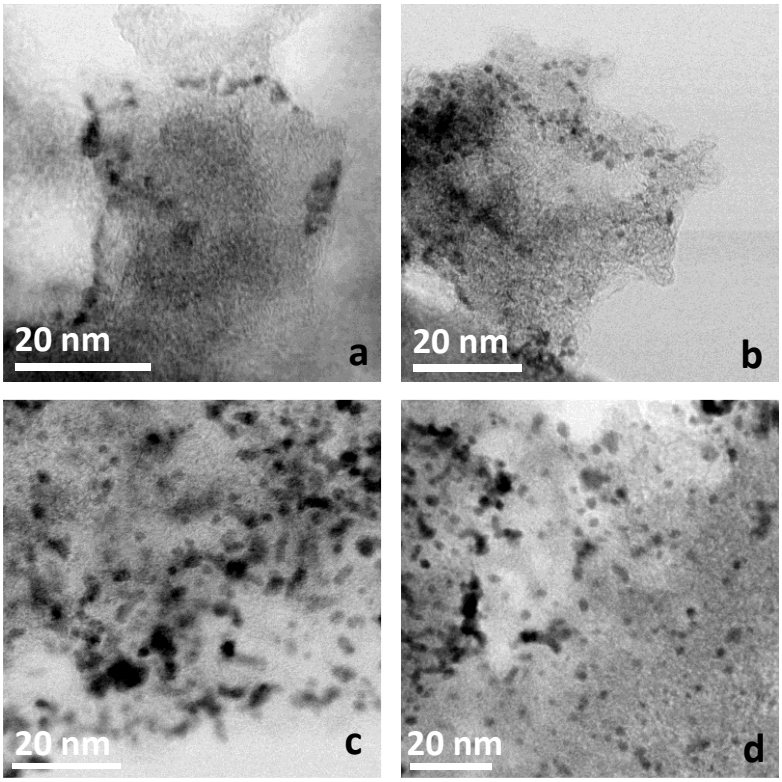

Figure V-5: HR-TEM images for a) RuO_2 (5%) / AC; b) RuO_2 (5%) – pre-treated SO_3H / AC; c) RuO_2 (5%) / AC after 5 runs; d) RuO_2 (5%) – pre-treated SO_3H / AC after 5 runs

In conclusion for this section, superiority of the bifunctional catalyst over the monofunctional catalyst has been demonstrated. Synergy between Ru nanoparticles and sulfonic functions has been highlighted even though they do not seem compatible at first sight. The recyclability of the bifunctional catalyst has been established and the catalyst has been confirmed undamaged by XRD, TEM and EDX analyses after 5 catalytic runs.

V.3 Transformation of starch into sorbitol

In the previous section, efficient bifunctional catalysts have been synthesized for the transformation of cellobiose into sorbitol. As the main goal of this thesis project is to produce sorbitol directly from biomass, the

best bifunctional catalysts have been assessed with more challenging substrates. The first catalytic tests of this type have been conducted on starch transformation into sorbitol. The hydrolysis of starch with sulfonated AC has been studied and only 59 % of selectivity into glucose was obtained. The hydrolysis of starch into glucose seems to be less controlled than with cellobiose. Indeed, starch is a mixture of two glucose polymers: amylose and amylopectin. Glucose units are mainly connected by α-1,4-glycosidic bond and by a few β-1-4- glycosidic bond in amylopectin. Its hydrolysis can lead to oligomers instead of glucose monomers. Bifunctional catalyst and monofunctional catalyst (only Ru) have been tested for the hydrogenolysis (Table V-12). Conversion of starch is difficult to estimate because starch itself cannot be analyzed by the column that is used in HPLC. Therefore, results have been presented as sorbitol / glucose molar ratio obtained at the end of the 2 hours catalytic test. It allows comparison between the two catalysts without knowing starch conversion. Hydrolysis of starch into glucose and further hydrogenation into sorbitol is a well-known process as reported in the literature[6]. Nevertheless the results are striking: the bifunctional catalyst is producing less sorbitol than the monofunctional one. Unfortunately there are no explanations for this lack of activity after the good results on cellobiose transformation into sorbitol with the same catalysts.

Table V-12: Hydrogenolysis of starch with monofunctional and bifunctional catalysts: Molar ratio between sorbitol and glucose obtained at the end of the test (150 °C, 30 bar of H_2, 2h, 150 mg of catalyst, 1 g of starch)

Catalyst	Sorbitol / Glucose molar ratio
RuO_2 (5%) / AC	18.86
RuO_2 (5%) – pre-treated SO_3H / AC	0.82

V.4 Transformation of cellulose into sorbitol

In this section cellulose direct transformation into sorbitol will be investigated. The main issue of using cellulose as substrate is that it is not soluble in water. It means that after the reaction, when the catalyst is filtrated, the cellulose that has not reacted will be also collected. The cellulose conversion can be calculated by subtracting the initial mass of the catalyst from the final mass of solid recovered.

V.4.1 Cellulose pre-treatment

Due to its insolubility in water, cellulose has difficulties to react in this medium. That is why a variety of pre-treatments can be conducted to make cellulose more reactive as explained in the General Introduction [7–10]. In our case a ball-milling of 24h has been chosen. The conditions have been detailed in the Experimental section. First, the reactivity of our bifunctional catalyst with and without prior ball-milling of the cellulose has been assessed (Table V-13).

Table V-13: Hydrogenolysis of cellulose with bifunctional catalyst (RuO_2 (5%) – pre-treated SO_3H / AC): Cellulose conversion, selectivity in xylitol, mannitol and sorbitol, yield in sorbitol (150 °C, 30 bar of H_2, 2h, 150 mg of catalyst, 1 g of cellulose); The estimated confidence interval on cellulose conversion and selectivities is 5 %

Pre-treatment	Cellulose conversion (%)	Xylitol selectivity (%)	Mannitol selectivity (%)	Sorbitol selectivity (%)	Sorbitol yield (%)
No ball-milling	20	7	0	10	2
Ball-milling (300 rpm)	25	11	7	28	7

Cellulose conversion in these soft conditions (150 °C) is low. Ball-milling of the cellulose has enhanced its reactivity as an increase of both conversion and selectivity in sorbitol are obtained. Two side-products have been identified, namely xylitol and mannitol (Scheme V-1). Mannitol is coming from the isomerization of sorbitol while xylitol and arabitol are

produced by the decarbonylation of sorbitol[11]. Arabitol has not been identified as reaction product in our case. These side-products were not present in the catalytic tests on cellobiose. Traces (< 1 %) of cellobiose and glucose can also be seen on the chromatograms but it has not been indicated in the results table for the sake of clarity and readibility.

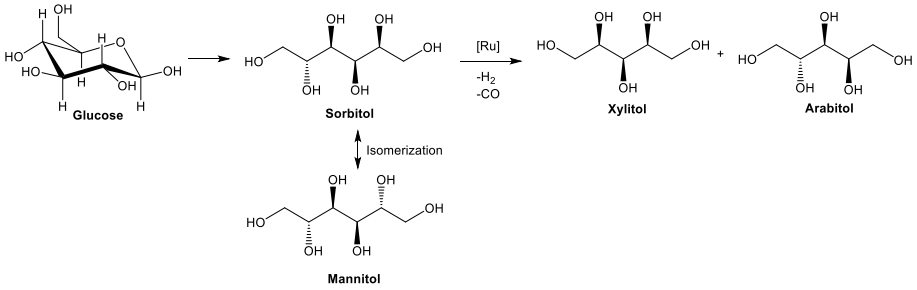

Scheme V-1: Formation of sorbitol, mannitol, xylitol and arabitol from glucose (adapted from [11])

V.4.2 Reaction conditions optimization

As low yields of sorbitol have been obtained in the previous conditions, an increase of the reaction time has been studied with the bifunctional catalyst and ball-milled cellulose (Table V-14). Increasing the reaction time has improved the cellulose conversion as well as the sorbitol selectivity. As explained in Section V.2, sorbitol can further react in these conditions to give side-products. Here it seems that even if it can happen, a longer reaction time manages to produce more sorbitol and counterbalances its degradation.

Table V-14: Hydrogenolysis of cellulose with bifunctional catalyst (RuO_2 (5%) – pre-treated SO_3H / AC): Cellulose conversion, selectivity in xylitol, mannitol and sorbitol, yield in sorbitol (150 °C, 30 bar of H_2, 150 mg of catalyst, 1 g of ball-milled cellulose (300 rpm)); The estimated confidence interval on cellulose conversion and selectivities is 5 %

Reaction time	Cellulose conversion (%)	Xylitol selectivity (%)	Mannitol selectivity (%)	Sorbitol selectivity (%)	Sorbitol yield (%)
2h	25	11	7	28	7
6h	29	10	8	34	10
24h	44	6	5	37	16

The next parameter that has been optimized was the temperature. In order to improve the cellulose reactivity, the temperature has been increased to 170 °C and 190 °C (Table V-15). The impact of the temperature is striking on the cellulose conversion: a slight increase at 170 °C and a huge improvement at 190 °C are observed. However the selectivity in sorbitol stays around 30 % with a maximum of 34 % at 170 °C. Indeed, it is known that increasing the temperature will favor the sorbitol degradation[7]. A test at 190 °C during 24h has been conducted and has confirmed that sorbitol selectivity is dropping when high temperature and too long reaction time are applied. However the cellulose conversion has reached almost 100 % and the global yield of sorbitol (20 %) is the same for both conditions. The optimal conditions to maximize the sorbitol yield should be somewhere between 2h and 24h. Unfortunately kinetic studies are difficult to build on this reaction. Indeed as the cellulose is not soluble in water, the solid has to be weighed after filtration to calculate the cellulose conversion by subtracting catalyst mass to the final combined mass. Aliquots cannot be taken during the reaction to have enough data points in order to build a kinetic curve.

Table V-15: Hydrogenolysis of cellulose with bifunctional catalyst (RuO_2 (5%) – pre-treated SO_3H / AC): Cellulose conversion, selectivity in xylitol, mannitol and sorbitol, yield in sorbitol (30 bar of H_2, 150 mg of catalyst, 1 g of ball-milled cellulose (300 rpm)); The estimated confidence interval on cellulose conversion and selectivities is 5 %

Temperature and time	Cellulose conversion (%)	Xylitol selectivity (%)	Mannitol selectivity (%)	Sorbitol selectivity (%)	Sorbitol yield (%)
150 °C / 2h	25	11	7	28	7
170 °C / 2h	35	8	6	34	12
190 °C / 2h	70	3	5	30	21
190 °C / 24h	98	2	4	20	20

A comparison between the monofunctional and the bifunctional catalyst has been conducted with two different reaction conditions: at 150 °C during 24h and at 190 °C during 2h (Table V-16). The results indicate that the same cellulose conversion has been obtained with both catalysts. However the bifunctional catalyst has produced almost twice the amount of sorbitol. Side products such as xylitol and mannitol (see Scheme V-1 above) have been less formed with the bifunctional catalyst. The same effect of sorbitol stabilization as it has been shown in the previous section can be observed here. This highlights the synergy between the Ru and the sulfonic functions and confirms that the bifunctional catalyst is definitely better than the monofunctional catalyst for sorbitol production.

Table V-16: Hydrogenolysis of cellulose with monofunctional and bifunctional catalyst: Cellulose conversion, selectivity in xylitol, mannitol and sorbitol, yield in sorbitol (30 bar of H_2, 150 mg of catalyst, 1 g of ball-milled cellulose (300 rpm)); The estimated confidence interval on cellulose conversion and selectivities is 5 %

Catalyst	Cellulose conversion (%)	Xylitol selectivity (%)	Mannitol selectivity (%)	Sorbitol selectivity (%)	Sorbitol yield (%)
RuO_2 (5%) / AC[a]	43	7	12	21	9
RuO_2 (5%) – pre-treated SO_3H / AC[a]	44	6	5	37	16
RuO_2 (5%) / AC[b]	69	8	15	13	9
RuO_2 (5%) – pre-treated SO_3H / AC[b]	70	3	5	30	21

[a]150 °C and 24 h; [b]190 °C and 2h

The experimental conditions of the ball-milling step have been investigated. The rotation speed was increased to 500 rpm to observe if the cellulose could be made even more reactive or not (Table V-17). Surprisingly, the results have shown the opposite trend, as the sorbitol selectivity has decreased. The ball-milling conditions at 300 rpm have therefore been kept for the subsequent catalytic tests on cellulose.

Table V-17: Hydrogenolysis of cellulose with bifunctional catalyst (RuO_2 (5%) – pre-treated SO_3H / AC): Cellulose conversion, selectivity in xylitol, mannitol and sorbitol, yield in sorbitol (170 °C; 30 bar of H_2, 2h, 150 mg of catalyst, 1 g of ball-milled cellulose (300 and 500 rpm)); The estimated confidence interval on cellulose conversion and selectivities is 5 %

Cellulose pre-treatment	Cellulose conversion (%)	Xylitol selectivity (%)	Mannitol selectivity (%)	Sorbitol selectivity (%)	Sorbitol yield (%)
Ball-milling at 300 rpm	35	8	6	34	12
Ball-milling at 500 rpm	31	7	6	25	8

V.4.3 Combined ball-milling of cellulose with catalyst

In order to maximize sorbitol yield, a new pre-treatment has been set up. As the cellulose is not soluble in water, increasing its proximity with the catalyst should enhance its reactivity. That is why doing a combined ball-milling pre-treatment of the cellulose with the catalyst has been imagined just before starting the reaction. This ball-milling is shorter than the

pre-treatment of cellulose alone, only 2h, and is detailed in the Experimental section (Chap. VII). Cellulose is still ball-milled during 24h before this second pre-treatment. The results obtained by doing so are presented in Table V-18. If these results are compared with the results without ball-milling of both cellulose and catalyst together (Table V-15) it can be seen that this combined ball-milling has a positive impact on the results. The cellulose conversion has increased for all temperatures. The selectivity in sorbitol has remained the same for the test at 150 °C but it has increased drastically for the tests at 170 °C and 190 °C. With this new method, almost 40 % of sorbitol yield can be reached at 190 °C in only 2h directly from cellulose. A catalytic test with the monofunctional catalyst has been conducted similarly and the results have also been better when implementing the combined ball-milling. However it has been confirmed that the bifunctional catalyst is better than the monofunctional one even in these new conditions.

Table V-18: Hydrogenolysis of cellulose with monofunctional and bifunctional catalysts: Cellulose conversion, selectivity in xylitol, mannitol and sorbitol, yield in sorbitol (30 bar of H_2, 2h, 150 mg of catalyst, 1 g of ball-milled cellulose (300 rpm) with combined ball-milling); The estimated confidence interval on cellulose conversion and selectivities is 5 %

Conditions	Cellulose conversion (%)	Xylitol selectivity (%)	Mannitol selectivity (%)	Sorbitol selectivity (%)	Yield in sorbitol (%)
150 °C + bifunctional catalyst	33	6	6	28	9
170 °C + monofunctional catalyst	40	8	13	33	13
170 °C + bifunctional catalyst	52	5	6	50	26
190 °C + bifunctional catalyst	73	2	6	54	39

As the combined ball-milling of the cellulose and the catalyst has extended the total ball-milling time of cellulose of 2h, it is legitimate to ask ourselves if this increase of activity is due to the extra ball-milling duration or the proximity between the cellulose and the catalyst. A catalytic test with

cellulose pre-treated during 26h has been carried out to address this issue (Table V-19). The results show that the ball-milling of cellulose during 26h has increased slightly the activity compared to 24h ball-milling. However the combined ball-milling of both cellulose and the catalyst has given the best results. It can be concluded that the combined ball-milling has a real effect on the reactivity between cellulose and the catalyst.

Table V-19: Hydrogenolysis of cellulose with bifunctional catalyst (RuO_2 (5%) – pre-treated SO_3H / AC): Cellulose conversion, selectivity in xylitol, mannitol and sorbitol, yield in sorbitol (170 °C; 30 bar of H_2, 2h, 150 mg of catalyst, 1 g of ball-milled cellulose (300 rpm) with and without combined ball-milling); The estimated confidence interval on cellulose conversion and selectivities is 5 %

Conditions	Cellulose conversion (%)	Xylitol selectivity (%)	Mannitol selectivity (%)	Sorbitol selectivity (%)	Sorbitol yield (%)
170 °C + combined ball-milling	52	5	6	50	26
170 °C with 26h ball-milled cellulose (no combined ball-milling)	37	5	7	38	14

Other conditions have been studied in order to optimize sorbitol production. As it was shown that sorbitol selectivity is decreasing when the reaction time is increased at 190 °C, it has been decided to increase the reaction time at lower temperature (Table V-20). It can be noticed that the conversion of cellulose and the selectivity in sorbitol have slightly increased at 150 °C with 24h of reaction time. At 170 °, a better conversion of cellulose has been obtained with longer reaction duration. However, this increase of conversion is very slight regarding the huge difference of reaction time. It suggests that poisoning of a cellulose by-product on the catalyst could occur or that something is happening to deactivate the catalyst that is slowing down the reaction drastically. A drop of catalyst activity in the case of cellobiose transformation had already been noticed in the previous section (see Figure V-3). Moreover, the sorbitol selectivity has decreased and has

even dropped to only 10 % after 24h. It can be concluded that at 150 °C the gain in conversion and sorbitol selectivity is too low to be relevant regarding the reaction time increase and that at 170 °C short reaction time is the best way to obtain high selectivity in sorbitol.

Table V-20: Hydrogenolysis of cellulose with bifunctional catalyst (RuO_2 (5%) – pre-treated SO_3H / AC): Cellulose conversion, selectivity in xylitol, mannitol and sorbitol, yield in sorbitol (30 bar of H_2, 150 mg of catalyst, 1 g of ball-milled cellulose (300 rpm) with combined ball-milling); The estimated confidence interval on cellulose conversion and selectivities is 5 %

Temperature and time	Cellulose conversion (%)	Xylitol selectivity (%)	Mannitol selectivity (%)	Sorbitol selectivity (%)	Sorbitol yield (%)
150 °C / 24h	44	4	5	36	16
170 °C / 6h	58	3	5	40	23
170 °C / 24h	66	0	1	10	7

V.4.4 Comparison with literature

As the superiority of bifunctional catalysts towards the monofunctional catalyst has been demonstrated, it is time to compare the results with the literature. In order to do that, two catalytic tests have been carried out using another cellulose grade: Avicel PH-101 (Table V-21). Indeed the Avicel PH-101 cellulose has been chosen as it is the most common one that can be found in the literature in similar studies[10]. Surprisingly, the results are here almost the same without and with the combined ball-milling of both catalyst and cellulose before the reaction. Only a slight increase of the cellulose conversion can be observed when implementing the combined ball-milling. If these results are compared with the ones obtained with the other cellulose type, it can be noticed that the Avicel PH-101 cellulose produces a little less sorbitol in the same conditions. As these results are almost similar to the ones obtained with the first cellulose grade, all the

conclusions that have been established above can stand for this second cellulose type.

Table V-21: Hydrogenolysis of cellulose with bifunctional catalyst (RuO_2 (5%) – pre-treated SO_3H / AC): Cellulose conversion, selectivity in xylitol, mannitol and sorbitol, yield in sorbitol (190 °C, 30 bar of H_2, 2h, 150 mg of catalyst, 1 g of ball-milled cellulose (300 rpm) with and without combined ball-milling); The estimated confidence interval on cellulose conversion and selectivities is 5 %

Catalyst	Cellulose conversion (%)	Xylitol selectivity (%)	Mannitol selectivity (%)	Sorbitol selectivity (%)	Sorbitol yield (%)
RuO_2 (5%) – pre-treated SO_3H / AC without combined ball-milling	64	0	4	38	24
RuO_2 (5%) – pre-treated SO_3H / AC with combined ball-milling	71	0	4	38	27

These results obtained in the best possible conditions, using the Avicel PH-101 cellulose allows us to compare our results with literature and to benchmark the performance obtained in comparison to all the other catalysts envisaged for sorbitol production.

Table V-22 is depicting the sorbitol production obtained directly from cellulose with various Ru based catalysts. Comparison between literature results and our work is not always an easy task because of the differences in reaction conditions. By looking at the entry 1, it can be observed that sorbitol has been produced from crystalline cellulose with monofunctional Ru catalyst in short reaction time but with a very high reaction temperature. The best catalyst presented in this work has shown similar result at lower temperature with joint ball-milling and longer reaction time (entry 13). Entry 2 is giving similar sorbitol productivity and is using the same reaction conditions than our work except for the reaction time and Ru loading. This highlights the improvement of catalyst activity by the sulfonic functions and the ball-milling procedure. Entries 3 and 4 are using bifunctional catalysts

with Ru nanoparticles on AC doped with heteropolyacids. Despite the harsh reaction conditions (lower cellulose / catalyst ratio, higher reaction time and temperature), the sorbitol yields obtained by these authors are lower than the ones obtained with the catalysts that have been made in this work. The fact that the joint ball-milling step is slightly decreasing the sorbitol yield in their case is unexpected. Indeed, the common catalyst/substrate ball-milling usually increases the catalytic activity of the system. Similar bifunctional catalysts using Ru and SO_3H-AC (sulfonation was achieved by using concentrated H_2SO_4) have been used (entries 5 and 6) with 10 wt. % of Ru loading. The difference without and with joint ball-milling is striking and it shows that joint ball-milling can lead to excellent sorbitol production. Higher Ru loading, lower substrate / catalyst ratio and higher reaction time are explaining the better activity of this catalyst compared with ours despite the lower reaction temperature. Entries 7 and 8 are using the same type of catalyst than us with the same Ru loading. However in their case 5 wt. % of Ru is leading to lower selectivity in hexitols (they have not separated the selectivities in sorbitol and mannitol). Despite using lower substrate / catalyst ratio and higher reaction time, the results they obtained are quite similar to ours, which indicates that our catalyst seem to be more active. Nevertheless, such comparisons are very delicate because the impact of each variation of experimental condition is difficult to predict. Sulfonated silica with Ru can be used to produce sorbitol at low temperature with low cellulose / catalyst ratio and longer reaction time (entry 9). Entry 10 is giving the results for a bifunctional catalyst with Ru on acidic zeolite. Low yield of sorbitol has been obtained but it can be attributed to the use of microcrystalline cellulose as substrate. The last two entries (11 and 12) are using a mix of two catalysts, Ru on mesoporous carbon and acidic catalyst (ZrP). Once again, the joint ball-milling of cellulose with catalysts is drastically

improving the sorbitol yield. Globally our best catalyst is very efficient and the sorbitol yield that can be obtained is competing with the literature results. Moreover, our reaction conditions with high cellulose / catalyst ratio, and short reaction time are beneficial for possible industrial applications.

Table V-22: Transformation of cellulose into sorbitol from literature

Entry	Catalyst	Cellulose pre-treatment	Cellulose / catalyst mass (mg)	Time (h)	Temperature (°C)	Cellulose conversion (%)	Sorbitol yield (%)	Mannitol yield (%)	Ref.
1	*4 wt. % Ru/AC*	Microcrystalline cellulose	1000 / 100	0.5	245	86	30	10	[12]
2	*2 wt. % Ru/AC*	Ball-milling	324 / 50	18	190	83	30	8	[13]
3	*0.4 wt. % Ru / AC – TPA ($H_3O_{40}PW_{12}{\cdot}nH_2O$)*	Ball-milling	750 / 300	6	205	98	16	n.d.	[14]
4	*0.4 wt. % Ru / AC – TPA ($H_3O_{40}PW_{12}{\cdot}nH_2O$)*	Joined ball-milling	750 / 300	6	205	100	13	n.d.	[14]
5	*10 wt. % Ru / AC-SO_3H*	Microcrystalline cellulose	50 / 20	24	165	20	9	4	[15]
6	*10 wt. % Ru / AC-SO_3H*	Ball-milling	50 / 20	24	165	81	59	7	[15]
7	*3 wt. % Ru / AC-SO_3H*	Ball-milling	1120 / 480	24	180	95	Sum = 42		[16]
8	*5 wt. % Ru / AC-SO_3H*	Ball-milling	1120 / 480	24	180	95	Sum = 10		[16]
9	*3 wt. % Ru / SiO_2-SO_3H*	Ball-milling	250 / 200	10	150	90	61	7	[2]
10	*3 wt. % Ru / BEA zeolite*	Microcrystalline cellulose	140 / 60	24	180	35	21	n.d.	[17]
11	*ZrP (900 mg) – 3 wt. % Ru / MC (mesoporous carbon)*	Microcrystalline cellulose	500 / 30	1.5	170	34	21	1	[18]
12	*ZrP (900 mg) – 3 wt. % Ru / MC*	Joined ball-milling	500 / 30	1.5	170	100	66	2	[18]
13	*RuO_2 (5%) – pre-treated SO_3H / AC*	Joined ball-milling	1000 / 150	2	190	71	27	3	Our work

V.5 Conclusion

Bifunctional catalysts combining Ru nanoparticles and sulfonic functions on the same carbon support have been synthesized to produce sorbitol directly from cellobiose or cellulose. Poisoning of the Ru nanoparticles by the sulfur is known in literature and has been highlighted in the preliminary results. To avoid that effect, optimization of the ratio between the Ru and the sulfur has been required, as well as finding an adequate synthesis procedure allowing to keep the two types of surface sites active. It has been demonstrated that the amount of sulfonic functions can be lowered by heat treatment or pre-treatment in water in the same conditions than the catalytic test to remove all the labile groups. By diminishing the amount of sulfonic functions, a better activity was obtained with the bifunctional catalyst but not as much as with the monofunctional catalyst used as reference. The amount of Ru had to be increased to 5 wt. % to find the best ratio between the two active sites and obtain a bifunctional catalyst that outperforms the monofunctional one. Synergy between the two sites has been highlighted. Indeed, sulfonic functions are enhancing the hydrolysis of cellobiose and cellobitol and Ru promotes hydrogenation. Moreover, the acidic functions are stabilizing the sorbitol by avoiding its degradation into side-products. These two positive effects together are largely compensating the poisoning of a part of the Ru nanoparticles. Kinetic studies have confirmed the advantage of the bifunctional catalyst against the monofunctional one, especially during long reaction time. Recyclability tests have been conducted and the bifunctional catalyst displayed a better sustainability than the monofunctional one.

After that, catalytic tests have been carried out with starch and cellulose. Unfortunately the tests with starch have not been conclusive as there was no improvement with the bifunctional catalyst. By opposition,

sorbitol has been produced successfully directly from cellulose. Test conditions have been optimized and it has been shown that short reaction time with high temperature is the best way to produce sorbitol. Ball-milling of the cellulose has also helped to produce more sorbitol. The best conditions that have been found are: 190 °C, 2h, 30 bar of H_2 and combined ball-milling of 1 g of cellulose and 150 mg of catalyst. These conditions are giving a total sorbitol yield of 39 % with cellulose from Sigma-Aldrich and 27 % with Avicel PH-101. A lot of parameters can be tuned even more to maximize the sorbitol production but our main goal has been achieved: producing sorbitol directly from cellulose and showing that a bifunctional catalyst has a better activity than a simple Ru / C catalyst.

Finally, comparison of our best catalyst with various catalysts from literature used for direct production of sorbitol from cellulose has been performed. Such comparison is difficult because of the different reaction conditions. However, it can be noticed that our best catalyst is giving excellent results that are competitive compared to published performance, which highlights the promising potential of synergy between Ru nanoparticles and sulfonic functions.

References

[1] M. Dreher, M. Steib, M. Nachtegaal, J. Wambach, F. Vogel, *ChemCatChem* **2014**, *6*, 626–633.

[2] W. Zhu, H. Yang, J. Chen, C. Chen, L. Guo, H. Gan, X. Zhao, Z. Hou, *Green Chem.* **2014**, *16*, 1534.

[3] Z. Q. Li, C. J. Lu, Z. P. Xia, Y. Zhou, Z. Luo, *Carbon N. Y.* **2007**, *45*, 1686–1695.

[4] J. Z. Bloh, R. Dillert, D. W. Bahnemann, *Phys. Chem. Chem. Phys.* **2014**, *16*, 5833–5845.

[5] C. Sassoye, G. Muller, D. P. Debecker, A. Karelovic, S. Cassaignon, C. Pizarro, P. Ruiz, C. Sanchez, *Green Chem.* **2011**, *13*, 3230–3237.

[6] R. Höfer, in *Ind. Biorefineries White Biotechnol.*, Elsevier, **2015**, pp. 157–235.

[7] B. Zada, M. Chen, C. Chen, L. Yan, Q. Xu, W. Li, Q. Guo, Y. Fu, *Sci. China Chem.* **2017**, *60*, 853–869.

[8] V. Chaturvedi, P. Verma, *3 Biotech* **2013**, *3*, 415–431.

[9] S. Haghighi Mood, A. Hossein Golfeshan, M. Tabatabaei, G. Salehi Jouzani, G. H. Najafi, M. Gholami, M. Ardjmand, *Renew. Sustain. Energy Rev.* **2013**, *27*, 77–93.

[10] Y. Liao, B. O. de Beeck, K. Thielemans, T. Ennaert, J. Snelders, M. Dusselier, C. M. Courtin, B. F. Sels, *Mol. Catal.* **2020**, *487*, 110883.

[11] P. J. C. Hausoul, L. Negahdar, K. Schute, R. Palkovits, *ChemSusChem* **2015**, *8*, 3323–3330.

[12] C. Luo, S. Wang, H. Liu, *Angew. Chemie - Int. Ed.* **2007**, *46*, 7636–7639.

[13] H. Kobayashi, H. Matsuhashi, T. Komanoya, K. Hara, A. Fukuoka, *Chem. Commun.* **2011**, *47*, 2366–2368.

[14] M. Almohalla, I. Rodríguez-Ramos, L. S. Ribeiro, J. J. M. Órfão, M. F. R. Pereira, A. Guerrero-Ruiz, *Catal. Today* **2018**, *301*, 65–71.

[15] J. W. Han, H. Lee, *Catal. Commun.* **2012**, *19*, 115–118.

[16] P. A. Lazaridis, S. A. Karakoulia, C. Teodorescu, N. Apostol, D. Macovei, A. Panteli, A. Delimitis, S. M. Coman, V. I. Parvulescu, K. S. Triantafyllidis, *Appl. Catal. B Environ.* **2017**, *214*, 1–14.

[17] A. Negoi, K. Triantafyllidis, V. I. Parvulescu, S. M. Coman, *Catal. Today* **2014**, *223*, 122–128.

[18] G. Zhang, T. Chen, Y. Zhang, T. Liu, G. Wang, *Catal. Letters* **2020**, *150*, 2294–2303.

Chapter VI

Conclusions and prospects

VI.1 General conclusion

This work has been divided into three major parts: a study of the glucose/cellobiose hydrogenation reaction with Ru catalysts, hydrolysis optimization with sulfonated carbon materials and fabrication of bifunctional catalysts for the direct transformation of cellulose into sorbitol.

Firstly, Ru nanoparticles have been deposited on three different carbon supports (CNF, AC and GNP). Two deposition methods have been compared: $NaBH_4$ method that has given poor dispersion and large nanoparticles and urea method that gave better dispersion and small nanoparticles. Nanoparticles size has been controlled by adapting heat-treatment on small nanoparticles. Reaction conditions of glucose hydrogenation have been studied to witness the impact of each factor on the conversion of glucose and the selectivity in sorbitol. Increasing temperature and reaction duration have boosted glucose conversion at the expense of sorbitol selectivity. H_2 pressure had no major influence between 30 bar and 50 bar. Intermediate experimental conditions that allow us comparisons between different catalysts have been chosen: 140 °C, 30 bar of H_2 during 2 h. Using these conditions, the optimal Ru nanoparticles size, namely 1-2 nm, has been successfully determined for hydrogenation of glucose into sorbitol. This optimal nanoparticles size has been targeted in all the following steps.

Secondly, nitrogen incorporation into carbon materials and its influence on Ru activity have been investigated. Two methods to dope carbon materials with nitrogen have been compared: urea adsorption on carbon materials and reaction between carbon surface and ethylenediamine (EDA). The first method gave disappointing results while the EDA method successfully incorporated nitrogen functions on carbon materials (AC and GNP). Heat-treatments have been applied after both methods to force

nitrogen incorporation within the carbon material polyaromatic structure. The carbon functionalization has been confirmed by XPS, which determined the type of nitrogen functions, and by CO_2-TPD and Boehm titrations, which informed us on the number of basic/nitrogen sites. N-doped carbon materials have then been used as supports for Ru nanoparticles. The nitrogen doping enhanced Ru nanoparticles dispersion and their crystallinity (as confirmed by TEM and XRD). These catalysts have been tested for cellobiose transformation into sorbitol. Cellobiose has been chosen instead of glucose as starting reactant to have a more realistic substrate as model for biomass and to study the reaction pathway towards sorbitol, including the possibility to catalyze the hydrolysis step. Kinetic studies have demonstrated that the preferential pathway follows first the hydrogenation of cellobiose to cellobitol and then hydrolysis of cellobitol to give glucose and sorbitol. Finally, catalytic tests have shown that nitrogen doping increased Ru activity and led to efficient and recyclable catalysts for producing sorbitol from cellobiose. Therefore, it can be concluded that N-doping of the carbon support is not giving active sites for hydrolysis of the starting glycosidic bond, but it is highly beneficial to boost the hydrogenation ability of the supported Ru particles.

Thirdly, the hydrolysis of cellobiose into glucose has been studied. Cellobiose hydrolysis can be improved by acidic catalysts. Therefore, seven different carbon materials have been functionalized with sulfonic functions. The functionalization has been carried out by a diazonium coupling strategy that is covalently grafting benzyl sulfonic functions on the carbon surface. The catalysts acidity has been measured by Boehm titration and in each case, an increase of the acidity has been witnessed. Presence of the sulfonic functions has also been proven by TPD and XPS analyses. The functionalized carbon materials have been tested in the hydrolysis of cellobiose into glucose

under inert atmosphere. An improvement of the glucose yield has been observed for all the functionalized carbons in comparison with the pristine ones. A maximum of 80 % of glucose yield has been achieved with the functionalized Reduced Graphene Oxide (RGO) at 150 °C after 2 hours. It has been discovered that below a certain amount of acidic functions (in our case below 120 mmol/100g in the solid catalyst) there is no improvement of the cellobiose hydrolysis in our reaction conditions. Recyclability of the acidic catalysts has been studied and despite a slight decrease of activity, the catalysts still showed excellent results after 6 runs. The activity decrease has been attributed to the fact that some sulfonic functions that are only adsorbed on the carbon surface can leach during the first catalytic reaction. This functionalization method is an excellent alternative to common sulfonation methods that are using concentrated H_2SO_4 which damages carbon materials and leads to leachable sulfonic functions in addition to brittle solid particles. Moreover it is applicable to almost all types of carbon materials, is easily scalable and provides great amount of acid sites of high strength with strongly bonded sulfonic functions. Hence it gives solid acid catalysts that can compete with commonly-known zeolites or resins.

Finally, the last section of this work has been dedicated to the elaboration of bifunctional catalysts by putting together Ru nanoparticles and the sulfonic functions on the same solid support. A new method to deposit Ru nanoparticles has been envisaged to avoid the basic conditions of the two first methods that would deactivate the previously grafted sulfonic functions. This method consists in pre-forming RuO_2 nanoparticles before depositing them on the carbon surface. The RuO_2 nanoparticles will be reduced during catalytic reaction under H_2. First results with bifunctional catalysts for the production of sorbitol from cellobiose have shown cross-poisoning between Ru and sulfonic functions. Therefore, optimization of the

ratio between these two active sites has been conducted. It led to a catalyst composed of 5 wt. % RuO_2 with sulfonic functions pre-treated in water. This bifunctional catalyst produced higher yield of sorbitol than the corresponding monofunctional catalyst with only Ru deposited on the same carbon support. This better sorbitol production has been attributed to a stabilization effect of the sulfonic functions on the sorbitol molecule itself. This effect has been demonstrated by a decrease of sorbitol degradation when sulfonic functions are present. Kinetic studies have highlighted this observation by obtaining better performance with bifunctional catalysts especially for long reaction times where sorbitol is more and more prone to degradation. Moreover, robustness of the bifunctional catalyst has been shown by recycling it up to 5 runs with only a slight decrease of activity. These excellent results have opened the door to valorization of more complex substrates such as starch and cellulose itself. Unfortunately, results have been disappointing for the transformation of starch into sorbitol. By opposition, higher yields of sorbitol have been obtained from insoluble cellulose with bifunctional catalysts than with corresponding monofunctional Ru/C catalysts. As this result was outstanding, reaction conditions have been varied to enhance even more sorbitol production. Moreover, pre-treatments of cellulose to improve its reactivity have been envisaged. Combining the best conditions that have been found and a cellulose pre-treatment by ball-milling, 39 % of sorbitol yield at 190 °C for 2 hours under 30 bar of H_2 with cellulose fibers from Sigma-Aldrich and 27 % of sorbitol yield in the same conditions for Avicel PH-101 cellulose have been obtained. This is amongst the best results reported in the literature for this whole process. As it is now, this bifunctional catalyst is not ready to be applicable to industrial large-scale production of sorbitol from cellulose. There are still optimizations to do in order to maximize sorbitol productivity.

However, the main objective of this work, which was to synthesize a bifunctional catalyst that is more efficient than a monofunctional Ru/C catalyst to produce sorbitol from cellulose, has been fulfilled.

VI.2 Future work

Since the bifunctional catalysts have been proven to be more efficient than the monofunctional ones, further optimization of the reaction conditions such as temperature or reaction duration would be interesting in order to maximize sorbitol yield and to be potentially applicable to industrial processes. Moreover, in order to apply these bifunctional catalysts in transformation of raw biomass, pre-treatments have to be further studied. Indeed, ball-milling is not a pre-treatment that can be easily applicable to large-scale installations because it is very costly and energy demanding[1]. Other pre-treatments that have not been tested in this work would be attractive for such applications. For example, the use of ionic liquids could be a good pre-treatment if their recovery and recyclability are optimized in order to decrease the overall cost[2]. Utilization of dilute acids to depolymerize is currently the most used pre-treatment method[3] and its combination with our bifunctional catalyst would be interesting to look at.

In this work, only one particular reaction has been focused on but the combination of Ru active sites with an acidic support can be used in other reactions than the transformation of cellulose into sorbitol. Indeed, a lot of reaction of hydrogenolysis require Ru catalysts with an acidic media. For example, the transformation of glycerol into propylene glycol and 1,3-propanediol has been performed with a Ru/C catalyst in combination with an acidic catalyst such as Amberlyst-15[4]. Our bifunctional catalyst is the perfect fit for this type of reaction. As said in the introduction, sorbitol can be dehydrated, under acidic conditions, into sorbitans which can lead to

isosorbide[5,6]. By changing the reaction conditions and using our bifunctional catalyst, it could be possible to obtain isosorbide directly from cellulose. Hydrodeoxygenation of phenolic molecules into arenes and cycloalkanes is one of the strategies to valorize lignin[7]. This kind of transformation requires both metal active sites such as Ru and acidic catalyst which is again the perfect match for the bifunctional catalyst that have been designed. Hydrodeoxygenation of vanillin into cycloalkanes has been recently demonstrated by using a bifunctional catalyst composed of Ru supported on the H-form of ZSM-5 zeolite[8]. This reaction could be tried with our type of bifunctional catalyst. The transformation of levulinic acid to *γ*-valerolactone is also a reaction that can be catalyzed with bifunctional catalysts like ours[9].

Fabrication of bifunctional catalysts with a different metal site but still with sulfonated carbon supports could also be very interesting. Other metals such as Ni, Pd or Pt are widely used for catalytic applications in combination with acids. For example, Pt nanoparticles supported on sulfonated mesoporous silica has been used to transform acetaldehyde and acetic acid into ethyl acetate through a combined, one-step hydrogenation/esterification[10]. In another work, Pd and Pt supported on zeolites have been used in the reductive amination of carbonyl compounds[11]. Utilization of supported Ni or W catalyst in the presence of H_2 can lead to the C-C bond cleavage of glucose to glycols[12]. For example, Ni supported on metal oxide support has favored the formation of 1,2-alkanediols (such as ethylene glycol, 1,2-propanediol or 1,2-butanediol) from cellulose[13]. All the reactions cited above could be studied with bifunctional catalysts composed of the corresponding metal nanoparticles supported on sulfonated carbons. Although sulfur is known to poison these metals, it has been shown in this work that bifunctional catalysts can still

display better activity than corresponding monometallic ones despite the potential poisoning, thanks to an optimized synthesis method.

Compartmentalization of the bifunctional catalysts could be an excellent way to avoid poisoning of the Ru by the sulfur. The idea would be to have a carbon material functionalized by sulfonic acid moieties covered by a mesoporous silica layer on which Ru nanoparticles would be deposited. The covering of carbon materials by a mesoporous silica layer has been developed in our team by Tommy Haynes[14]. The silica layer would avoid the proximity between Ru and S and would prevent the poisoning effect. As the silica layer presents mesopores, substrates could diffuse to the acidic functions on the carbon core to be hydrolyzed. Hydrogenation reactions would be performed by the Ru at the surface of the silica layer. This kind of system would be difficult to apply for bulky substrates such as cellulose because of the need to diffuse through the silica layer porosity but it could be interesting for smaller molecules that can be hydrogenolyzed. This is particularly true in the field of biomass valorization because the conditions are highly demanding for the catalytic materials and in this way at least one of the two active sites would be protected from deactivation.

In this project, it has additionally been shown that nitrogen doping of the carbon materials is enhancing the Ru activity when these N-doped carbons are used as supports. However, this doping has not been used in the fabrication of bifunctional acidic catalysts. It would be interesting to make fully integrated catalysts supported on N-doped carbons to see if there can be a further improvement of the catalytic activity in comparison with the metal/acidic bifunctional catalysts. The main issue that could appear with this type of catalyst would be that sulfonic functions hide (or limit the accessibility to) the nitrogen functions and that no performance amelioration could be witnessed. However, if such a “tri”functional catalyst could be

prepared, one could take advantage of a solid presenting both acidic and basic sites on neighboring locations, together with redox-active nanoparticles, opening even more doors in terms of versatility for applications in biomass valorization reactions.

References

[1] S. Haghighi Mood, A. Hossein Golfeshan, M. Tabatabaei, G. Salehi Jouzani, G. H. Najafi, M. Gholami, M. Ardjmand, *Renew. Sustain. Energy Rev.* **2013**, *27*, 77–93.

[2] P. Alvira, E. Tomás-Pejó, M. Ballesteros, M. J. Negro, *Bioresour. Technol.* **2010**, *101*, 4851–4861.

[3] A. M. J. Kootstra, H. H. Beeftink, E. L. Scott, J. P. M. Sanders, *Biotechnol. Biofuels* **2009**, *2*, 1–14.

[4] Y. Kusunoki, T. Miyazawa, K. Kunimori, K. Tomishige, *Catal. Commun.* **2005**, *6*, 645–649.

[5] B. Zada, M. Chen, C. Chen, L. Yan, Q. Xu, W. Li, Q. Guo, Y. Fu, *Sci. China Chem.* **2017**, *60*, 853–869.

[6] J. Keskiväli, S. Rautiainen, M. Heikkilä, T. T. T. Myllymäki, J. P. Karjalainen, K. Lagerblom, M. Kemell, M. Vehkamäki, K. Meinander, T. Repo, *Green Chem.* **2017**, *19*, 4563–4570.

[7] K. L. Luska, P. Migowski, S. El Sayed, W. Leitner, *Angew. Chemie - Int. Ed.* **2015**, *54*, 15750–15755.

[8] H. Kim, S. Yang, Y. H. Lim, J. M. Ha, D. H. Kim, *J. Hazard. Mater.* **2022**, *423*, 126525.

[9] Y. Wang, Z. Rong, Y. Wang, T. Wang, Q. Du, Y. Wang, J. Qu, *ACS Sustain. Chem. Eng.* **2017**, *5*, 1538–1548.

[10] Y. Tang, S. Miao, B. H. Shanks, X. Zheng, *Appl. Catal. A Gen.* **2010**, *375*, 310–317.

[11] M. E. Domine, M. C. Hernández-Soto, M. T. Navarro, Y. Pérez, *Catal. Today* **2011**, *172*, 13–20.

[12] P. Barbaro, F. Liguori, N. Linares, C. M. Marrodan, *Eur. J. Inorg. Chem.* **2012**, *2012*, 3807–3823.

[13] X. Wang, L. Meng, F. Wu, Y. Jiang, L. Wang, X. Mu, *Green Chem.* **2012**, *14*, 758–765.

[14] T. Haynes, O. Ersen, V. Dubois, D. Desmecht, K. Nakagawa, S. Hermans, *Appl. Catal. B Environ.* **2019**, *241*, 196–204.

Chapter VII

Experimental section

VII.1 Reagents and materials

The activated coal (AC; SX+ type) was obtained from NORIT, and sieved to keep only the fraction with granulometry below 50 µm. The reduced graphene oxide N002-PDR (RGO) was obtained from Angstron Materials. The multi-walled carbon nanotubes (MWCNT) were obtained from Nanocyl (Belgium) (NC 7000 Thin MWCNTs, 95+% C purity). The carbon black (CB) was obtained as 250 G type from IMERYS GRAPHITE & CARBON. The carbon nanofibers (CNF; LHT and LHT-OX type) were obtained from Applied Sciences Inc (USA). The graphene nanoplatelets (GNP; M15 and C750 types) were purchased from Sigma-Aldrich. Thionyl chloride, urea, nitric acid (HNO_3), ethylenediamine, sulfanilic acid (99%), isopentyl nitrite (96%), ruthenium (III) chloride hydrate (Ru content around 42 %), sodium carbonate (Na_2CO_3), sodium borohydride ($NaBH_4$), hydrogen peroxide (H_2O_2) (30% w/w in water), glucose, mannitol, xylitol, sorbitol, D-(+)-cellobiose (≥99%), cellulose (reference C6288, crystalline and high purity) and cellulose (microcrystalline, Avicel PH-101) were also supplied by Sigma-Aldrich and used as received.

VII.2 Syntheses

VII.2.1 Ru deposition

$NaBH_4$ method: 300 mg of carbon support was dispersed in 100 mL of Na_2CO_3 solution (2.5 wt. %) and was stirred during 15 minutes. As 3 wt. % of Ru loading on the support is targeted, 22.1 mg of $RuCl_3$ hydrate dissolved in 20 mL of demineralized water was added to the dispersion and stirred for 20 minutes. After that, 5 g of $NaBH_4$ in 20 mL of demineralized water were added at once to the dispersion and the mix was stirred during 2 hours.

Finally, the solid was filtrated out, washed extensively with demineralized water and oven dried overnight.

Urea method: 150 mg of urea was dissolved in 100 mL of a demineralized water dispersion containing 250 mg of carbon support. As 3 wt. % of Ru loading on the support is targeted, 18.4 mg of $RuCl_3$ hydrate was then added. After one hour stirring, the heating was turned on and fixed at 120 °C (urea starts to decompose at 90 °C) and the solution remained at this temperature for one hour before cooling down. Then, at room temperature, 2 g of sodium formate were added and the solution was left under agitation for one hour. After that, the solution was set to 130 °C (formate degradation temperature) for one hour. Then, the solution was left at room temperature under agitation overnight. Following this, the solid was filtrated out, washed extensively with demineralized water and oven dried overnight. Finally, the solid was heat-treated under reductive atmosphere in order to obtain the desired particles size (Alphagaz mix: 5% H_2 / 95% Ar) at 400 °C or 600 °C for two hours following the temperature program below:

a. Temperature rising at 100 °C/h to the desired temperature (400 °C/600 °C).

b. Two hours plateau at the desired temperature

c. Temperature decrease at 100 °C/h to room temperature.

Pre-formed RuO_2 method: Colloidal suspension of RuO_2 was synthesized via slow hydrolysis/condensation of $RuCl_3$ hydrate by using H_2O_2 as oxidizing agent. It was adapted from a literature procedure[1]. In order to have 1 wt.%, 3 wt.% or 5 wt.% of Ru on the carbon support, 24.1 mg, 73.6 mg, 125.3 mg of $RuCl_3$ was respectively added to 40 mL of demineralized water (solution A) and 1 mL of H_2O_2 was added to 20 mL of demineralized water (solution B). Solution B was added drop by drop to solution A. The final mixture was agitated during 5 minutes. After that, the glass berlin capped by

an aluminum foil containing the mixture was placed in an oven at 95 °C for 2h. The solution was cooled down at room temperature and added to 1 g of AC. The dispersion was agitated during 30 minutes. The solid was recovered by evaporation of the solvent in a rotavapor, at 60°C under reduced pressure, and it was dried overnight at 100 °C.

VII.2.2 Acidic functionalization

The carbon functionalization was carried out by a diazonium coupling method (Scheme 1)[2]. Typically, 1 g of carbon powder was dispersed in 60 mL distilled water. 1.5 g of sulfanilic acid were added and the suspension was stirred at 70 °C during 10 minutes. The suspension was cooled down at 30 °C before adding 1.2 mL of isopentyl nitrite. The mixture was stirred during 16h. Then the solid was filtered out and washed with distilled water and ethanol. The resulting material was dried overnight at 100 °C.

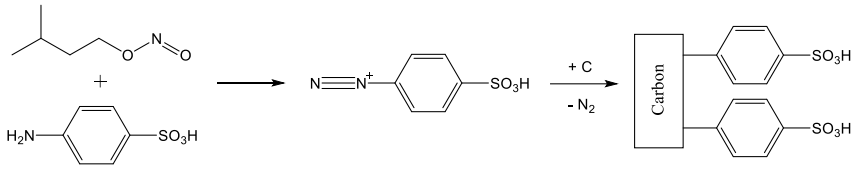

Scheme 1: Diazonium coupling on carbon materials for sulfonic acid grafting

Heat treatment: Catalysts were treated thermally at different temperatures to change the amount of surface sulfonic functions. In order to do that, solids were placed in a tubular oven and heated under N_2 to 200 °C, 300 °C or 400 °C with an increase of temperature of 100 °C / h. When the targeted temperature was reached, it was maintained during 2 h before being decreased to room temperature.

VII.2.3 Nitrogen doping

Urea method: 1 g of carbon support was dispersed in an alcoholic solution (20:80 water/ethanol) containing 1 g of urea in a round-bottom flask and was stirred for 4 h. The solvent was then evaporated using a rotavapor and the resulting solid was oven dried overnight at 100 °C.

The solid was then heat-treated in a furnace under inert atmosphere (N_2 or Ar) following the temperature program below:

a. Temperature rising at 100 °C/h to the desired temperature (500 °C / 700 °C / 900 °C).

b. Two hours plateau at the desired temperature.

c. Temperature decrease at 100 °C/h to room temperature.

Ethylenediamine method: 1 or 2 g of support was dispersed in respectively, 100 mL or 200 mL of HNO_3 solution (2.5 mol/L) in a three-neck round-bottom flask. The suspension was then heated under reflux and agitation at 105 °C. After 24h, the mixture was filtrated on a Büchner and extensively washed with water until constant pH. Finally, the resulting solid was oven dried overnight at 100 °C.

The oxidized support was dispersed in 100 mL of toluene in a three-neck round-bottom flask. 6 mL of pure thionyl chloride were then added using a 12 mL syringe and the suspension was heated under reflux and agitation at 110 °C. After 5 hours, the mixture was filtrated and extensively washed with 500 mL of toluene. The resulting solid was then oven dried overnight at 100 °C.

The chlorinated support was dispersed in a mixture of 70 mL toluene and 30 mL ethylenediamine in a three-neck round-bottom ask. The suspension was then heated under reflux and agitation at 110 °C. After 24h, the mixture was filtrated and washed extensively with ethanol. The resulting solid was then oven dried overnight at 100 °C.

The solid was then heat-treated in a furnace (Carbolite STF 16/-/450) under inert atmosphere (N_2) following the same temperature program than above with a targeted temperature of 700 °C or 900 °C.

VII.2.4 Heat-treatment

All heat-treatments have been conducted in a furnace (Carbolite STF 16/-/450) under either inert atmosphere (N_2) or reductive atmosphere (Alphagaz mix: 5% H_2 / 95% Ar) with solids in a ceramic crucible following the temperature program below:

a. Temperature rising at 100 °C/h to the desired temperature

b. Two hours plateau at the desired temperature.

c. Temperature decrease at 100 °C/h to room temperature.

VII.2.5 Catalytic tests

The tests were carried out in a 300 mL stainless steel Parr autoclave. 1 g of glucose / cellobiose / starch / cellulose was added to a certain mass of catalyst (20 mg / 150 mg / 300 mg) in 120 mL of mQ water. These testing conditions were based on precedents in the literature [3],[4]. The low cellobiose concentration ensures absence of diffusional limitations. Then, the autoclave was sealed and the system was purged three times with nitrogen and heated up under autogenic pressure of N_2 for the hydrolysis tests and under H_2 pressure (30 or 40 or 50 bar) for the hydrogenation tests (this pressure is set when the temperature is reached). At the controlled temperature, the agitation was started at 1700 rpm for several hours. After this fixed duration of catalytic test, the system was then cooled down to room temperature and the solution was filtrated. The solid catalyst was washed and dried. The filtrate was then diluted to 250 mL with mQ water and analyzed by HPLC. For kinetic studies, at various time intervals, liquid samples were taken and two times diluted with mQ water before analyzing it similarly. The pressure within the autoclave was brought back to 30 bar of N_2 or H_2 after each sampling.

HPLC analyses were performed with a Waters system equipped with Waters 2414 refractive index (RI) detector (detector temperature = 30 °C).

Two columns were used. The first one is a Carbohydrate Transgenomic CarboSep CHO682 column, with mQ H_2O (18 MΩ.cm at 25 °C) as eluent, a flux of 0.4 mL/min, a column temperature of 80 °C and 20 µL of injected volume. The second one is an Aminex HPX 87C column, with mQ H_2O (18 MΩ.cm at 25 °C) as eluent, a flux of 0.5 mL/min, a column temperature of 85 °C and 25 µL of injected volume.

The conversion of cellobiose was calculated as follows:

$$Cellobiose\ conversion\ (\%) = \frac{n\ cellobiose\ converted}{initial\ n\ cellobiose} * 100$$

The selectivity in glucose was calculated as follows:

$$Selectivity\ in\ glucose\ (\%) = \frac{n\ glucose\ produced}{2 * (n\ cellobiose\ converted)} * 100$$

The selectivity in sorbitol was calculated as follows:

$$Selectivity\ in\ sorbitol\ (\%) = \frac{n\ sorbitol\ produced}{2 * (n\ cellobiose\ converted)} * 100$$

The selectivity in cellobitol was calculated as follows:

$$Selectivity\ in\ cellobitol\ (\%) = \frac{n\ cellobitol\ produced}{n\ cellobiose\ converted} * 100$$

The yield in glucose from cellobiose was calculated as follows:

$$Yield\ in\ glucose\ (\%) = \frac{n\ glucose\ produced}{2 * initial\ n\ cellobiose} * 100$$

The yield in sorbitol from cellobiose was calculated as follows:

$$Yield\ in\ sorbitol\ (\%) = \frac{n\ sorbitol\ produced}{2 * initial\ n\ cellobiose} * 100$$

For the catalytic reaction on cellulose substrate, the formulae are slightly different.

The conversion of cellulose was calculated as follows:

$$Cellulose\ conversion\ (\%) = \frac{(initial\ cellulose\ mass - recovered\ cellulose\ mass)}{initial\ cellulose\ mass} * 100$$

The selectivity in glucose was calculated as follows:

$$Selectivity\ in\ glucose\ (\%) = \frac{n\ glucose\ produced}{(n\ cellulose\ converted)} * 100$$

The selectivity in sorbitol was calculated as follows:

$$Selectivity\ in\ sorbitol\ (\%) = \frac{n\ sorbitol\ produced}{(n\ cellulose\ converted)} * 100$$

The selectivity in xylitol was calculated as follows:

$$Selectivity\ in\ xylitol\ (\%) = \frac{n\ xylitol\ produced}{(n\ cellulose\ converted)} * 100$$

The selectivity in mannitol was calculated as follows:

$$Selectivity\ in\ mannitol\ (\%) = \frac{n\ mannitol\ produced}{(n\ cellulose\ converted)} * 100$$

The yield in glucose from cellulose was calculated as follows:

$$Yield\ in\ glucose\ (\%) = \frac{n\ glucose\ produced}{initial\ n\ cellulose} * 100$$

The yield in sorbitol from cellulose was calculated as follows:

$$Yield\ in\ sorbitol\ (\%) = \frac{n\ sorbitol\ produced}{initial\ n\ cellulose} * 100$$

VII.3 Characterization methods

VII.3.1 Boehm titrations

Boehm titration method was used to evaluate the catalysts acidity and basicity[5],[6]. NaOH solutions were prepared by dilution of Titrisol ampoules (VWR) containing precise and known quantities of sodium hydroxide. HCl solutions were prepared by the dilution of concentrated hydrochloric acid. The HCl concentrations were determined by titration with the standard NaOH solutions. These solutions were prepared with mQ water that had been previously decarbonated by nitrogen flushing.

For titrating the acid groups, 60 mg of sample were dispersed in 30 mL of NaOH 0.01 mol/L and the solution was decarbonized for one hour under Ar flux. The mixture was then agitated for 23 h under Ar atmosphere.

The suspension was then filtrated and two times 10 mL of the resulting filtrate were back-titrated, under Ar flux, using the HCl 0.005 mol/L solution. The indicator used is phenolphthalein. The amount of acid functions on the catalyst is determined by calculating the difference between the initial amount of NaOH and the amount of NaOH titrated by the HCl.

For titrating the basic groups, 60 mg of sample were dispersed in 30 mL of HCl 0.01 mol/L and the solution was decarbonized for one hour under Ar flux. The mixture was then agitated for 23 h under Ar atmosphere. The suspension was then filtrated and two times 10 mL of the resulting filtrate were back-titrated, under Ar flux, using the NaOH 0.005 mol/L solution. The indicator used was phenolphthalein. The amount of basic functions in the catalyst was determined by calculating the difference between the initial amount of HCl engaged and the amount of remaining HCl after 24 hours, titrated by the NaOH.

VII.3.2 X-ray photoelectron spectroscopy (XPS)

XPS analyses were carried out at room temperature with a SSI-Xprobe (SSX 100/206) photoelectron spectrometer from Surface Science Instruments (USA), equipped with a monochromatized microfocus Al X-ray source. Samples were stuck onto small sample holders with double face adhesive tape and then placed on an insulating ceramic carousel (Macor®, Switzerland). Charge effects were avoided by placing a nickel grid above the samples and using a flood gun set at 8 eV. The binding energies were calculated with respect to the C-(C, H) component of the C1s peak fixed at 284.4 eV. Data treatment was performed using the CasaXPS program (Casa Software Ltd., UK). The peaks were decomposed into a sum of Gaussian/Lorentzian (85/15) after subtraction of a Shirley-type baseline.

The depth of the XPS analyses can be determined as follow: 63 % of the signal originates from a layer of thickness equal to $\lambda \cos(\theta)$, 86 % from a

layer of thickness 2λ cos(θ), and 95 % from a layer of thickness 3λ cos(θ)[7]. As the carbon supports we are using have a low density, the inelastic mean free path (λ) is around 3.5 nm. During our analyses, θ was equal to 55°. Therefore, we can conclude that 63 % of the signal originates from the first 2 nm, 86 % from a depth of 4 nm, and 95 % of the signal comes from 6 nm depth.

VII.3.3 Transmission electron microscopy (TEM)

TEM analyses have been conducted as follows. The powder samples were suspended in hexane under ultrasonic treatment, then a drop of the supernatant was deposited on a holey carbon film supported on a copper grid (Holey Carbon Film 300 Mesh Cu, Electron Microscopy Sciences) which was dried overnight under vacuum at room temperature before analysis. The images were obtained on a LEO 922 OMEGA energy filter transmission electron microscope. TEM analyses have been partially carried out by Tommy Haynes.

VII.3.4 High resolution transmission electron microscopy (HR-TEM)

HR-TEM analyses have been carried out on a JEOL 2100 FEG S/TEM working at 200 kV voltage, equipped with a probe corrector for spherical aberrations. For these measurements, samples were dispersed in an ethanol solution and a drop of each suspension was deposited on a copper grid covered with a holey carbon membrane. These analyses have been carried out by Walid Baaziz, working with Prof. Ovidiu Ersen at Institut de physique et de chimie des Matériaux de Strasbourg (IPCMS).

VII.3.5 Scanning transmission electron microscopy (STEM) and Energy dispersive X-ray (EDX)

STEM analyses have been carried out on a JEOL 2100 FEG S/TEM by using a spot size of 0.13 nm with a current density of 140 pA and a camera

focal distance of 8 cm, corresponding to inside and outside annular detector diameters of 73 and 194 mrad. EDX mapping has been performed using a JEOL Silicon Drift Detector (SDD) with sensor size of 60 mm². These analyses have been carried out by Walid Baaziz, working with Prof. Ovidiu Ersen at Institut de physique et de chimie des Matériaux de Strasbourg (IPCMS).

VII.3.6 X-ray crystallography (XRD)

Powder X-ray diffraction (PXRD) patterns were recorded at room temperature on a Siemens D5000 diffractometer equipped with a Ni filter using CuKα radiation (BraggBrentano geometry) operated at 40 kV and 40 mA. Diffractograms were taken between 5° and 80° (2θ) with a step size of 0.02° (2θ).

The crystallite size (d) can be determined as a function of peak width (B), peak position (2θ) and wavelength of the incident X-ray beam (λ), according to Scherrer's equation:

$$d = \frac{0.94\,\lambda}{B\cos(\theta)}$$

where B is obtained as the full width at half maximum intensity (FWHM) of selected X-ray diffraction peak.

VII.3.7 Temperature programmed desorption (TPD)

TPD-CO_2 analyses were performed on Hiden Catlab reactor combined with a QGA Hiden quadrupole mass spectrometer. During the first stage, the sample was heated to 850 °C at 10 °C/min under an inert flux of argon at 50 mL/min. Then, the temperature was maintained for two hours after which it is let to cool down to 60 °C. Carbon dioxide was then injected with argon (CO_2/Ar: 15/85) at 30 mL/min additionally to the first argon inlet. Then comes the second stage: carbon dioxide inlet was stopped and only argon flows at 50 mL/min through the sample at 60 °C for one hour. Next,

the sample was heated again from 60 °C to 800 °C at 10 °C/min in flowing argon.

TPD-NH_3 analyses were performed on Hiden Catlab reactor combined with a QGA Hiden quadrupole mass spectrometer. Samples were pretreated under Ar (30 ml/min, 5.0 AirLiquide) at 200 °C during two hours to remove all the water before the analysis. NH_3 adsorption was performed at 70 °C during 1 hour by flowing a mixture of Argon (20 ml/min) and 5% NH_3 in He (10 ml/min). The catalyst was then flushed in Ar (30 ml/min) during 2 hours and then, the NH_3 desorption measurement was performed under Ar (30 ml/min) from 70 to 600 °C (heating rate of 10 °C /min).

VII.3.8 Total organic content (TOC)

Total organic content (TOC) analyses have been performed in the MOCA platform at UCLouvain on solutions after catalytic test by using a Shimadzu TOC-L analyzer with a ASI-L autosampler using the combustion catalytic oxidation method at 680 °C.

VII.3.9 Inductively coupled plasma (ICP)

To evaluate ruthenium content, ICP analyses have been conducted in the MOCA platform at UCLouvain on a Thermo 6000 series Duo, with axial and radial measurement modes. The sample is first burnt to eliminate the carbon that can cause interferences. Then, ruthenium is mineralized by sodium peroxide (Na_2O_2) and analyzed by ICP method.

VII.3.10 BET specific surface area

The textural characteristics of the different carbon supports was characterized by nitrogen adsorption–desorption isotherms. The measurements were achieved by using a Micromeritics ASAP 2020 analyzer at -196 °C. Before analysis, the samples (0.02 - 0.10 g) were degassed for 10 h at 200 °C with a heating rate of 10 °C/min under 0.133 Pa pressure. The analysis of the isotherms provided specific surface areas calculated with the

Brunauer-Emmett-Teller (BET) equation. Linearization has been done with relative pressure P/P_0 between 0.06 and 0.2 and the C constant has been positive for all samples.

References

[1] C. Sassoye, G. Muller, D. P. Debecker, A. Karelovic, S. Cassaignon, C. Pizarro, P. Ruiz, C. Sanchez, *Green Chem.* **2011**, *13*, 3230–3237.

[2] D. R. Stellwagen, F. Van Der Klis, D. S. Van Es, K. P. De Jong, J. H. Bitter, *ChemSusChem* **2013**, *6*, 1668–1672.

[3] P. J. C. Hausoul, L. Negahdar, K. Schute, R. Palkovits, *ChemSusChem* **2015**, *8*, 3323–3330.

[4] Y. Niu, H. Wang, X. Zhu, Z. Song, X. Xie, X. Liu, J. Han, Q. Ge, *Microporous Mesoporous Mater.* **2014**, *198*, 215–222.

[5] H.-P. Boehm, E. Diehl, W. Heck, R. Sappok, *Angew. Chemie Int. Ed. English* **1964**, *3*, 669–677.

[6] S. L. Goertzen, K. D. Thériault, A. M. Oickle, A. C. Tarasuk, H. A. Andreas, *Carbon N. Y.* **2010**, *48*, 1252–1261.

[7] M. J. Genet, C. C. Dupont-Gillain, P. G. Rouxhet, in *Med. Appl. Colloids* (Ed.: E. Matijevic), Springer New York, New York, NY, **2008**, pp. 177-307 (Chap. 5).

Supporting Information

Contents

S1. Catalytic tests repeatability

The confidence interval has been determined for each Chapter based on several tests conducted with the same catalyst in the same conditions.

Table 1: Repeatability of catalytic tests for Chapter II; results from the hydrogenation of glucose into sorbitol at 140 °C under 30 bar of H_2 during 2 h with 20 mg of catalyst (Ru 3 wt. %) and 1 g of glucose; The estimated confidence interval on glucose conversion and sorbitol selectivity is 7 %

Catalyst	Conversion (%)	Sorbitol selectivity (%)	Yield in sorbitol (%)
Ru (3 wt. %) / LHT	30	70	21
Ru (3 wt. %) / LHT	40	80	32

Table 2: Repeatability of catalytic tests for Chapter III; conversion of 1 g of cellobiose and selectivity into glucose, cellobitol and sorbitol and yield in sorbitol after 6 hours (160 °C; 1700 rpm; 30 bar H_2; 20 mg of catalyst); The estimated confidence interval on each value is 5 %

Catalyst	Conversion (%)	Selectivity in glucose (%)	Selectivity in cellobitol (%)	Selectivity in sorbitol (%)	Yield in sorbitol (%)
Ru / N-doped AC	100	1	31	66	66
Ru / N-doped AC	97	2	38	60	58

Table 3: Repeatability of catalytic tests for Chapter IV; Conversion of cellobiose and selectivity in glucose (N_2 autogenic pressure; 150 °C; 2h; 1700 rpm; 1g of cellobiose; 300 mg of catalyst); The estimated confidence interval on cellobiose conversion and glucose selectivity is 4 %

Catalyst	Conversion (%)	Selectivity in glucose (%)
SO_3H/AC (1^{st} run)	81	96
SO_3H/AC (2^{nd} run)	67	97
SO_3H/AC (3^{rd} run)	50	95
SO_3H/AC (4^{th} run)	54	95
SO_3H/AC (5^{th} run)	42	97
SO_3H/AC (1^{st} run)	85	98
SO_3H/AC (2^{nd} run)	64	99
SO_3H/AC (3^{rd} run)	55	99
SO_3H/AC (4^{th} run)	63	98
SO_3H/AC (5^{th} run)	50	98

Table 4: Repeatability of catalytic tests for Chapter V for cellobiose transformation into sorbitol; Cellobiose conversion, selectivity in glucose, cellobitol and sorbitol, yield in sorbitol (150 °C, 30 bar of H_2, 2h, 150 mg of catalyst); The estimated confidence interval on cellobiose conversion and selectivities is 3 %

Catalyst	Conversion (%)	Selectivity in glucose (%)	Selectivity in cellobitol (%)	Selectivity in sorbitol (%)	Yield in sorbitol (%)
RuO_2 (5%) – SO_3H / AC	76	29	44	17	13
RuO_2 (5%) – SO_3H / AC	74	25	45	17	13
RuO_2 (5%) – pre-treated SO_3H / AC	100	6	29	53	53
RuO_2 (5%) – pre-treated SO_3H / AC	96	8	30	52	50

Table 5: Repeatability of catalytic tests for Chapter V for cellulose transformation into sorbitol; Cellulose conversion, selectivity in xylitol, mannitol and sorbitol, yield in sorbitol (190 °C; 2 h; 30 bar of H_2, 150 mg of catalyst, 1 g of ball-milled cellulose (300 rpm)); The estimated confidence interval on cellulose conversion and selectivities is 5 %

Catalyst	Cellulose conversion (%)	Xylitol selectivity (%)	Mannitol selectivity (%)	Sorbitol selectivity (%)	Sorbitol yield (%)
RuO_2 (5%) – pre-treated SO_3H / AC	70	3	5	30	21
RuO_2 (5%) – pre-treated SO_3H / AC	62	9	8	23	14

S2. List of molecules injected in HPLC

Table 6: List of molecules injected in HPLC

Molecule	Supplier and purity	Observed in catalytic tests
Arabinose	Sigma-Aldrich - ≥ 99 %	**X**
Dulcitol	Sigma-Aldrich - ≥ 99 %	**X**
Erythritol	Sigma-Aldrich - ≥ 99 %	**X**
Fructose	Sigma-Aldrich - ≥ 99 %	✓
Galactose	Sigma-Aldrich - ≥ 99 %	**X**
HMF	Sigma-Aldrich - 99 %	**X**
Lactitol	Sigma-Aldrich - 98 %	**X**
Maltose	Sigma-Aldrich - 99 %	**X**
Mannose	Sigma-Aldrich - ≥ 99 %	**X**
Mannitol	Sigma-Aldrich - ≥ 98 %	✓
Sucrose	Sigma-Aldrich - ≥ 99.5 %	**X**
Xylitol	Sigma-Aldrich - ≥ 99 %	✓

S3. TPD analyses of pristine and N-doped GNP

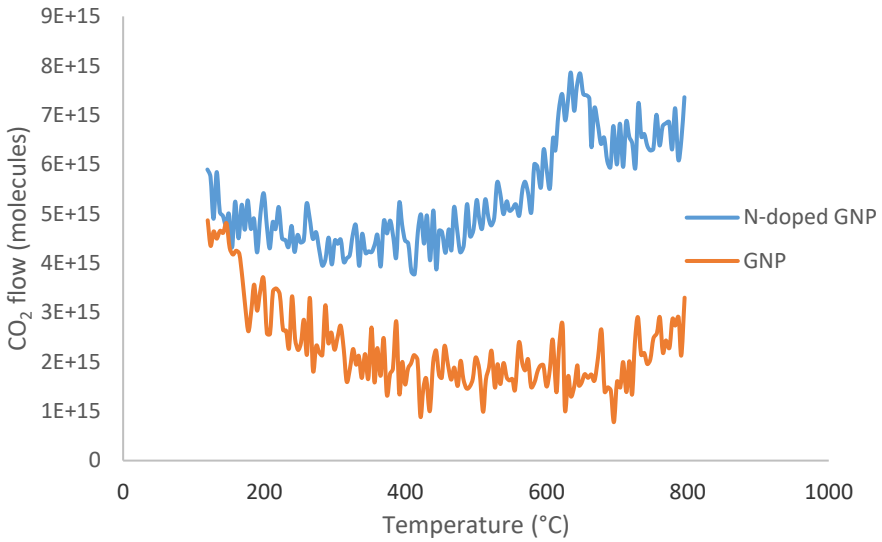

Figure 1: CO_2 flow as a function of the temperature for GNP-C750 and N-doped GNP

S4. XPS analyses of final catalysts

Table 7: Pristine and N-doped supports with Ru nanoparticles heat-treated under reductive atmosphere

Catalyst	Ru (at. %)	$Ru_{3p3/2}$ (eV)
Ru / pristine AC	1.91	461.9
Ru / EDA-AC	1.53	461.6
Ru / N-doped AC	0.83	461.7
Ru / pristine GNP	1.55	461.9
Ru / N-doped GNP	1.76	462.0

S5. XPS analysis of the used Ru / N-doped GNP catalyst

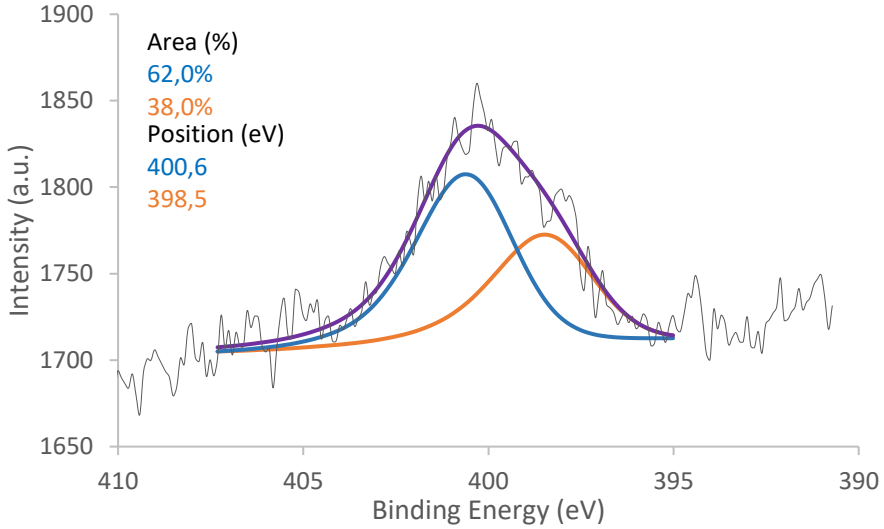

Figure 2: N1s peaks (in blue: amine; in orange: pyridine/pyrrole) from XPS analysis of Ru / N-doped GNP after three catalytic tests

S6. TEM image of the used Ru / N-doped GNP catalyst

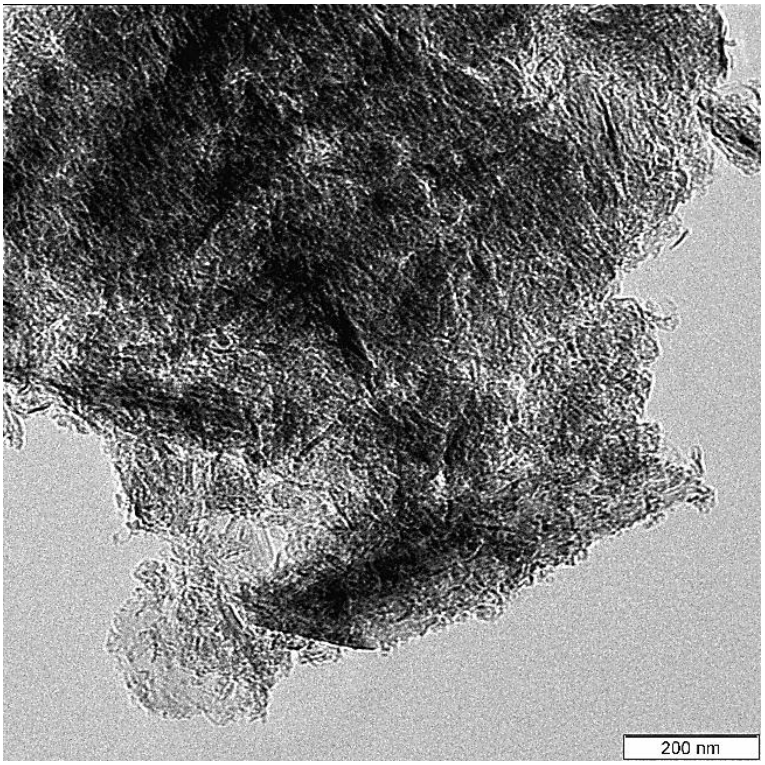

Figure 3: TEM image of Ru / N-doped GNP after 3 catalytic tests

S7. XPS S_{2p} spectra for all carbon materials before and after functionalization

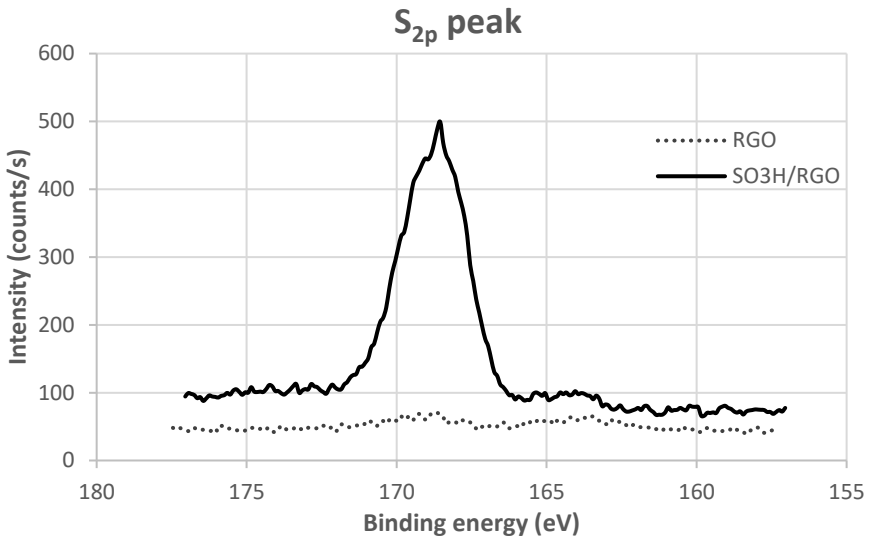

Figure 4: S_{2p} XPS peak for RGO and functionalized RGO samples

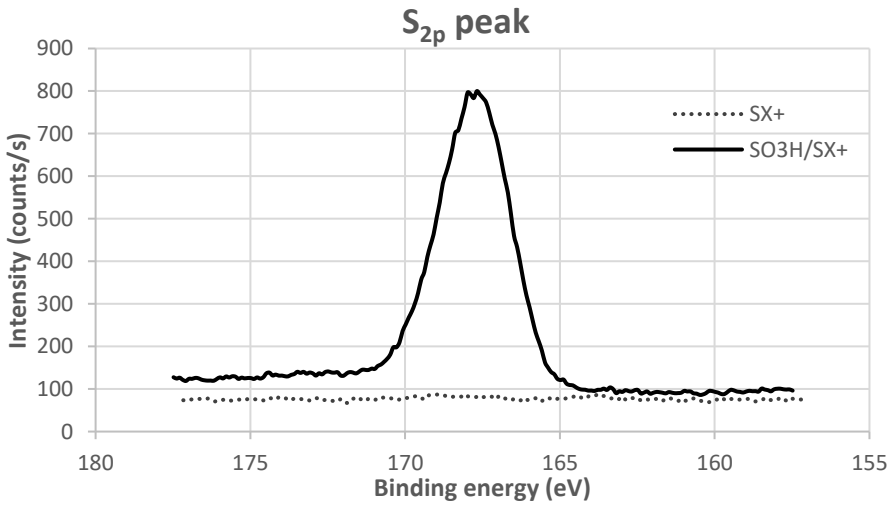

Figure 5: S_{2p} XPS peak for SX+ and functionalized SX+ samples

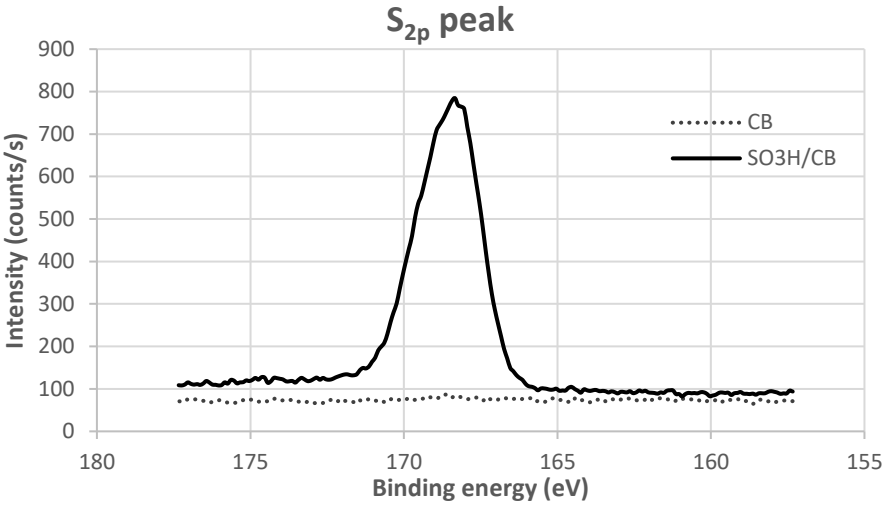

Figure 6: S_{2p} XPS peak for CB and functionalized CB samples

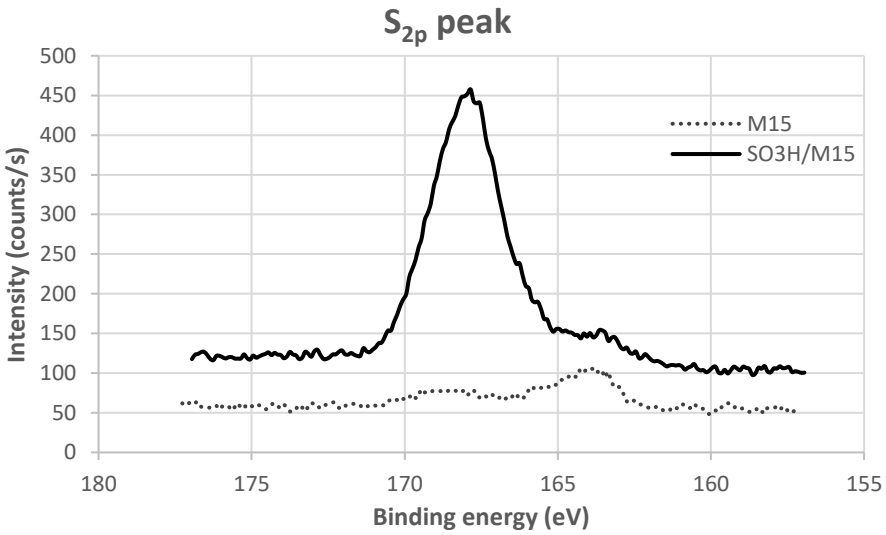

Figure 7: S_{2p} XPS peak for GNP-M15 and functionalized GNP-M15 samples

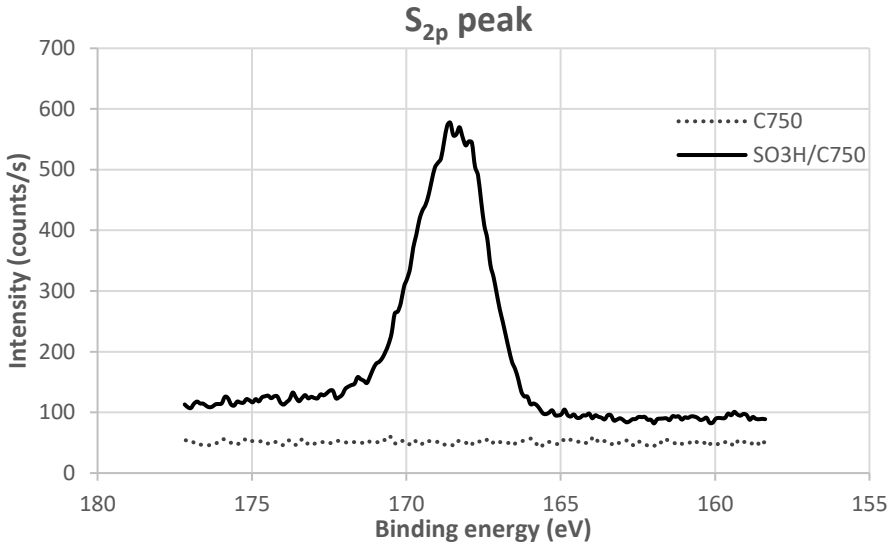

Figure 8: S_{2p} XPS peak for GNP-C750 and functionalized GNP-C750 samples

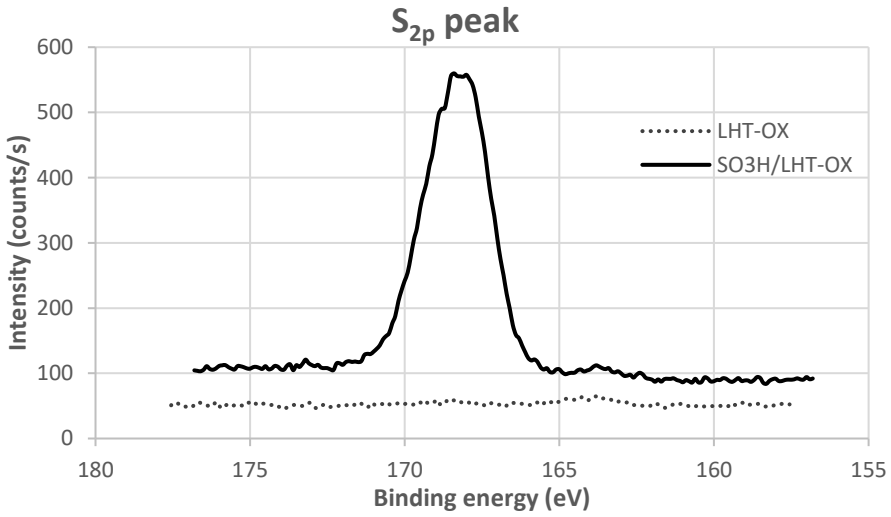

Figure 9: S_{2p} XPS peak for LHT-OX and functionalized LHT-OX samples

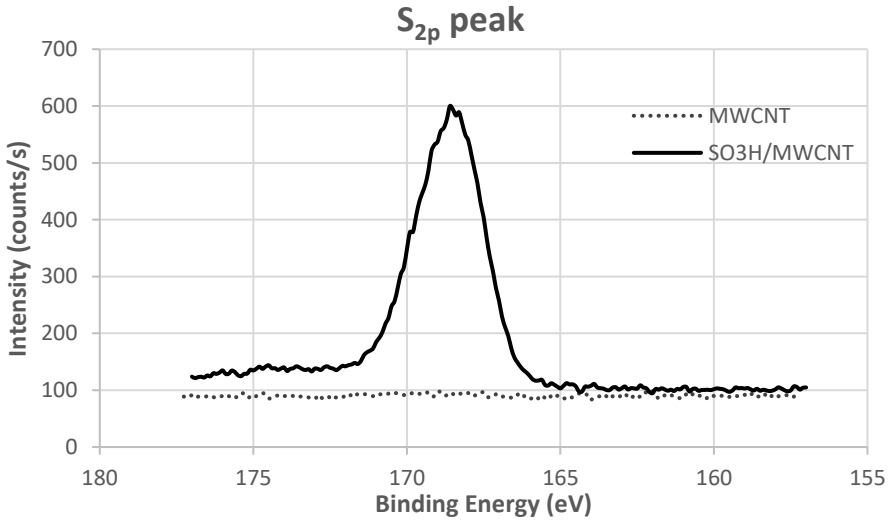

Figure 10: S_{2p} XPS peak for MWCNT and functionalized MWCNT samples

S8. XPS N_{1s} and C_{1s} analyses for representative carbon samples

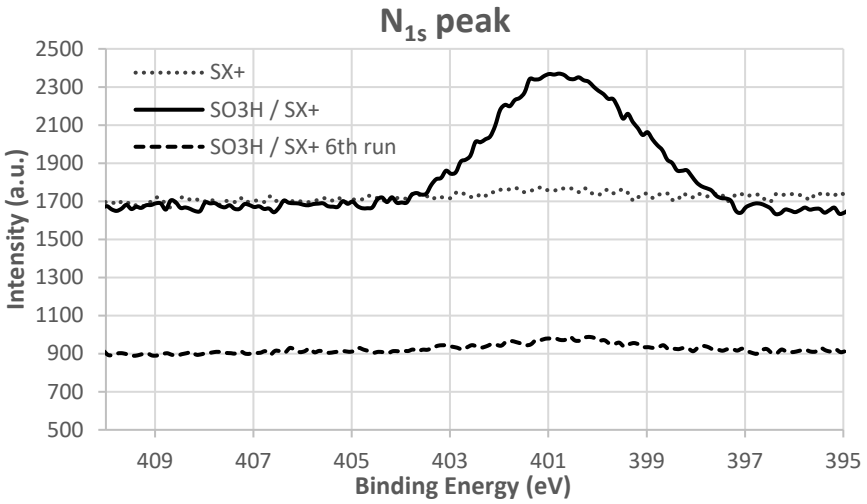

Figure 11: N_{1s} peak measured by XPS for pristine and functionalized SX+ before and after catalytic test

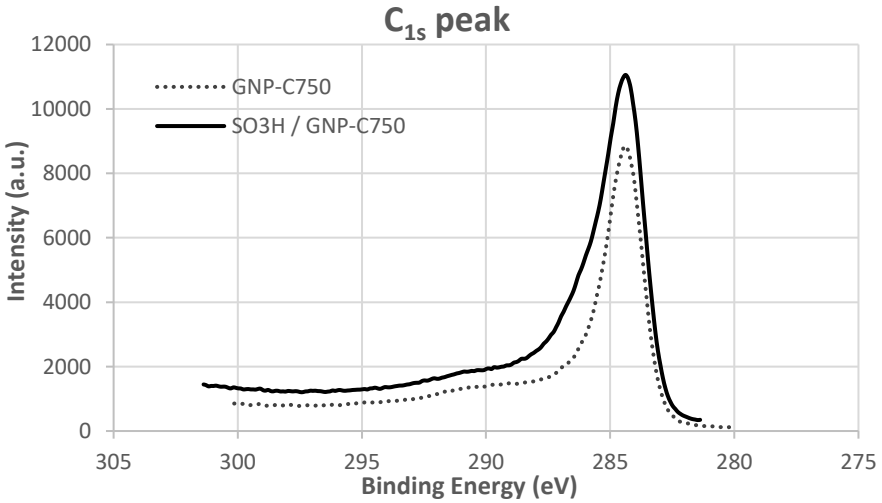

Figure 12: C_{1s} peak measured by XPS for pristine and functionalized GNP-C750

S9. NH_3-TPD analyses for each support with and without functionalization

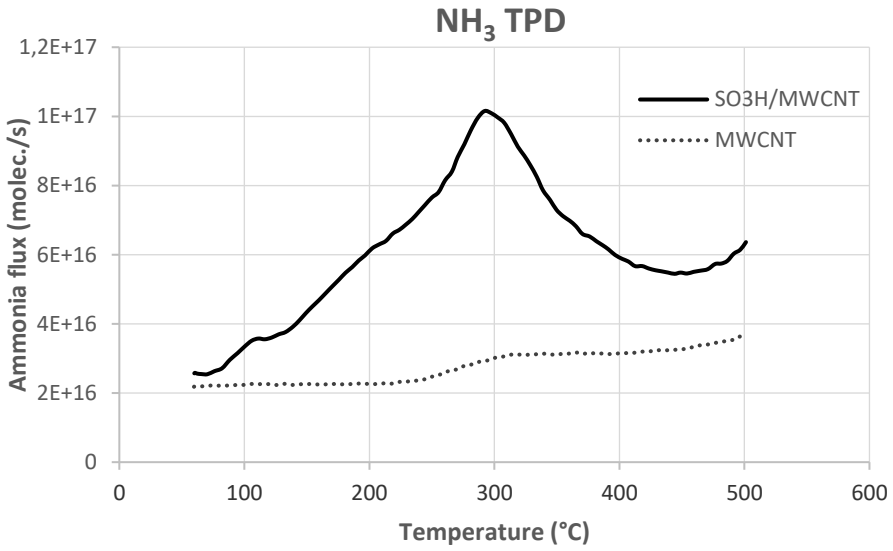

Figure 13: NH_3 flux as a function of temperature for MWCNT and functionalized MWCNT

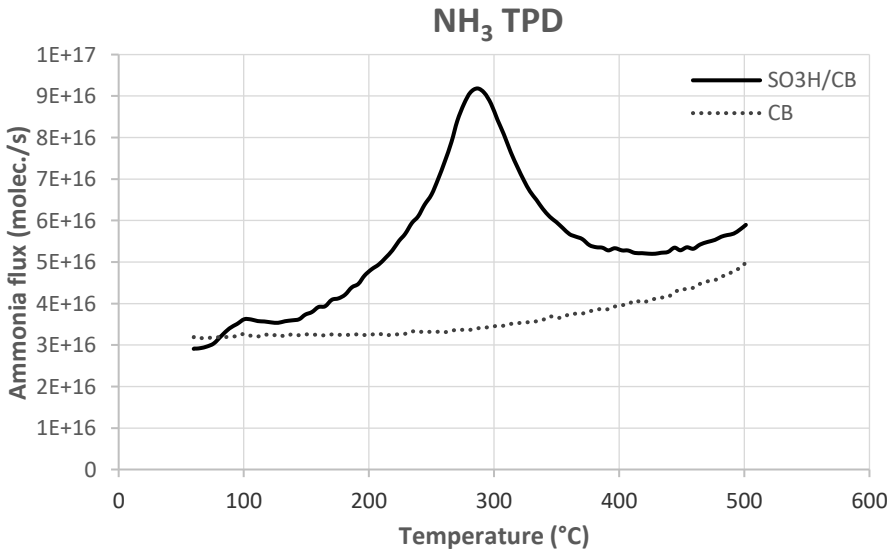

Figure 14: NH_3 flux as a function of temperature for CB and functionalized CB

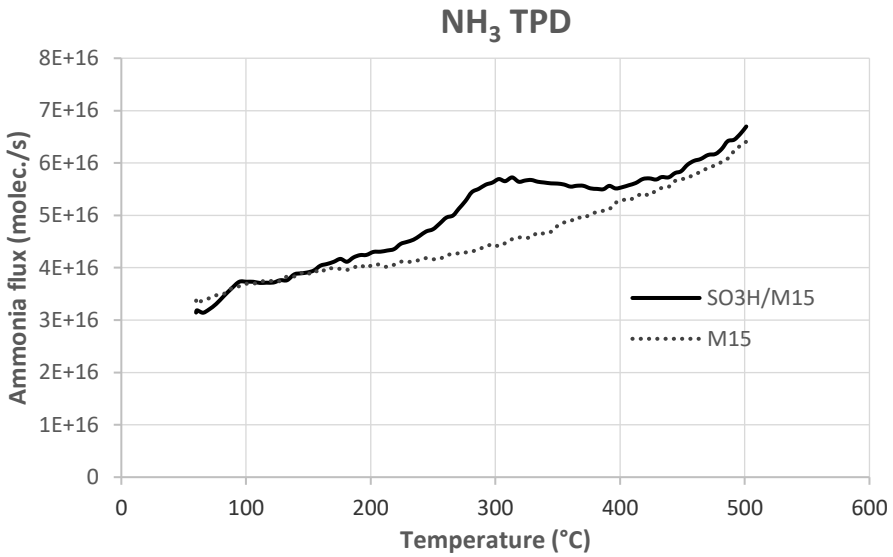

Figure 15: NH_3 flux as a function of temperature for GNP- M15 and functionalized GNP-M15

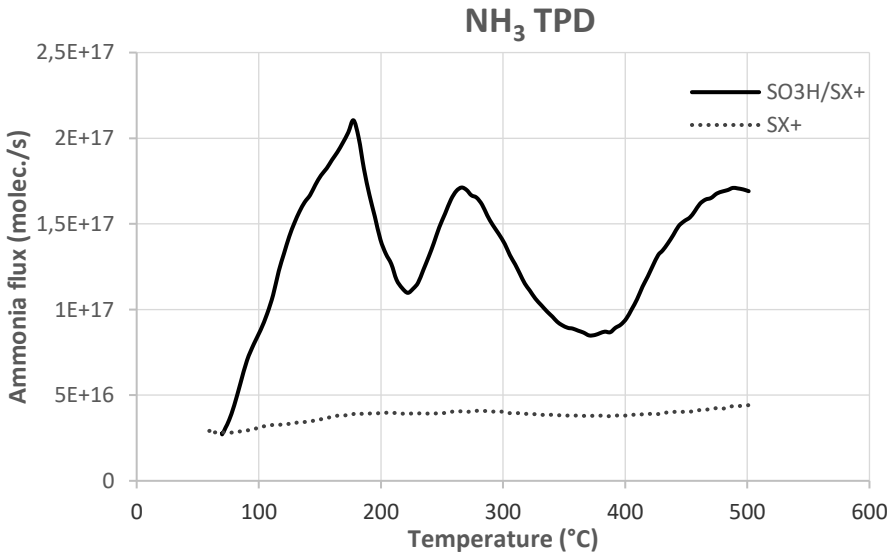

Figure 16: NH_3 flux as a function of temperature for SX+ and functionalized SX+

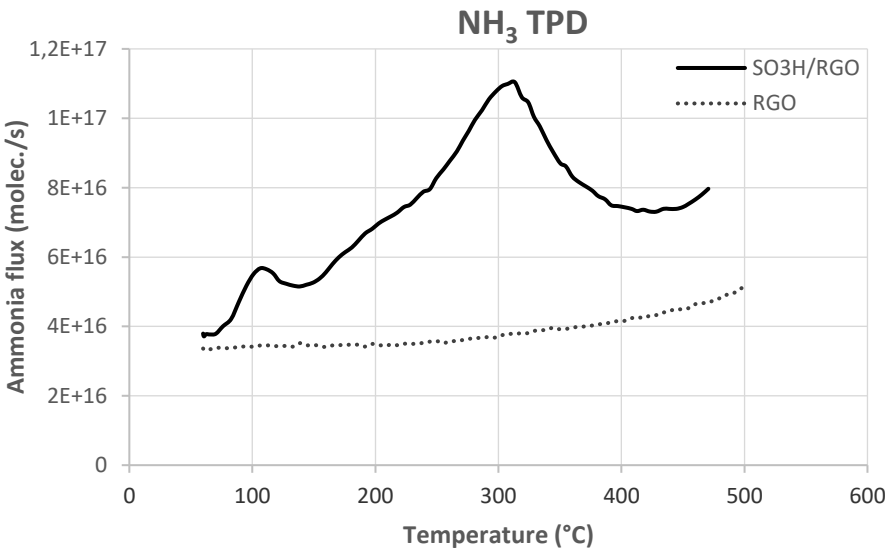

Figure 17: NH_3 flux as a function of temperature for RGO and functionalized RGO

S10. SO_2 signal followed by MS during NH_3-TPD analysis

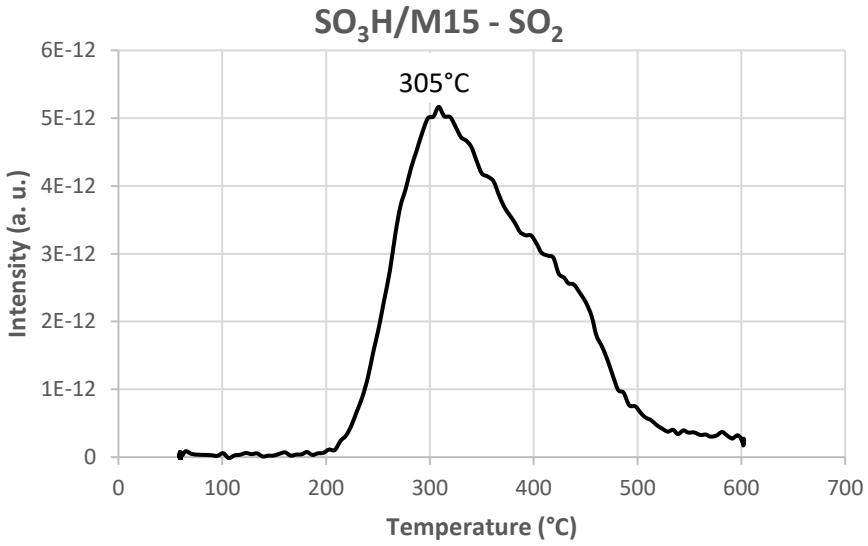

Figure 18: SO_2 signal followed by MS during the NH_3-TPD analysis of functionalized GNP-M15

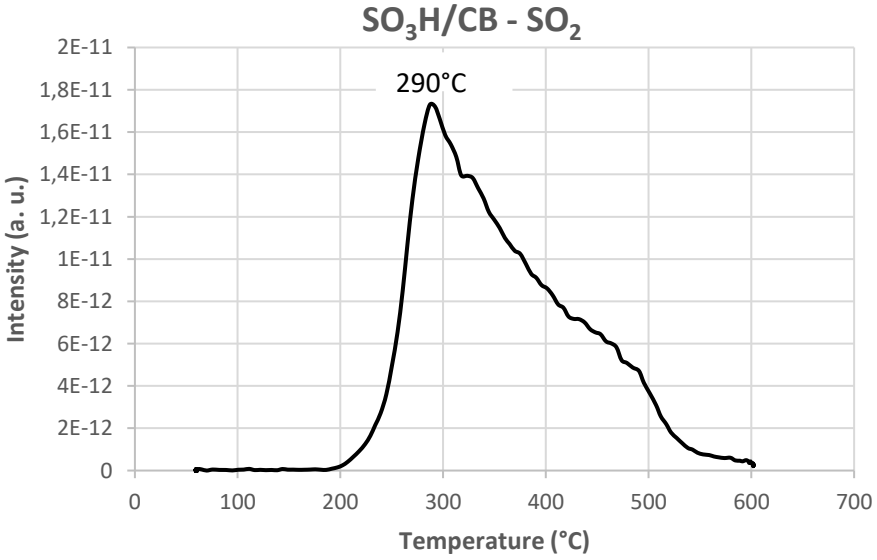

Figure 19: SO_2 signal followed by MS during the NH_3-TPD analysis of functionalized CB

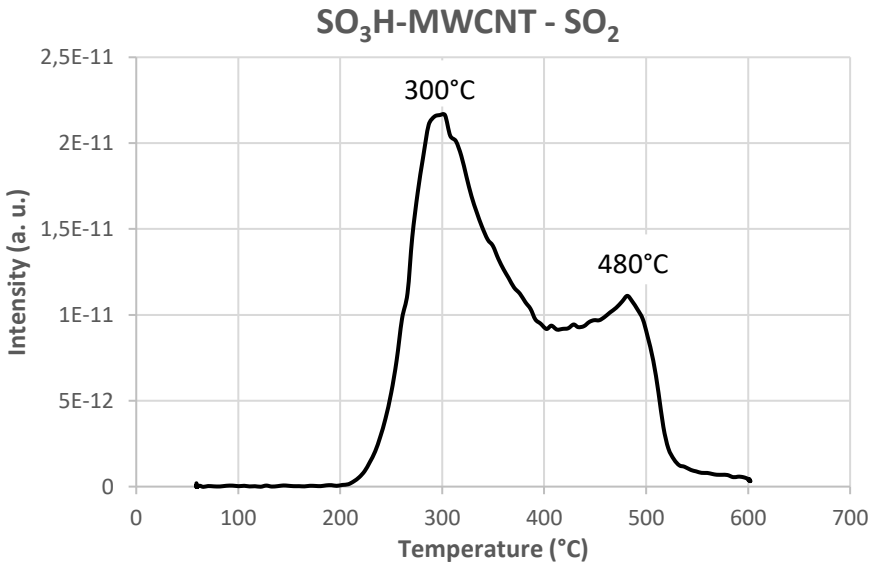

Figure 20: SO_2 signal followed by MS during the NH_3-TPD analysis of functionalized MWCNT

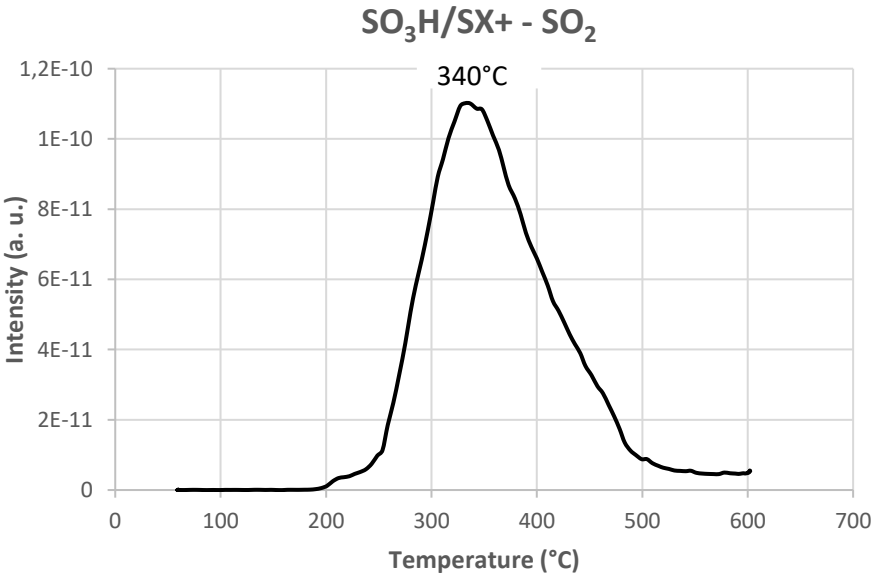

Figure 21: SO_2 signal followed by MS during the NH_3-TPD analysis of functionalized SX+

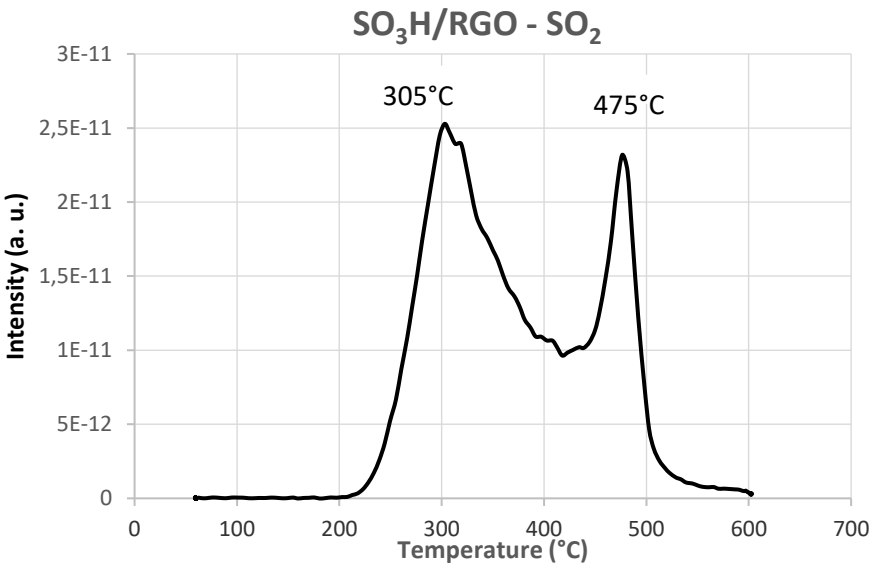

Figure 22: SO_2 signal followed by MS during the NH_3-TPD analysis of functionalized RGO

S11. Kinetic curves for bifunctional catalysts prepared with different SO_3H heat-treatments

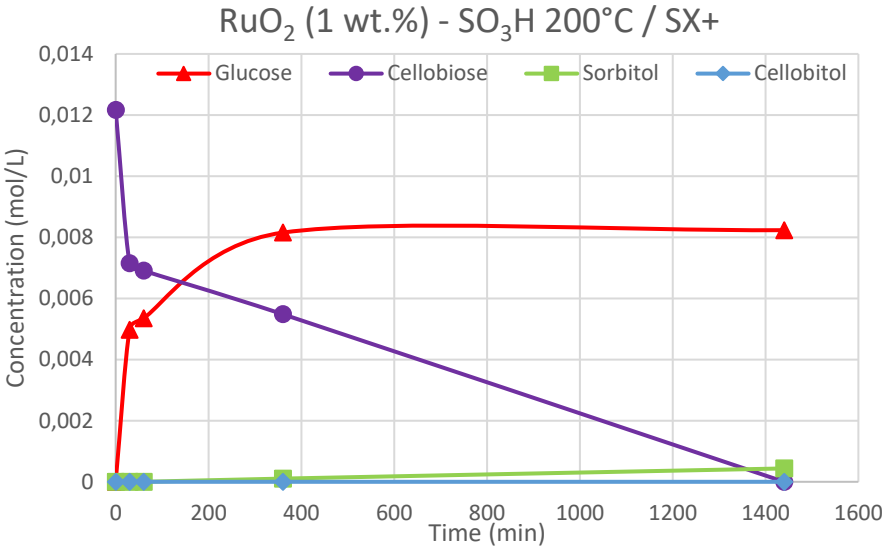

Figure 23: Kinetic curves for the transformation of cellobiose into sorbitol with three catalysts: RuO_2 (1 wt.%) – SO_3H treated at 200°C

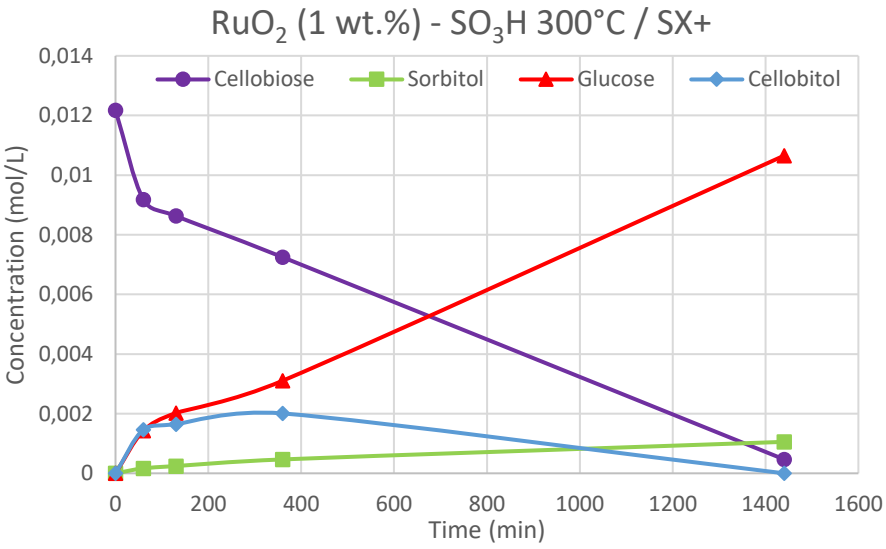

Figure 24: Kinetic curves for the transformation of cellobiose into sorbitol with three catalysts: RuO_2 (1 wt.%) – SO_3H treated at 300°C

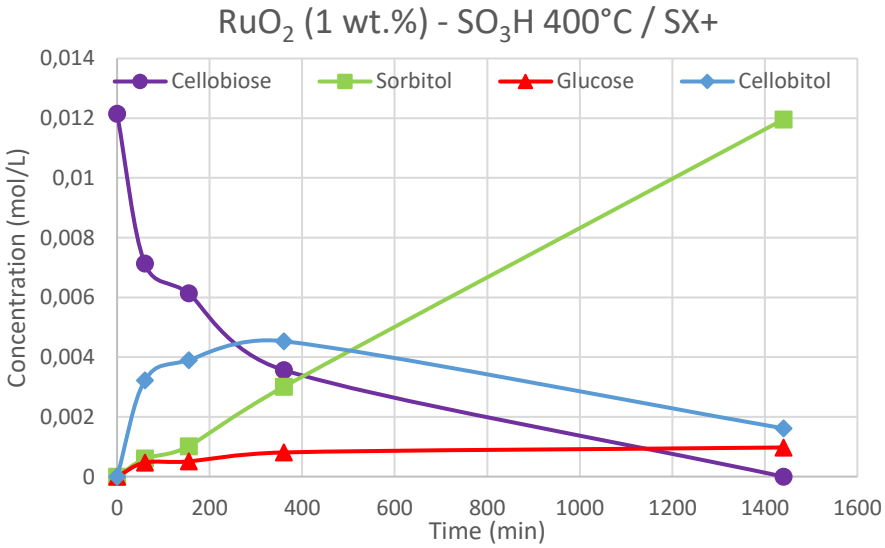

Figure 25: Kinetic curves for the transformation of cellobiose into sorbitol with three catalysts: RuO_2 (1 wt.%) – SO_3H treated at 400°C / SX+

S12. Conversion of cellobiose, selectivity and yield in sorbitol corresponding to the kinetic curves in main text in Chap V (Figure V-2)

Table 8: Results of the kinetic study for the hydrogenolysis of cellobiose with RuO_2 (5 wt.%) / AC; Cellobiose conversion, selectivity in glucose, cellobitol and sorbitol, yield in sorbitol (150°C, 30 bar of H_2, 150 mg of catalyst)

Time (min)	Cellobiose conversion (%)	Glucose selectivity (%)	Cellobitol selectivity (%)	Sorbitol selectivity (%)	Sorbitol yield (%)
60	100	2	58	16	16
130	100	3	48	22	22
360	100	3	31	28	28
1440	100	0	0	28	28

Table 9: Results of the kinetic study for the hydrogenolysis of cellobiose with RuO_2 (5 wt.%) – pre-treated SO_3H / AC; Cellobiose conversion, selectivity in glucose, cellobitol and sorbitol, yield in sorbitol (150°C, 30 bar of H_2, 150 mg of catalyst)

Time (min)	Cellobiose conversion (%)	Glucose selectivity (%)	Cellobitol selectivity (%)	Sorbitol selectivity (%)	Sorbitol yield (%)
60	84	6	50	26	22
120	88	6	48	31	27
360	91	6	47	39	35
1440	100	0	5	68	68

S13. C_{1s} and Ru_{3d} peaks from XPS analyses for different AC supported catalysts

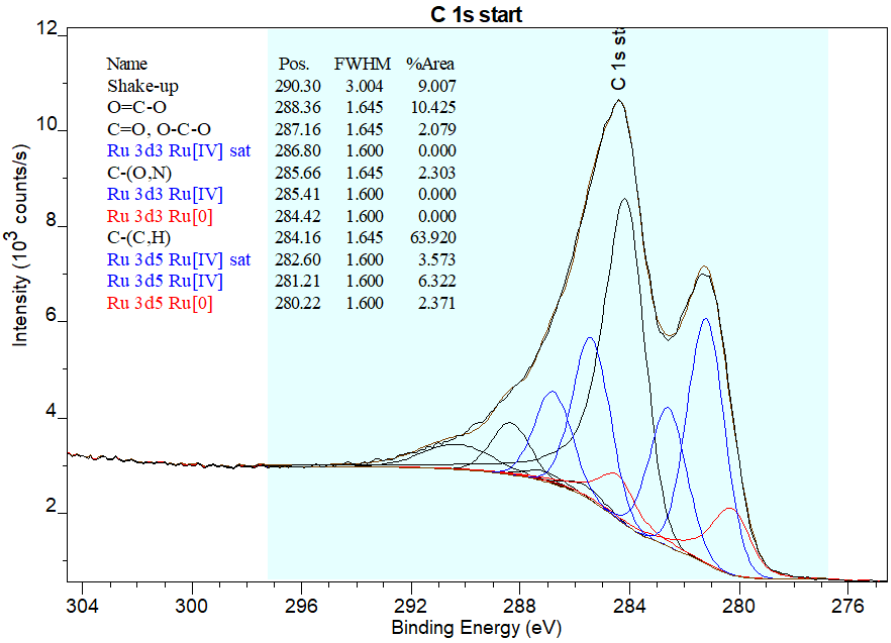

Figure 26: C_{1s} and Ru_{3d} peaks from XPS analysis of RuO_2 (5 wt. %) / AC catalyst

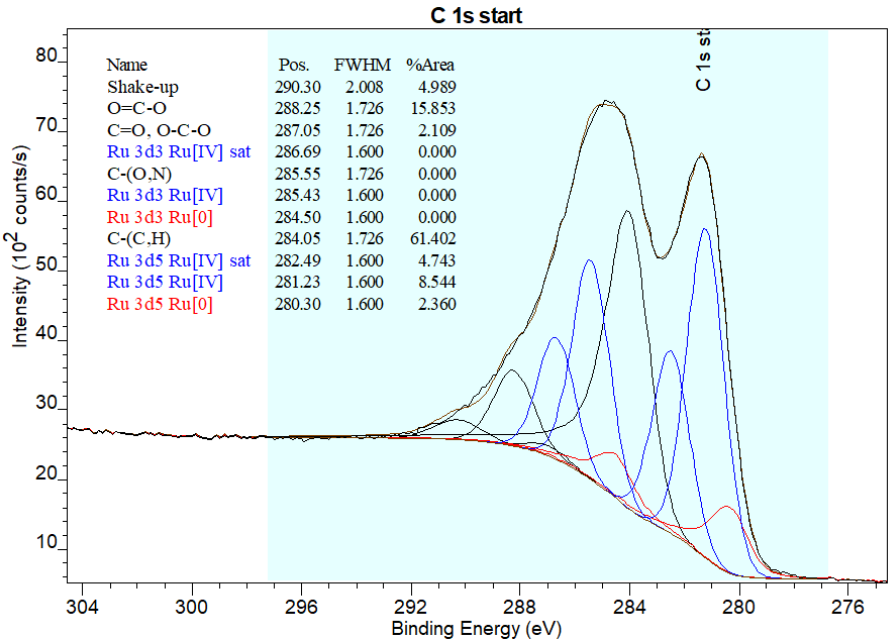

Figure 27: C_{1s} and Ru_{3d} peaks from XPS analysis of RuO_2 (5 wt. %) – pre-treated SO_3H / AC catalyst

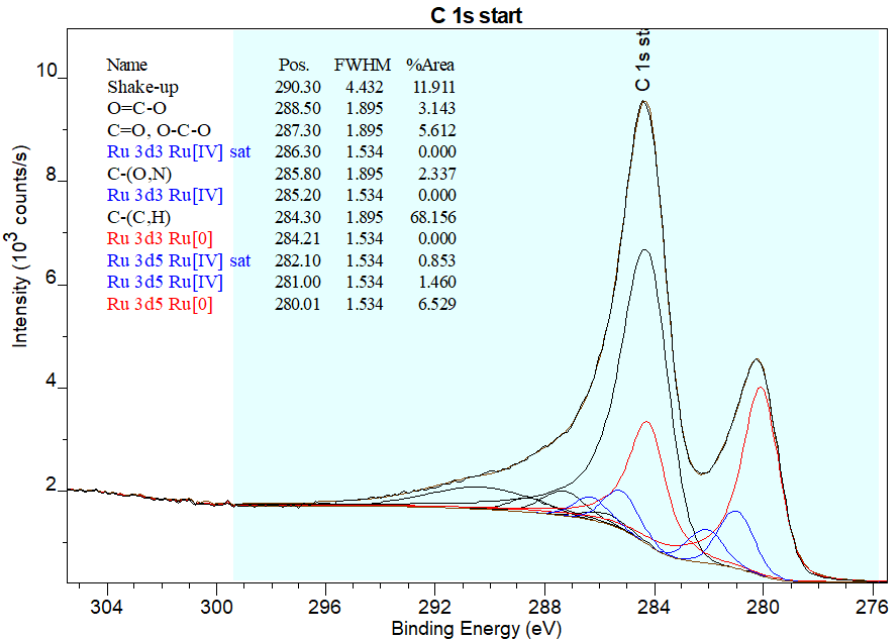

Figure 28: C_{1s} and Ru_{3d} peaks from XPS analysis of RuO_2 (5 wt. %) / AC catalyst after 5 runs

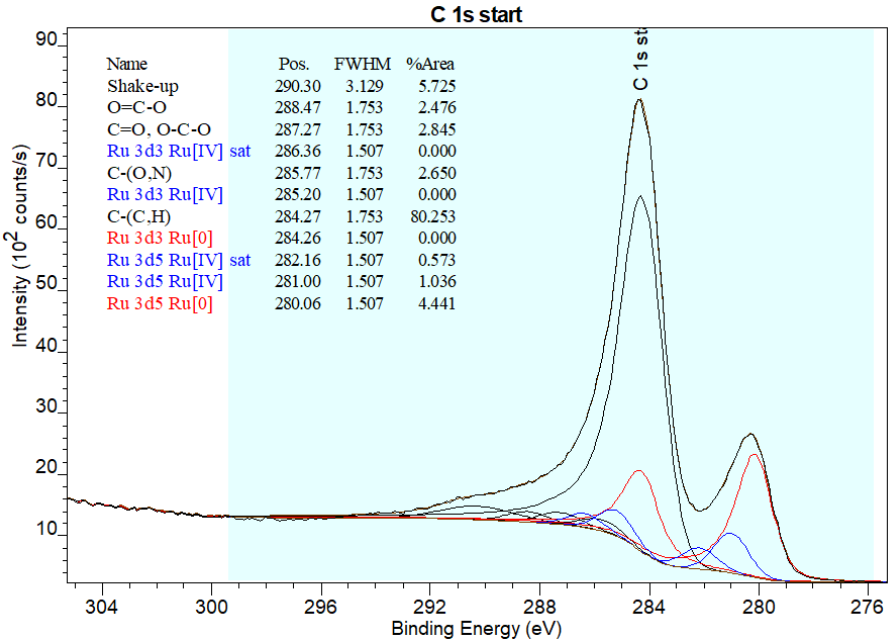

Figure 29: C_{1s} and Ru_{3d} peaks from XPS analysis of RuO_2 (5 wt. %) – pre-treated SO_3H / AC catalyst after 5 runs

S14. Atomic percentages of C_{1s} and Ru_{3d} determined by XPS analyses of monofunctional and bifunctional catalysts loaded with 3 wt.% of Ru

Table 10: Atomic contents in C and Ru for RuO_2 (3 wt.%) / AC and RuO_2 (3 wt.%) – pre-treated SO_3H / AC

Catalyst	C_{1s} (at. %)	Ru_{3d} (IV) (at. %)	Ru_{3d} (0) (at. %)
RuO_2 (3%) / AC	73.4	4.4	0.4
RuO_2 (3%) – pre-treated SO_3H / AC	59.4	5.9	0.6

S15. HR-TEM, STEM and EDX mapping analyses for monofunctional and bifunctional catalysts, before and after catalytic reaction

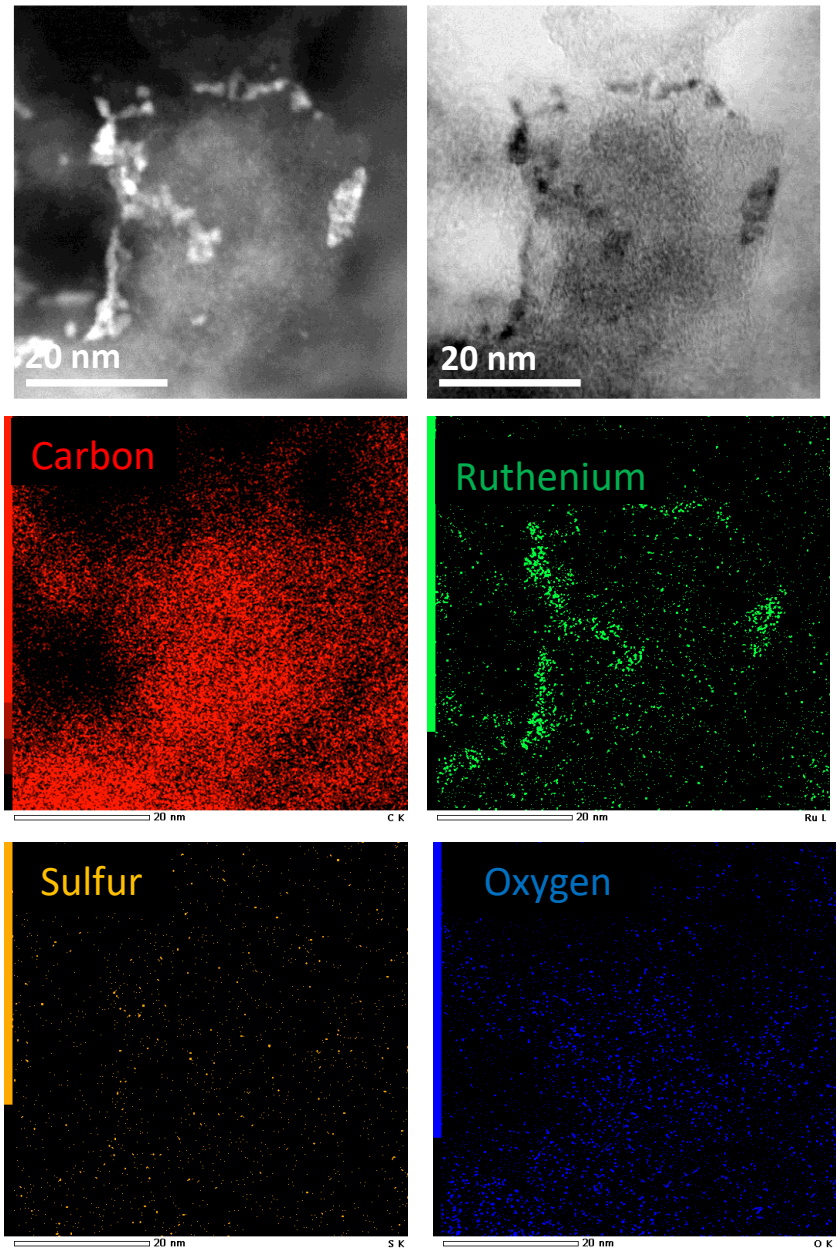

Figure 30: HR-TEM, STEM and EDX mapping analyses for RuO_2 (5%) / AC before catalytic test

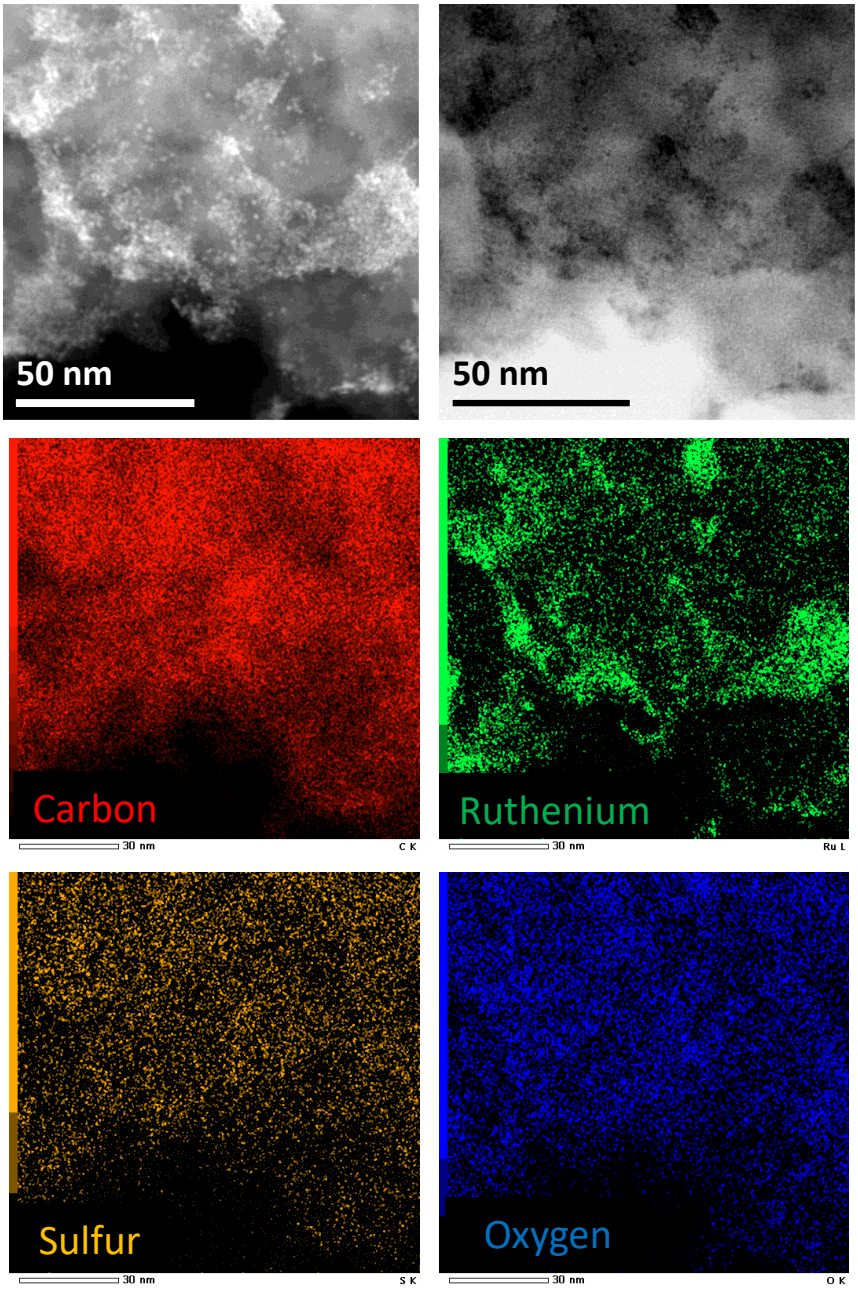

Figure 31: HR-TEM, STEM and EDX mapping analyses for RuO_2 (5%) – pre-treated SO_3H / AC before catalytic test

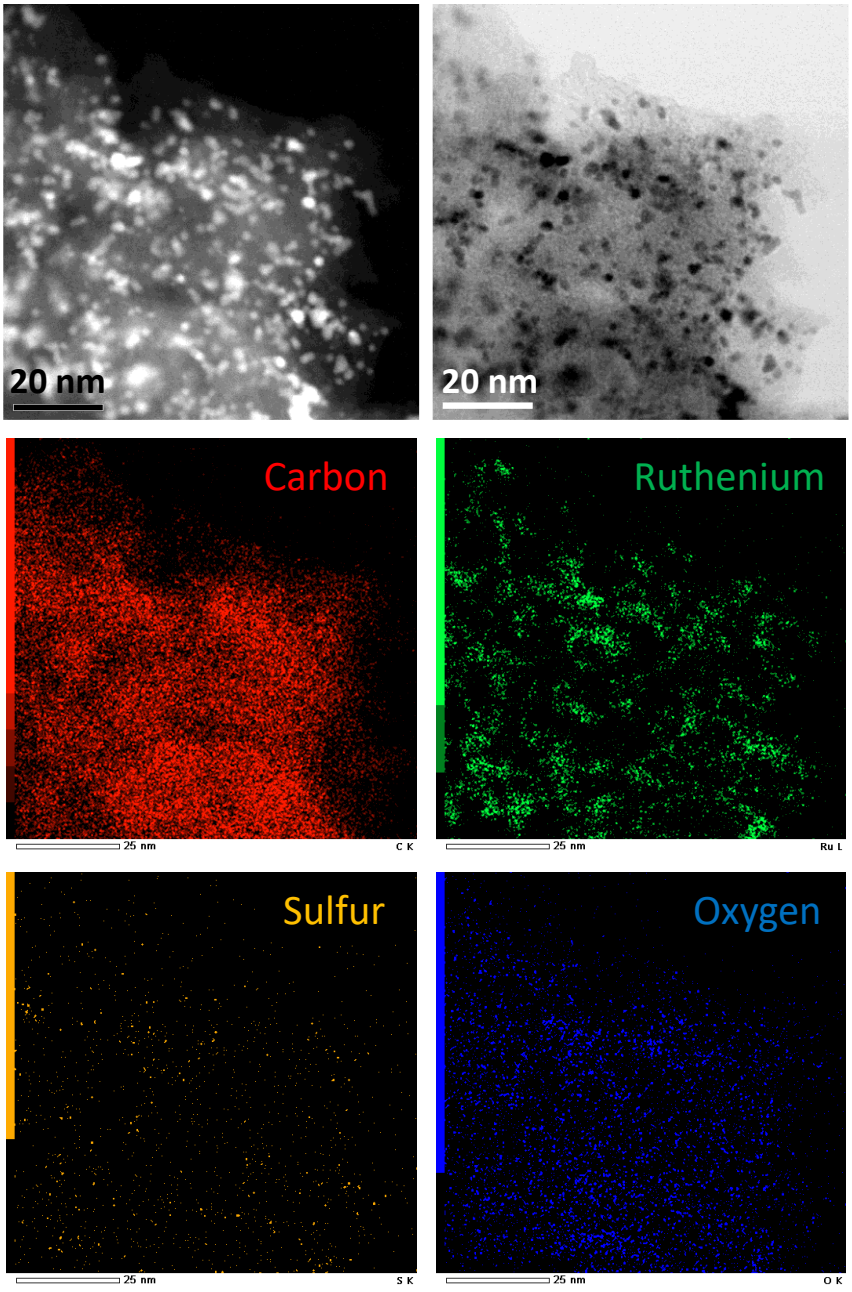

Figure 32: HR-TEM, STEM and EDX mapping analyses for RuO_2 (5%) / AC after 5 runs

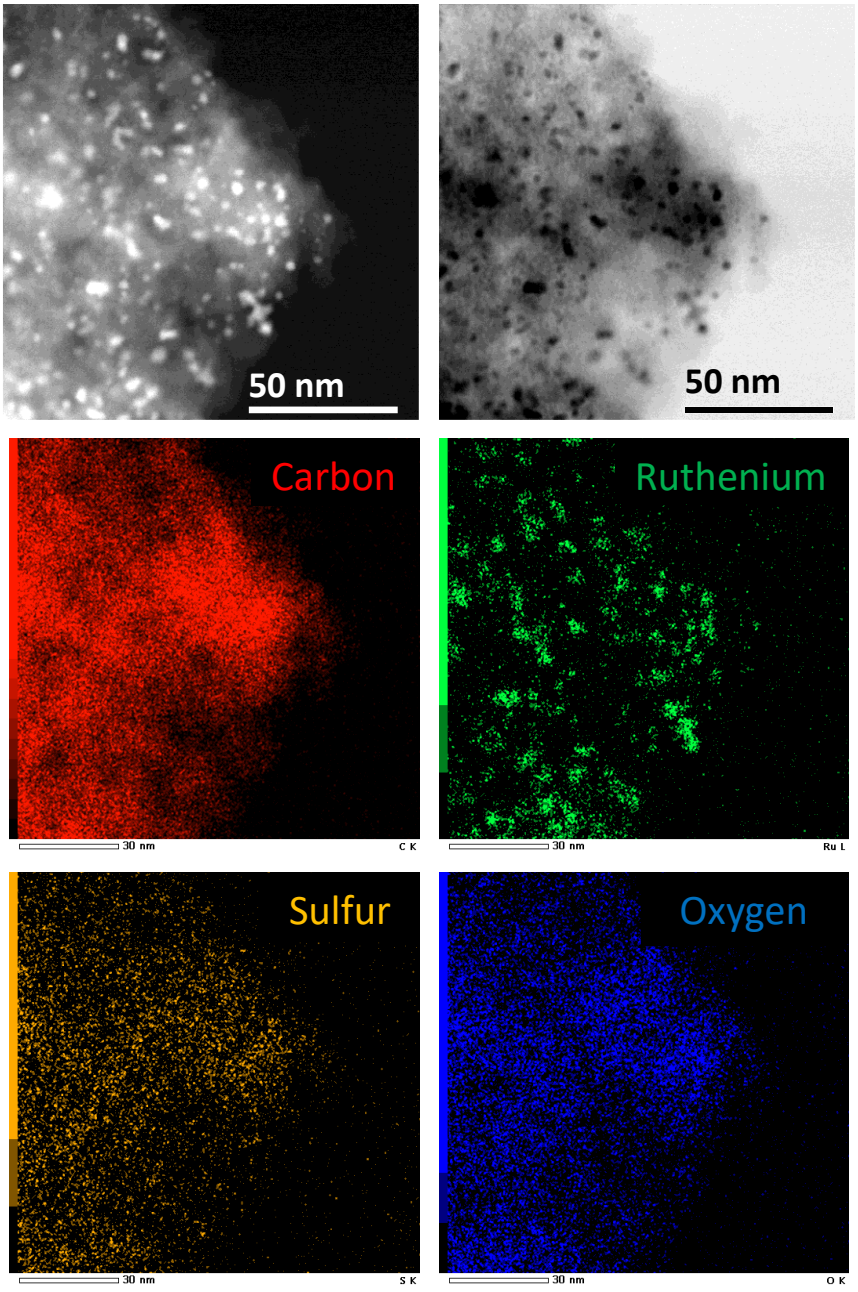

Figure 33: HR-TEM, STEM and EDX mapping analyses for RuO_2 (5%) – pre-treated SO_3H / AC after 5 runs

Publications

- S. Carlier, W. Baaziz O. Ersen, S. Hermans, Synergy between sulfonic functions and Ru nanoparticles supported on activated carbon for the valorization of cellobiose into sorbitol, *In preparation*, **2022**.

- S. Carlier, J. Gripekoven, M. Philippo, S. Hermans, Ru on N-doped carbon supports for the direct hydrogenation of cellobiose into sorbitol, *Applied Catalysis B: Environmental*, **2021**, 282.

- S. Carlier, S. Hermans, Highly efficient and recyclable catalysts for cellobiose hydrolysis: systematic comparison of carbon nanomaterials functionalized with benzyl sulfonic acids, *Frontiers in Chemistry*, **2020**, 8, 347.

- T. Haynes, S. Hubert, S. Carlier, V. Dubois, S. Hermans, Influence of water-miscible organic solvent on the activity and stability of silica-coated Ru catalysts in the selective hydrolytic hydrogenation of cellobiose into sorbitol, *Catalysts*, **2020**, 10, 149.

- N. Mager, P. Libioulle, S. Carlier, S. Hermans, Water-soluble single source precursors for homo- and hetero-metallic nanoparticle catalysts supported on nanocarbons, *Catalysis Today*, **2018**, 301, 153-163.

- N. Mager, W. S. Lamme, S. Carlier, S. Hermans, pH controlled adsorption of water-soluble ruthenium clusters onto carbon nanotubes and nanofibers surfaces, *Phys. Chem. Chem. Phys.*, **2016**, 18, 32210-32221.

Contributions to Conference

- Oral presentation accepted at **17th International Congress on Catalysis** 2020 in San Diego, United States (congress canceled)
- Oral presentation at **Europacat 2019** in Aachen, Germany (August 18 to August 23, 2019)
- Poster at **PREPA12** in Louvain-la-Neuve, Belgium (July 8 to July 12, 2018)
- Oral presentation at **Europacat 2017** in Florence, Italy (August 27 to August 31, 2017)